

# **NANOSCALE POLYMERIC PARTICLES via AEROSOL-PHOTOPOLYMERIZATION**

zur Erlangung des akademischen Grades eines  
DOKTORS DER INGENIEURWISSENSCHAFTEN (Dr.-Ing.)

der Fakultät für Chemieingenieurwesen und Verfahrenstechnik des  
Karlsruher Instituts für Technologie (KIT)

genehmigte

**DISSERTATION**

(Tag der mündlichen Prüfung: 06.02.2015)

Dipl.-Ing. Ertan Akgün

aus Izmir

Referent: Prof. Dr. Jürgen Hubbuch

Korreferent: Prof. Dr. Gerhard Kasper



## Acknowledgements

I would like to express my sincere and warmest thanks to the following people who directly or indirectly contributed to this work:

Dr. rer. nat. Michael Wörner, for providing me this great PhD opening, and also for his numerous discussions and very supportive comments.

Prof. Dr. Jürgen Hubbuch, for the possibility to conduct my PhD project in his research group and for his constructive comments.

Prof. Dr. Gerhard Kasper, who is one of the initiators of the project IP3 JointLab and also one of our project partners, for his discussions and fruitful advices.

Prof. Dr. Karlheinz Schaber, who made me aware of the presence of this project.

Siegfried Almstedt for his efforts on the construction and maintenance of the photoreactors.

Patrick Pionneau, who always was ready to support when required.

Christopher Anderlohr, one of our project partners within the JointLab, for providing his TEM equipment.

Our further project partners from and outside of JointLab.

All members of Prof. Hubbuch's research group.

My diploma students Meric Seker, Malin Reller, and Alex Muntean, and my further lab students.

All my friends who are not mentioned here by name.

All crossfit members for the challenging and priceless time.

Zuhal Bozer, my sister, and Muzaffer Bozer, her husband, for their support. I also thank my niece Asena and my nephew Volkan for the funny times.

My parents Ümit Akgün and Enver Akgün for their support and contribution before, during, and after my studies. I could not reach this point without their initiative.

# Contents

<b>Abstract</b> .....	<b>v</b>
<b>Zusammenfassung</b> .....	<b>vii</b>
<b>1. Introduction</b> .....	<b>9</b>
1.1 Polymerization Processes .....	10
1.2 Polymerization Mechanisms .....	12
1.3 Free Radical Polymerization .....	12
1.4 Rate of Photopolymerization .....	17
1.5 Photopolymerization of Multifunctional Monomers .....	18
1.6 Aerosol Generation Techniques .....	19
1.7 Atomization of Liquid Solutions .....	20
1.8 Aerosol-Photopolymerization .....	21
1.9 Experimental Setup of Aerosol-Photopolymerization .....	21
1.10 Polymer Reaction Engineering .....	23
<b>2. Research Proposal</b> .....	<b>29</b>
<b>3. Patents, Publications &amp; Manuscripts</b> .....	<b>31</b>
Patent Application 1 .....	33
Patent Application 2 .....	34
Perspectives of Aerosol-Photopolymerization: Nanoscale Polymer Particles .....	35
Perspectives of Aerosol-Photopolymerization: Organic-Inorganic Hybrid Nanoparticles ..	47
Perspectives of Aerosol-Photopolymerization: Nanostructured Polymeric Particles .....	60
Defined Polymer Shells on Nanoparticles via a Continuous Aerosol-Based Process .....	83
Cationic Aerosol-Photopolymerization .....	96
<b>4. Conclusions &amp; Outlook</b> .....	<b>105</b>
<b>5. References</b> .....	<b>107</b>
<b>Curriculum Vitae</b> .....	<b>119</b>

## Abstract

This PhD thesis focuses on the process of aerosol-photopolymerization for the generation of various polymeric particles. Such structures are most often prepared by liquid-based methods via the well-established thermal initiation step, and aerosol-photopolymerization is presented as an alternative, aerosol-based technique which employs photoinitiated polymerization. To the starting point of this thesis, aerosol-photopolymerization had not been researched in detail. Therefore, the advantages and drawbacks of this process, and its broad aspects are discussed within this thesis.

As an initiating step, a photoreactor with a XeCl\* excimer irradiation source was designed and constructed. It consists of concentric quartz glass tubes with the UV source at the center. Water circulation served for temperature control in the most outer shell. The first experiments were performed by employing the excimer photoreactor for the generation of spherical, nanoscale polymer particles. A monomer formulation was prepared by dissolving the solid photoinitiator Irgacure 907 in the liquid monomer without using any other solvent. This step was a proof of concept for testing the experimental setup under which conditions successful polymerization takes place. Methyl methacrylate (MMA) and butyl acrylate (BA) were chosen as the monofunctional monomers. MMA was either photopolymerized in the presence of the multifunctional monomer 1,6-hexanediol diacrylate (HDDA) or could be copolymerized with BA. The low propagation rate coefficient of MMA restricted its polymerization during a photoreactor passage of about 1 min whence it required a comonomer. BA possesses a much higher propagation rate coefficient than MMA and could be polymerized with and without a comonomer during the same aerosol residence time in the photoreactor.

After polymer nanospheres had been successfully obtained, the aim was to get more sophisticated particles via the same experimental setup. Zinc oxide (ZnO) was chosen as the model inorganic substance for the production of organic-inorganic hybrid nanoparticles in the form of polymer-matrix nanocomposites. ZnO nanoparticles were suspended in the monomer formulations which were used for polymer particle synthesis. Upon the same experimental procedure, polymer spheres containing the pre-dispersed ZnO nanoparticles were obtained. Since ZnO is capable of absorbing UV photons, practically the same hybrid particles were generated by preparing the same monomer formulation but without any conventional photoinitiator. In other words, ZnO nanoparticles themselves assisted the polymerization process as the photoinitiator.

Since the excimer photoreactor required time-intensive cleaning, it was not efficient for the trial of new monomer formulation recipes. A second photoreactor was arranged for a faster clean-up. This photoreactor consists of a single quartz glass tube surrounded by UV fluorescent tubes, and is operated at ambient temperature. Practically all of the particles resulting from this PhD thesis could be generated by both of the employed photoreactors, the excimer photoreactor and the photoreactor equipped with UV fluorescent tubes.

The third particle type resulting from this thesis are nanocaps which represent an example of non-spherical polymeric particles. For the production of nanocaps, additives were required in the monomer formulation. Apart from the solution consisting of liquid monomer, crosslinker, and the dissolved photoinitiator, a second solution was prepared by dissolving

glycerol in ethanol or another similar solvent. This solvent has to dissolve the first solution, the monomer solution, upon mixing. The prepared final solution is then processed via aerosol-photopolymerization for the synthesis of nanocaps. During photoreactor passage, ethanol evaporates and the presence of glycerol delays the gelation while a three-dimensional polymer network is formed within each particle. After a certain point, glycerol is no longer soluble within each polymerizing droplet upon the evaporation of ethanol and conversion of monomers. This leads to a controlled collapse of each sphere and cap-shaped particles are formed. The same particles were also formed with ZnO nanoparticles distributed in the polymer matrix.

Porous spherical particles possessing rough surface characteristics were obtained via aerosol-photopolymerization as well. A porogen, solvent miscible with monomer but immiscible with the obtained polymer afterwards, was employed for this. For successful pore formation, the porogen should be less volatile than ethanol, for example like 2-ethylhexanol. Nanospheres, nanocaps, and mosaic particles were loaded with caffeine for drug release experiments. Caffeine represents a molecularly distributed substance in the polymer matrix in comparison to ZnO nanoparticles, and the results revealed release rates depending on the degree of crosslinking, particle shape, and the employed additives.

An integrated, aerosol-based process was realized for the generation of core-shell particles in cooperation with another working of JointLab, the joint initiative between BASF and KIT. Two aerosol streams were prepared, one having monomer droplets and the other one having core particles as the dispersed phase. The aerosols were electrostatically charged with opposite signs and mixed for bipolar coagulation to take place. Each core particle had to collide with a monomer droplet in order to become coated by the liquid monomer after a certain residence time for coagulation. Once wetted core particles were obtained, aerosol-photopolymerization served for the polymerization of the monomer coating into a solid shell. Various core materials such as gold, silica, and salt particles were encapsulated via this technique by the same polymers prepared as nanoscale polymer spheres, either poly(HDDA) or poly(HDDA-crosslinked MMA). Bipolar coagulation, which is based on physical charging, enabled the coating process to be independent of material choice provided that the core particle surface can be completely wetted by the liquid monomer, and aerosol-photopolymerization served for the rapid solidification of the liquid shell surrounding each core particle.

Although this PhD thesis is based on an experimental work, basic modeling and simulation has been performed to estimate the time for the photopolymerization of monofunctional monomers. Propagation and termination rate coefficients were defined as functions of monomer conversion and parameters such as initiation and propagation rate coefficient were varied to simulate the conversion of photoinitiator and monomer for 1 min of photopolymerization. The results revealed strong dependency of monomer conversion on the propagation rate coefficient. For high photoinitiator conversion, high initiation rates are required which can be realized by either choosing a photoinitiator with high UV absorptivity and high quantum yield, using more amounts of photoinitiator, or increasing the UV irradiance in the photoreactor.

## Zusammenfassung

Die vorliegende Doktorarbeit beschäftigt sich mit dem Prozess der Aerosol-Photopolymerisation zur Generierung von verschiedenen polymerbasierten Partikeln. Solche Materialien werden am häufigsten durch flüssigkeitsbasierende Methoden hergestellt, wobei fast ausschließlich thermische Initiierung für den Polymerisationsprozess eingesetzt wird. Daher wird die Technik der Aerosol-Photopolymerisation als Alternativverfahren unter Anwendung von photochemischer Initiierung vorgestellt.

Als erstes wurde ein Photoreaktor, basierend auf einem XeCl\* Excimer-Strahler, ausgelegt und konstruiert. Er bestand aus konzentrischen Quarzglasrohren mit dem Strahler im Zentrum. Wasserumlauf in einem Außenmantel diente zur Temperaturkontrolle. Die ersten Experimente wurden mit diesem Photoreaktor durchgeführt, um kugelförmige, nanoskalige Polymerpartikel herzustellen. Dazu wurde eine Monomerlösung vorbereitet, in dem der feste Photoinitiator im flüssigen Monomer gelöst wurde, ohne zusätzliches Lösungsmittel zu verwenden. Dies sollte als Test dienen, um herauszufinden, unter welchen Bedingungen eine erfolgreiche Polymerisation durchgeführt werden kann. Als monofunktionelle Monomere wurden Methylmethacrylat (MMA) und Butylacrylat eingesetzt (BA). MMA wurde entweder in Anwesenheit des multifunktionellen Monomers (Vernetzer) 1,6-Hexandioldiacrylat (HDDA) verwendet oder mit BA copolymerisiert. Der niedrige Kettenwachstumskoeffizient von MMA erlaubte keine vollständige Polymerisation dieses Monomers ohne Zugabe eines schnelleren Comonomers während der Aerosolverweilzeit von etwa 1 Minute im Photoreaktor.

Nach der erfolgreichen Generierung von kugelförmigen, nanoskaligen Polymerpartikeln, waren komplexere Strukturen von Interesse, die mit demselben experimentellen Aufbau hergestellt werden sollten. Für die Herstellung von organisch-anorganischen Hybridnanopartikeln wurde Zinkoxid als anorganische Modellsubstanz eingesetzt. Hierfür wurden kommerziell erhältliche ZnO-Nanopartikeln verwendet, um Polymer-Matrix Nanokomposite zu erzeugen. Ähnliche Hybridpartikel wurden ebenfalls generiert ohne einen konventionellen Photoinitiator in der Monomerformulierung zu lösen, da ZnO-Nanopartikeln selbst im UV-Bereich absorbieren und den Polymerisationsprozess initiieren können.

Der Excimer-Photoreaktor war zeitintensiv bezüglich Reinigung und hat sich als nicht praktisch erwiesen für das schnelle Austesten von neuen Monomerformulierungen. Daher wurde ein zweiter, einfacherer Photoreaktor konstruiert. Er bestand aus einem Quarzglasrohr umgeben von Fluoreszenzstrahlern, die im UV-Bereich emittieren. Dieser Photoreaktor wurde ausschließlich bei Umgebungstemperatur betrieben. Alle Partikelstrukturen aus dieser Doktorarbeit konnten sowohl mit dem ersten Photoreaktor als auch mit dem zweiten Photoreaktor hergestellt werden.

Die dritte Generation von Polymerpartikeln dieser Doktorarbeit waren die „Nanocaps“. Diese nicht-kugelförmigen Polymerpartikel wurden mit Zusatzstoffen in der Monomerformulierung hergestellt. Außer der Monomerlösung, bestehend aus Monomer, Photoinitiator und Vernetzer, wurde eine zweite Lösung vorbereitet, in dem Glycerol in Ethanol oder einem ähnlichen Lösungsmittel gelöst wurde. Dieses Lösungsmittel musste nach dem Mischen beider Lösungen alle Bestandteile lösen können. Während der Aerosol-

Photopolymerisation der finalen Monomerformulierung wurden Nanocaps erzeugt. Die Ausbildung dieser Strukturen beruht auf der Verdampfung von Ethanol im Photoreaktor und der Wirkung von Glycerol, das als Weichmacher die Gelbildung verzögert, währenddessen ein dreidimensionales Polymernetzwerk in den jeweiligen Tröpfchen gebildet wird. Das führt zum kontrollierten Kollabieren der polymerisierenden Tröpfchen, die dabei von Kugelgestalt in capstrukturierte Partikeln übergehen. Dieselben strukturierten Partikel konnten wie bei den kugelförmigen Nanopartikeln auch mit ZnO-Nanopartikeln, verteilt in der Polymermatrix, generiert werden.

Poröse, kugelförmige Partikeln mit rauen Oberflächen wurden ebenfalls mit der Aerosol-Photopolymerisation erzeugt. Dazu wurde ein Porogen als Lösungsmittel verwendet, das mischbar mit dem Monomer ist, allerdings nicht mit dem gebildeten Polymer. Weniger flüchtige Porogene wie z.B. 2-Ethylhexanol bewirkten Porenbildung während der Polymerisation. Nanokugeln, Nanocaps und Mosaikpartikeln wurden mit Coffein beladen, um Freisetzungsversuche durchzuführen. Im Gegensatz zu ZnO-Nanopartikeln, wird Coffein in der Polymermatrix molekulardispers verteilt. Die Experimente zeigten, dass die Freisetzungskinetik durch den Vernetzungsgrad, der Partikelform und verwendeten Zusatzstoffen beeinflusst werden kann.

Ein integrierter, aerosolbasierter Prozess wurde für die Generierung von Kern-Schale-Partikeln in Kooperation mit einer anderen Arbeitsgruppe innerhalb des JointLabs, die Kooperation zwischen BASF und KIT, realisiert. Zwei Aerosolströme, einer mit Monomertröpfchen als disperser Phase und einer mit Kernpartikeln, wurden erzeugt. Die Aerosole wurden jeweils elektrostatisch mit gegensätzlicher Polarität geladen und anschließend gemischt. Nach einer gewissen Koagulationsverweilzeit sollten bevorzugte 1-zu-1 Kollisionen zwischen Tröpfchen und Kernpartikeln zustande kommen, sodass die Kernpartikeln mit der Monomerflüssigkeit umhüllt werden. Die flüssigen Hüllen wurden im nachgeschalteten Photoreaktor zu festen Schalen polymerisiert. Verschiedene Kernmaterialien wie Gold-, Silica- und Salzpartikeln wurden mit den Polymeren poly(HDDA) und poly(HDDA-vernetztes MMA) verkapselt. Die bipolare Koagulation ermöglichte materialunabhängige Beschichtung solange die Monomerlösung die Kernpartikel komplett benetzen kann, und die Aerosol-Photopolymerisation sorgte für die rapide Umwandlung der flüssigen Monomerhülle in die feste Polymerschale.

Obwohl diese Dissertation vorwiegend experimentell ausgerichtet war, sind auch grundlegende Modellierungen und Simulationen durchgeführt worden um die Dauer der Polymerisation von monofunktionellen Monomeren abzuschätzen. Kettenwachstums- und Kettenabbruchskoeffizienten wurden als Funktion des Monomerumsatzes definiert und Parameter wie der Initiierungs- und Kettenwachstumskoeffizient variiert, um den Monomerumsatz während 1 Minute Photopolymerisation zu simulieren. Die Ergebnisse zeigten, dass der Kettenwachstumskoeffizient der entscheidende Faktor ist. Darüber hinaus werden hohe Initiierungsraten benötigt, die nur mittels photoinitiiertes Polymerisation möglich sind. Dies kann entweder durch Wahl geeigneter Photoinitiatoren mit hohen UV Absorptionen und hohen Quantenausbeuten für die Radikalbildung, durch höhere Photoinitiatorkonzentrationen in der Formulierung oder durch Erhöhung der Bestrahlungsstärke im Photoreaktor realisiert werden.

## 1. Introduction

Photopolymer technology is a huge scientific area dealing with the application of electromagnetic radiation to form polymers or initiate reactions in polymeric materials. Between 1990 and 1995, over 4000 distinct references to some aspect of photopolymer technology were reported per year as a result of tremendous patent and open literature activities in this field. The applications are widespread and photopolymers are used in electronic materials, printing materials, optical and electro-optical materials, fabrication of devices and polymeric materials, adhesives and coating materials (Peiffer, 1997).

Photoinitiated polymerization, or photopolymerization, is a subdivision of photopolymer technology and was used as early as in the beginning of 1900 when Berthelot and Gaudechon (Berthelot and Gaudechon, 1910) polymerized ethylene by UV radiation. Photopolymerization has played a decisive role in the early development of polymer chemistry. It has been applied for various purposes such as detection and identification of photochemically produced free radicals, study of non-steady state polymerization kinetics, and electrophoresis where biological compounds are involved since no elevated temperatures are required (Oster and Yang, 1968). More recent and common applications of photopolymerization are its use for producing photoactive polymer-based systems for the coatings industry, paints and printing inks, adhesives, composite materials, and dental restorative formulations (Andrzejewska, 2001). Further applications are in photolithography, optoelectronics, stereolithography, and holography (Decker, 1996). Light sensitive poly(vinyl cinnamate) was developed as the first synthetic photopolymer material at Kodak for imaging (Minsk et al., 1954). Upon the development of free radical chain polymerization at DuPont (Plambeck, 1956), the utilization of photopolymer technology extended. In 1997, a yearly worldwide market of more than 10 billion dollars was estimated (Peiffer, 1997). Tough, new applications of photopolymer systems have still been developing such as 3D imaging for the direct construction of solid plastic objects from computer-drawn images (Crivello and Reichmanis, 2014).

Photopolymerization is generally accepted as the photoinitiated polymerization of monomers and oligomers to obtain crosslinked polymers although it is possible to photopolymerize monofunctional vinyl monomers (Crivello and Reichmanis, 2014). Therefore, a tremendous amount of published work about photoinitiated free radical and cationic polymerization report on the photopolymerization of multifunctional monomers, also called radiation curing (Andrzejewska, 2001; Bowman and Kloxin, 2008; Decker, 1992, 1996; Decker et al., 2001; Decker and Moussa, 1990; Peiffer, 1997). Upon the development of systems that efficiently undergo facile homolytic photocleavage or electron transfer reactions, free radical generation has been realized with high quantum yields. Hence, photoinitiators covering almost the whole UV spectrum were rapidly developed between 1960 and 1970 by companies such as Ciba-Geigy, BASF, AKZO, and Cray-Valley (Crivello and Reichmanis, 2014). Radiation curing offers substantial advantages such as very rapid reaction rates, spatial resolution by irradiating certain polymerization domains, operation at ambient temperature (Decker, 1996), very low energy requirements, elimination of organic volatile solvents (Crivello and Reichmanis, 2014), solvent-free formulations, and production of polymers possessing tailor-made properties. These points make photopolymerization quite

attractive for ultrafast drying of protective coatings, varnishes, printing inks and adhesives and high-definition images required in the manufacture of microcircuits and printing plates (Decker, 1996). Due to the very fast nature of photoinitiated crosslinking polymerization, calorimetric studies requiring a few seconds could not reveal kinetic results with high resolution (Tryson and Shultz, 1979). At first, this limited the performed research to be carried out at low intensities for monitoring in real-time. On the other side, industrial applications prefer intense UV radiation for thin film (thickness < 10  $\mu\text{m}$ ) polymerizations in the presence of air (Decker, 1996). Upon the application of spectroscopic methods such as IR (Decker, 1992; Decker and Moussa, 1990), UV (Decker, 1992), and FTIR spectroscopy (Li et al., 2006) for thin film photopolymerization, real-time results could be obtained. Thin films both possess diverse applications and allow the utilization of the mentioned real-time spectroscopic methods during photopolymerization (Decker, 1996). Applications of photopolymerization mostly cover UV curing in which the photons are delivered from a stationary irradiation source onto a flat surface substrate which is passed under the irradiation source by a conveyor or a moving web. Aside from this in-line processing, robot-guided movable irradiation sources have recently been applied to complex geometries as well. Photocurable automotive finishes or curing of coatings on completely assembled furniture are some examples (Crivello and Reichmanis, 2014).

Apart from thin films, particulate micron-sized and submicron polymeric materials also attract a broad range of industry areas ranging from optics and photonics to nanomedicine. Depending on the purpose of application, the particles can be spherical or non-spherical. The latter can possess specific or random shapes. In addition, the particles can be composed of polymeric part only or different materials can be integrated to fulfill multifunctionality within the particle. Shielding of UV radiation via transparent materials (Althues et al., 2007; Yuwono et al., 2004), multicomponent magnetic nanoparticles (Zeng and Sun, 2008), nanocomposites for color switching (Caseri, 2010), needle-free particle delivery into skin (Michinaka and Mitragotri, 2011), imaging and treatment in medicine (Berry and Curtis, 2003), and targeted drug delivery (van Vlerken and Amiji, 2006) are some of these examples. Various techniques exist for the production of polymer particles or polymeric composites. Most common are the methods which are based on the liquid phase such as suspension (Shim et al., 2002) or emulsion polymerization (Hecht et al., 2012) from which the former is suitable for larger particle generation whereas the latter is more appropriate for the synthesis of smaller particles (Odian, 2004). Nanoparticles can be synthesized by employing special kinds of emulsion polymerization, the microemulsion polymerization (particle size of 1 nm – 100 nm) or the miniemulsion polymerization (particle size of 50 nm – 1  $\mu\text{m}$ ), upon the polymerization of nanoscale monomer droplets which most often are stabilized by surfactants (Landfester et al., 1999). An overview of the common polymer and polymeric particle preparation methods is presented in the subsequent sub-chapter.

## **1.1 Polymerization Processes**

Polymerization reactions can be realized by employing different processes. Bulk (mass) and solution polymerization are carried out as homogeneous polymerizations whereas precipitation, suspension, and emulsion polymerization fall below the category of heterogeneous polymerization.

*Bulk or mass polymerization* is the simplest process and results in polymers with as low contamination as possible. However, its implementation for radical chain polymerization is difficult regarding the temperature control because the reactions are highly exothermic in nature, possess high activation energies, and tend toward the gel effect. Strong stirring is required for a better temperature control due to the rapidly increasing viscosity of the reaction medium. Local hot spots may occur, and these may lead to runaway reactions. Such drawbacks reduce the interest for bulk polymerization in industrial use. To overcome the heat dissipation and viscosity difficulties, bulk chain polymerizations are usually carried out to low conversions with subsequent separation and recycling of unreacted monomer. If favored, thin layer polymerization can be carried out for up-conversion once the low-converted polymer is obtained in a larger, upstream reactor.

*Solution polymerization* occurs if the monomer is dissolved in a solvent, resulting in easier handling of stirring due to the lower medium viscosity and a more efficient heat transfer. However, the presence of a solvent may both enhance transfer reactions to the solvent and reduce polymer purity.

*Precipitation polymerization* is homogeneous at the beginning and becomes heterogeneous during the progress of monomer conversion. A monomer is polymerized either in bulk or in solution, and the formed polymer is insoluble in the reaction medium. Examples are bulk polymerization of vinyl chloride and solution polymerization of acrylonitrile in water.

*Suspension polymerization* is carried out with monomer droplets having diameters of 50-500  $\mu\text{m}$ . Initiators which are soluble in the monomer are referred to as oil-soluble initiators. In suspension polymerization, each monomer droplet constitutes a miniature bulk polymerization system. Monomers such as styrene, acrylic and methacrylic esters, vinyl chloride, vinyl acetate, and tetrafluoroethylene are used for suspension polymerization. The amount of suspension stabilizers is less than 0.1 wt.-%. If the droplet diameter is about 1  $\mu\text{m}$ , the suspension polymerization is called microsuspension polymerization.

*Emulsion polymerization* is employed for radical chain polymerizations and is similar to suspension polymerization, but is quite different in mechanism and reaction characteristics. The monomer droplets to be polymerized are smaller and the dependence of polymer molecular weight on reaction parameters differs too. It is utilized for a variety of industrial products such as paints, coatings, finishes, and floor polishes. The product of an emulsion polymerization process is referred to as a latex. In contrast to other methods, emulsion polymerization is unique in increasing the polymer molecular weight without decreasing the polymerization rate. Its reaction mechanism allows to attain both high molecular weights and high reaction rates. The amount of stabilizers is much higher than in suspension polymerization. The higher surface area of monomer droplets is stabilized with surfactant as high as 1-5 wt.-% in concentration. By polymerizing smaller monomer droplets in emulsion polymerization, miniemulsion or microemulsion polymerization can be performed (O'dian, 2004).

*Aerosol-based processes* can be employed as alternative – and relatively new – techniques for the generation of polymeric particles. After spraying the liquid monomer to form gas-carried monomer droplets, the droplets were contacted with initiator vapor for the generation of micrometer-sized polystyrene particles (Shin et al., 1996). The “contact challenge” between monomer and initiator was overcome by spraying a multiacrylate monomer mixture

containing the photoinitiator with the help of a volatile solvent using a vibrating-orifice aerosol generator (Esen and Schweiger, 1996). The produced droplet aerosol was photopolymerized to a particle aerosol with monodisperse polymer particles being 5-50  $\mu\text{m}$  in diameter. A similar work with a modified vibrating-orifice aerosol generator resulted in monodisperse polymer particles having 5-100  $\mu\text{m}$  diameter (Gao et al., 2007). Apart from these free radical initiated polymerization, cationic photopolymerization in aerosols was employed for preparing microbeads as well (Vorderbruggen et al., 1999).

## 1.2 Polymerization Mechanisms

Polymerization reactions can be classified into two groups regarding the reaction mechanism, step polymerization and chain polymerization.

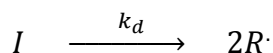
In step-growth polymerization, functional groups of educts react with each other and polymer molecular weight increases rather slowly. A monomer can react with another monomer to a dimer, or with a dimer to a trimer in a step-wise manner. The characteristic feature of this mechanism is that reaction occurs between any species, e.g. a tetramer can also react with a trimer to form a heptamer.

In chain-growth polymerization, an initiator is required to produce a species having a reactive center which is capable of further chain growth. This species may be a free radical, a cation, or an anion. Propagation via this active center by the successive addition of a large number of monomer molecules results in polymer chains with high molecular weights at relatively fast rates. Once a monomer is added to an active center, the active center is moved towards the new chain end. A monomer can react with a reactive center only, no reaction occurs between a monomer and another monomer or any different-sized species.

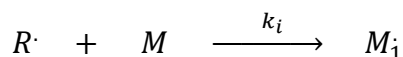
## 1.3 Free Radical Polymerization

The following part focuses on the free radical polymerization which is subcategory of the chain-growth polymerization.

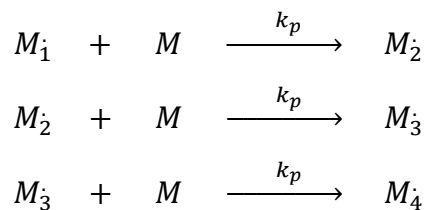
Radical chain polymerization consists of a sequence of three steps – (i) initiation, (ii) propagation, and (iii) termination. Two reactions are involved in the initiation step. The first reaction produces free radicals, usually by the homolytic scission of the initiator  $I$  to free radicals  $R\cdot$  with  $k_d$  as the dissociation rate coefficient:



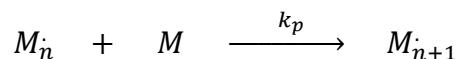
The free radical  $R\cdot$  arising from initiator cleavage is called the *primary radical* or the *initiator radical*. This is added to a monomer molecule  $M$  during the second reaction of the initiation step and forms a monomer radical  $M_1$ :



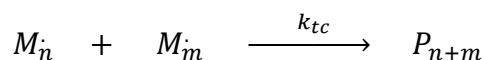
Above,  $M_1$  represents the chain-initiating radical (monomer radical) and  $k_i$  the rate coefficient for this initiation reaction. Propagation reactions start upon the addition of a monomer molecule to  $M_1$  and proceed via the successive addition of monomer molecules as represented below:



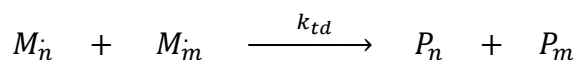
etc., and the propagation step can be generalized as shown below:



where  $k_p$  stands for the propagation rate coefficient and  $M_n$  is the radical chain having  $n$  monomeric units. Most monomers have a propagation rate coefficient between  $10^2$  and  $10^4$  L mol<sup>-1</sup> s<sup>-1</sup> (Beuermann et al., 1997; Buback et al., 1995) or even above (Beuermann et al., 1996), which makes free radical polymerization much faster than step-growth polymerization. The growing radical chains terminate after a certain time of polymerization. Bimolecular radical-radical termination reactions stop the growth of the concerned radical species, either by *combination (coupling)* or by *disproportionation*. Larger dead polymer chains are formed upon combination reaction as illustrated below. Dead polymers are no longer capable of growing to larger chains.



with  $k_{tc}$  as the rate coefficient for termination by combination and  $P_{n+m}$  as the dead polymer chain of length  $n+m$ . The probability of termination by disproportionation is less than the combination reaction (Odian, 2004). A hydrogen radical being *beta* to one radical center is transferred to the other radical center so that two polymer molecules, one being saturated and one unsaturated, are formed:



## Initiation

Thermal, photochemical, and redox methods can be applied to generate free radicals. No matter which technique is used, an initiator system has to be readily available, stable under ambient or refrigerated conditions, and possess a practical rate of radical generation at temperatures ideally below 150 °C.

In photoinitiated polymerization, radicals are generated by ultraviolet (UV) or visible light irradiation. Either some compound in the system undergoes excitation by absorbing radiation and subsequently decomposing into radicals (Norrish type I), or the excited species interacts with a second compound for radical formation (Norrish type II). The former method (Norrish type I) is used throughout this doctoral thesis by working with photoinitiators capable of forming radical species upon absorption.

### Photoinitiated Free Radical Polymerization

During this PhD project, a crosslinker (multifunctional) monomer was most often employed during photopolymerization. Methyl methacrylate (MMA) was never used as the sole monomer to produce PMMA. The short process residence time does not allow MMA to polymerize to PMMA completely. Nevertheless, the following discussion on photoinitiated polymerization is for simplicity illustrated for the polymerization of MMA.

The ongoing reactions in photoinitiated free radical polymerization do not differ from thermally initiated free radical polymerization except in the initiation step. Once an initiator molecule is decomposed to its radical fragments, the subsequent reactions proceed in the identical manner. The discussion of this sub-chapter is exemplarily shown on the photoinitiated free radical polymerization of MMA with Irgacure 907<sup>®</sup> employed as the photoinitiator.

Figure 1 represents the molecular structures of the photoinitiator Irgacure 907 and the monomer methyl methacrylate (MMA).

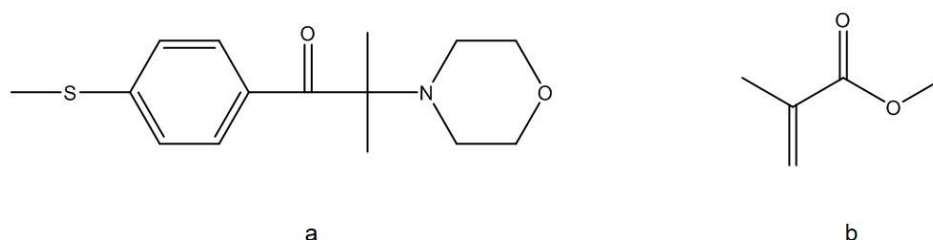


Figure 1 Chemical structures of (a) the photoinitiator Irgacure 907<sup>®</sup> and (b) the monomer methyl methacrylate (MMA).

Upon UV irradiation, Irgacure 907 decomposes into its radical fragments which are called primary radicals:

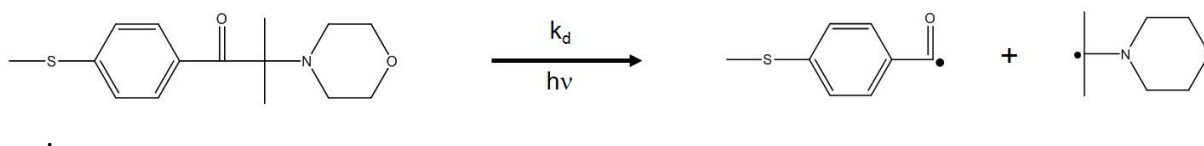


Figure 2 Decomposition reaction of Irgacure 907 by UV radiation upon homolytic bond dissociation into two primary radical fragments.

The generated primary radicals are capable of reacting with the carbon-carbon double bonds of the monomer molecules to initiate chain growth. The next figure shows the addition of one of the primary radical fragments to an MMA molecule:

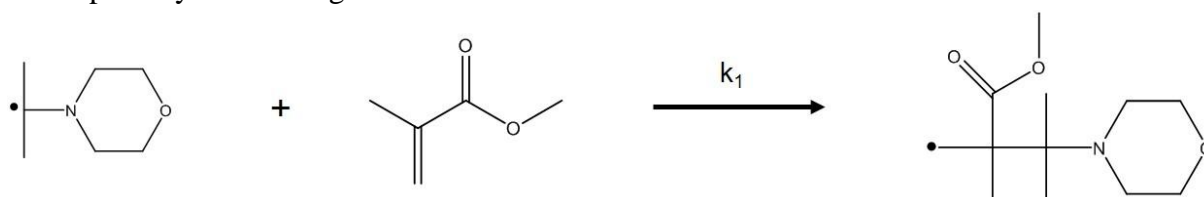


Figure 3 Initiation reaction of a primary radical fragment with MMA.

As mentioned earlier, the reaction above constitutes the second step of the initiation reactions. The reaction coefficient of this reaction where the first MMA unit is added to a primary radical is denoted as  $k_1$ . Similarly, the second primary radical fragment originating from photoinitiator cleavage as well also reacts with a monomer molecule. For simplicity, the reaction rate coefficient of this reaction, as represented below, can be assumed as  $k_1$  too. In reality, however, they can differ to some orders of magnitude (Lalevee et al., 2006).

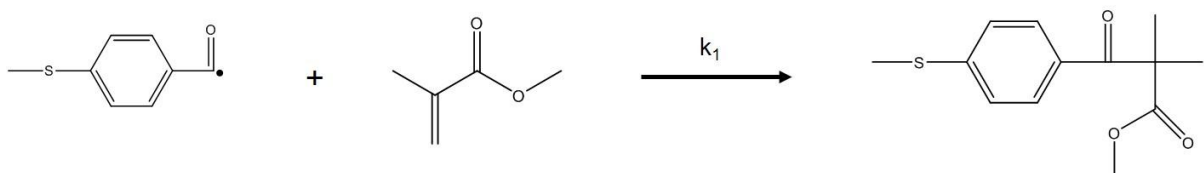


Figure 4 Reaction of the other primary radical fragment with MMA.

The radical chains consisting of one monomeric unit each can grow to larger polymer chains via further addition reactions of monomer molecules. In the following figure, one more MMA molecule adds to one of the growing chains where  $k_{p,2}$  denotes the propagation rate coefficient of the reaction in which the second MMA molecule is added to the radical molecule having one monomeric unit:

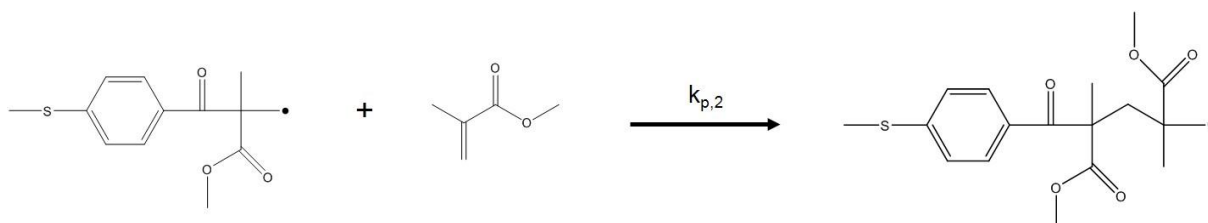


Figure 5 First propagation step.

Propagation reactions proceed sequentially via the addition of single monomeric units. The addition of a third monomer is illustrated below:

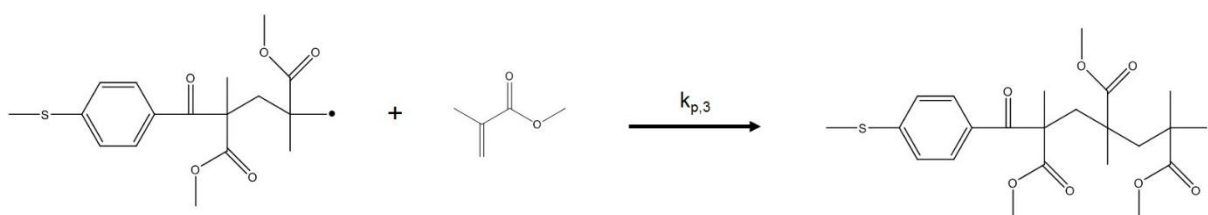


Figure 6 Propagation reaction via the addition of the third monomer to the growing chain.

The propagation rate coefficient for the reaction where 3<sup>rd</sup> monomer is added onto a chain is  $k_{p,3}$ . Since the propagation rate coefficients of each propagation step are nearly equal to each other, a single propagation rate coefficient  $k_p$  can be used for each chain growth step:

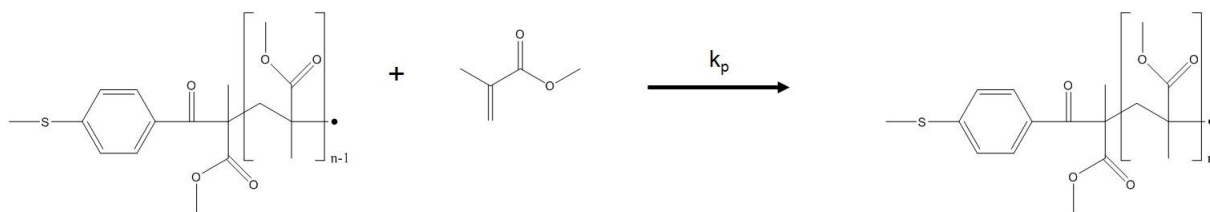


Figure 7 Generalized propagation reaction.

Each radical polymer chain can grow until it terminates, which can take place by termination reaction with another radical chain, by chain transfer reaction resulting in termination of this chain but formation in another radical molecule usually being not as reactive as the terminated chain, or by combination with a primary radical. The last one is rather improbable since typical initiator concentrations are low in polymerization systems. The probability for chain transfer is also not much if no chain transfer agents are present in the mixture. Therefore, the most probable case for a radical polymer chain termination is the classical termination reaction between two radical chains. This most often occurs by combination where the corresponding radicals combine to form a larger dead polymer chain. The next figure illustrates the combination reaction between radical polymer chains consisting of 3 and 4 monomeric units:

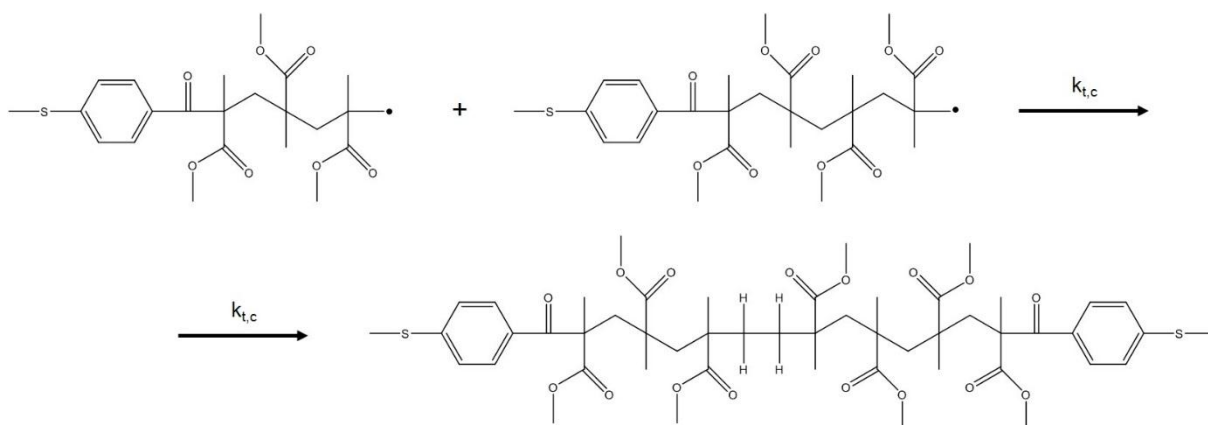


Figure 8 Termination by combination between two radical polymer chains to form a dead polymer chain.

Whether the radical chain ends originating from the photoinitiator molecules are the same at the ends of a dead chain is a matter of statistics. In a real polymerization system, both cases will appear. Since dead polymer chains are usually thousands of grams per mole in molecular weight, chain end molecules do not have an impact on the properties of the final polymer product. Apart from combination, termination can occur by disproportionation as well. Two polymer molecules will be formed during this reaction, hence leading to lower molecular weights of the polymer. One of the chains will be saturated and the other one unsaturated due to hydrogen atom transfer from one radical molecule to the second one. Termination by disproportionation is usually less probable compared to combination.

Initiation, propagation, and termination occur sequentially. A fourth kind of reaction, chain transfer, can result in termination of a growing radical chain too. Chain transfer can occur to chain transfer agents, to monomer, to polymer, or to solvent. In chain transfer agents, at least one weak chemical bond is present which is responsible for chain transfer reactions. Upon the transfer of e.g. a hydrogen atom to a radical species, the radical reactive center is transferred from the growing polymer chain. This results in termination of this chain but forms another radical species, mostly less active than the previously growing chain. Chain transfer agents can be employed specifically for branching.

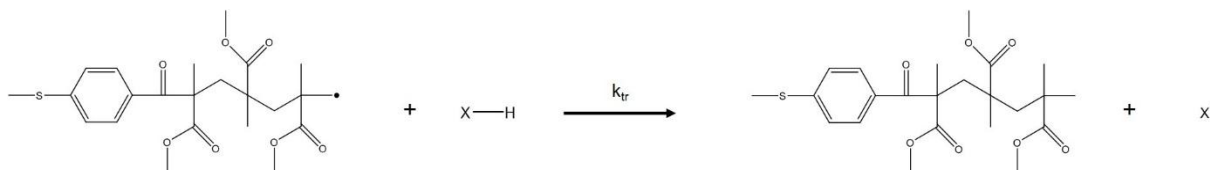


Figure 9 Chain transfer reaction via abstraction of a hydrogen atom from a chain transfer agent XH.

The addition of monomeric units to each growing polymer chain usually continues until  $10^3$ - $10^6$  monomer units are covalently bonded within this chain.

#### 1.4 Rate of Photopolymerization

The rate expression for chain polymerization initiated by free radicals can be derived by assuming steady-state conditions where the change of radical concentration maintains zero as a result of the equality between the initiation rate and the termination rate.

The monomer in the reaction system disappears according to the following equation:

$$\frac{-d[M]}{dt} = R_i + R_p$$

with  $R_i$  and  $R_p$  as the rates of initiation and propagation, respectively. Since the concentration of a monomer is far higher than the free radical concentration in a reaction mixture, the expression can be simplified to

$$\frac{-d[M]}{dt} = R_p$$

Hence, the rate of polymerization can be regarded as the propagation rate which is the sum of a number of individual propagation steps:

$$R_p = k_p[M\cdot][M]$$

Above,  $[M\cdot]$  represents the total concentration of all radical chains which are of the size  $[M_1]$  and larger. This term can be eliminated by the mentioned steady-state assumption where the initiation rate equals the termination rate. Bimolecular termination mechanism is assumed so that termination occurs between 2 chain radicals of any size:

$$R_i = R_t = 2k_t[M\cdot]^2$$

Transformation of the equation above to

$$[M\cdot] = \left(\frac{R_i}{2k_t}\right)^{1/2}$$

and substituting into the propagation rate expression containing the sum of radical chains results in the following polymerization rate expression:

$$R_p = k_p[M] \left(\frac{R_i}{2k_t}\right)^{1/2}$$

The initiation rate expression depends on the type of initiation. In the case of photoinitiation, the rate expression can be represented as

$$R_i = 2\phi I_a$$

where  $\phi$  is the quantum yield for initiation (fraction of the radicals produced in the homolysis reaction that initiated polymer chains) and  $I_a$  is the volumetric intensity of absorbed irradiation in moles (*Einsteins* in photochemistry) of light quanta per liter-second. The factor of 2 indicates that two radical species are produced upon the photolysis of a photoinitiator molecule. Then the rate expression for polymerization becomes:

$$R_p = k_p[M] \left(\frac{\phi I_a}{k_t}\right)^{1/2}$$

The absorbed irradiation  $I_a$  can be expressed by means of further parameters with the help of the Beer-Lambert law:

$$I'_a = I_0 - I_0 e^{-\alpha[PI]d}$$

where  $I'_a$  is the surface area absorbed intensity of radiation,  $\alpha$  the absorption coefficient of the photoinitiator  $PI$ ,  $d$  the distance for radiation absorption, and  $I_0$  the incident radiation intensity.

## 1.5 Photopolymerization of Multifunctional Monomers

Apart from the steady-state assumption which actually does not suit the aerosol-photopolymerization experiments possessing an average aerosol residence time of about 1 min in this work, the aforementioned rate expressions are not powerful enough for describing the photopolymerization kinetics of multifunctional monomers which is a highly challenging task.

Crosslinker (multifunctional) monomers such as multiacrylates and multimethacrylates display kinetic phenomena that differ from the polymerization of monofunctional monomers. In contrast to linear polymerization, the existence of more than one carbon-carbon double bond in a molecule results in a crosslinked, three-dimensional molecular network. First, one of the double bonds reacts with a growing radical polymer chain. Reactions proceed afterwards either via further monomer addition, via the attack on the pendant double bond by an intramolecular reaction, or via intermolecular reaction with the double bond of another chain. Intramolecular reactions can cause extensive cyclization and formation of microgels

which are compact structures (Andrzejewska, 2001). The absence of cyclization can result in a higher degree of crosslinking when crosslinker monomers are copolymerized with monofunctional monomers (Elliott and Bowman, 2001). Microgelation delays the gel point, leading to many unreacted pendant double bonds entrapped in the microgel regions. These microgels also cause heterogeneities within the built network, which becomes glassy and prevents the attainment of a maximum conversion beyond which no significant double bond conversion occurs due to the viscous, crosslinked environment upon vitrification (Andrzejewska, 2001). Radicals can be entrapped in linear systems and cause heterogeneity as well (Zhu et al., 1990), but it may become pronounced in radiation curing as functions of crosslinking density and initiation rate (Anseth et al., 1996). These entrapped radicals can remain present in the crosslinked polymer for months or even years (Bowman and Kloxin, 2008).

Rapid formation of a three-dimensional network restricts the mobility of chains, especially of the larger ones which are supposed to terminate each other. Therefore, center-of-mass diffusion reduces drastically, and polymer radicals mainly approach each other via segmental diffusion or by propagation. Nevertheless, further crosslinking also limits segmental diffusion and reaction diffusion becomes dominant for termination (Andrzejewska, 2001) and the overall kinetics gets diffusion-controlled resulting in network formation which depends on monomer conversion (Lovell et al., 2001). Diffusion limitations reduce the rate coefficient of termination dramatically, which leads to the phenomenon called autoacceleration (also called gel effect or Trommsdorf-Norrish effect) (Andrzejewska, 2001). Apart from that, the polymerizing medium usually does not have enough time for volume relaxation as crosslinking reactions proceed due to the very rapid chemical reaction rates. This results in a density difference between monomer and the formed polymer and is overcome during a certain time period after the polymerization has taken place. However, the formation of this excess volume allows for further reactions, increasing the overall carbon-carbon double bond conversion upon the addition reaction of rest monomer molecules (Anseth et al., 1995).

For aerosol-photopolymerization experiments in this thesis, crosslinked polymeric nanoparticles were prepared most often, either via the polymerization of a multifunctional monomer only or in the presence with a monofunctional monomer. Depending on the monomer propagation rate coefficient, some monofunctional monomers were also polymerized without a crosslinker within the short average aerosol residence time of about 1 min.

Various published work can be found on the experimental investigations on radiation curing (Decker, 1992; Decker and Moussa, 1990; Johnson et al., 2007; Li et al., 2006; Scherzer and Decker, 1999; Tryson and Shultz, 1979; Ye et al., 2011) and a number of models have been proposed to overcome the challenges arising during multivinyl free radical photopolymerization (radiation curing) and accurately predict the polymerization kinetics (Lovestead et al., 2002; Lovestead et al., 2005; Lovestead et al., 2003)

## **1.6 Aerosol Generation Techniques**

Although classical wet chemistry or lithographic methods are traditionally most often employed for particle generation, aerosol-based routes represent alternative techniques upon

the advancement of aerosol technology. The main drawbacks of liquid methods are the batch processing routes and the incorporation of impurities such as surfactants which contaminate the product. In contrast, aerosols represent a platform for the preparation of highly pure nanoparticles via continuous processes. Nanostructured materials of well-defined morphology and chemical composition can be obtained by aerosol routes (Biskos et al., 2008).

There are two main ways for the generation of aerosol nanoparticles. The first one is the atomization (spraying) of a solution of specific composition to form droplets which become solid particles via crystallization upon subsequent evaporation of the solvent (Biskos et al., 2008) or via photopolymerization (Akguen et al., 2013). The second strategy for aerosol nanoparticle manufacturing is the gas-to-particle conversion via nucleation and growth by condensation and coagulation controlled via saturation degree (Schenkel and Schaber, 1995). Solutions can be atomized either by mechanical methods such as nebulization or by the application of an electrostatic potential between the solution and a counter electrode such as electrohydrodynamic atomization (electrospraying). The methods involved for the gas-to-particle synthesis are furnace, flame, plasma, or laser reactors, glowing wires (Biskos et al., 2008) and spark discharges (Seipenbusch et al., 2003).

### **1.7 Atomization of Liquid Solutions**

This part deals with the atomization of solutions which is also called spraying. Different atomizers can be employed depending on the forces applied to break up the liquid solution into small gas-carried droplets. The most common methods are pneumatic, ultrasonic, and electrospray atomization for nanoparticle preparation. In contrast, methods such as spinning-disk atomizers produce larger particles in lower concentrations.

In ultrasonic atomization, the air-liquid interface is vibrated for droplet formation. Mechanical energy is applied from a piezoelectric crystal to the system, agitating the solution surface and creating capillary waves which break up to micron-sized droplets. Air stream passing over the solution takes the droplets for the formation of the droplet aerosol.

In electrohydrodynamic atomization, monodisperse droplets can be generated. Control of the liquid flow and the applied electrostatic potential between the solution and the counter electrode enable the production of droplets within a narrow size range having mean diameters from nanometers up to several micrometers.

In pneumatic atomization, pressurized gas is required which is introduced via an orifice, expanding perpendicularly to the end of a tube connected to the liquid reservoir. The low pressure at the tube end draws the liquid from the reservoir to the gas stream as a result of the Bernoulli effect. High forces at the gas-liquid interface break up the solution into small droplets which become gas-carried afterwards. The produced droplet aerosol is directed to an impactor plate for the separation of coarse droplets from the main aerosol stream (Collision-type atomizers). The isolated, coarse droplets can either be directed back to the reservoir or break up into smaller droplets and exit the atomizer with the aerosol stream (Biskos et al., 2008). Pneumatic atomization was realized throughout this thesis.

In their aerosol-photopolymerization setup, Esen and Schweiger (Esen and Schweiger, 1996) employed a vibrating-orifice aerosol generator (Berglund and Liu, 1973) and Gao et al. (Gao et al., 2007) utilized a modified version of it. Such aerosol generators fall within the category of ultrasonic atomization where monodisperse droplet aerosols with average

geometric standard deviation of almost 1 can be generated by the uniform break-up of liquid jets. Although a broad size of the dispersed phase between 1 and 50  $\mu\text{m}$  diameter can be obtained, a major drawback of these employed aerosol generators is the limiting droplet concentrations of only up to 500 droplets  $\text{cm}^{-3}$ . This low value limits its industrial use.

## 1.8 Aerosol-Photopolymerization

Once the aerosol with monomer droplets is produced, it is passed through the photoreactor where the gas-carried monomer droplets become gas-carried polymer particles. Nitrogen is chosen as the carrier gas due to free radical polymerization reactions which would be inhibited by oxygen.

As the photoinitiator, Irgacure 907<sup>®</sup> was used throughout this thesis except for some experiments where other photoinitiators were tested for comparison. Irgacure 907 possesses a high molar extinction coefficient  $\epsilon$  of 16000  $\text{L mol}^{-1} \text{cm}^{-1}$  at the emission wavelength of 313 nm which is comparable to 308 or 312 nm. This value is e.g. 6500  $\text{L mol}^{-1} \text{cm}^{-1}$  for Irgacure 819 or 194  $\text{L mol}^{-1} \text{cm}^{-1}$  for Irgacure 651 (Scherzer and Decker, 1999). As the multifunctional monomer, 1,6-hexanediol diacrylate (HDDA) was used most often, the monofunctional monomers employed mostly were methyl methacrylate (MMA) and butyl acrylate (BA).

As UV sources, an excimer irradiation source and UV fluorescent tubes were employed. The former is a quasi-monochromatic irradiation source (Kogelschatz, 1990). Such UV sources are based on excited rare gas dimers such as  $\text{Ar}_2^*$  (126 nm),  $\text{Kr}_2^*$  (146 nm),  $\text{Xe}_2^*$  (172 nm),  $\text{F}_2^*$  (157 nm) or their chlorides, fluorides and bromides such as  $\text{ArCl}^*$  (175 nm),  $\text{KrCl}^*$  (222 nm),  $\text{XeCl}^*$  (308 nm),  $\text{ArF}^*$  (193 nm),  $\text{KrF}^*$  (248 nm),  $\text{XeF}^*$  (351 nm),  $\text{XeBr}^*$  (282 nm). Depending upon the choice, emission can be realized between wavelengths of 120 and 360 nm. A distinct advantage of this type of UV sources is their flexibility in geometry and operation conditions, e.g. their emission intensity can be tuned.  $\text{XeCl}^*$  excimer source was utilized during this thesis for irradiation at 308 nm wavelength. In comparison to excimer sources, UV fluorescent tubes emit polychromatic radiation (270-360 nm) but possess an emission maximum at 312 nm being close to the value of the employed  $\text{XeCl}^*$  excimer source so that the same photoinitiator, Irgacure 907<sup>®</sup>, was used for both kind of photoreactors.

## 1.9 Experimental Setup of Aerosol-Photopolymerization

The process of aerosol-photopolymerization consists of two main devices, an aerosol generator (atomizer) and a photoreactor. The aerosol generator sprays the monomer formulation with the help of nitrogen gas to produce a droplet aerosol with nitrogen as the continuous, carrier phase and the monomer formulation droplets as the dispersed, carried phase. In the simplest case, a photoinitiator (PI) is dissolved in a liquid monomer (M). More complex formulations can be prepared by mixing or suspending additional substances such as solvents, solutes, and inorganic nanoparticles, or by preparing a comonomer system. The produced droplet aerosol is then passed through the photoreactor where nitrogen-carried monomer droplets are photopolymerized to nitrogen-carried polymeric particles. The particle aerosol leaving the photoreactor is either passed through a liquid for obtaining a suspension or through a filter membrane for dry particle collection. The process flow is depicted in the Figure 10:



Figure 10 Schematic process flow of aerosol-photopolymerization. M: monomer, PI: photoinitiator.

An aerosol generator utilizing a two-component nozzle was used throughout this thesis (ATM 220, Topas). Such nozzles produce polydisperse droplets, but mainly in the submicron range and with a concentration as high as  $10^7$ - $10^8$   $\text{cm}^{-3}$ . The most critical part of this aerosol generator is its two-component (two-stream) nozzle based on the injection principle, producing a highly concentrated polydisperse droplet aerosol. This aerosol generator (atomizer) is so designed that the formed droplet aerosol is directed towards the glass wall of the vessel, and the wall acts as a baffle for separating the coarse spray droplets from the aerosol and keeps the droplet size mainly below  $1 \mu\text{m}$ . The smaller droplets follow the nitrogen stream while the larger ones flow down the vessel wall back to the formulation. The volumetric aerosol flow rate can be changed between 1 and  $5 \text{ L min}^{-1}$  s by adjusting the nozzle inlet pressure between 1 and 6 bars.

The produced monomer droplet aerosol is directed to the photoreactor possessing an average aerosol residence time of about 1 min or shorter depending on the aerosol volumetric flow rate or photoreactor length. One of the photoreactors is equipped with a XeCl\* excimer irradiation source emitting quasi-monochromatic at 308 nm (width of half height  $\approx 3$  nm) and consists of concentric, cylindrical quartz glass tubes. The UV irradiation source is placed at the center where nitrogen is circulated for temperature control. The UV source is enclosed by the aerosol zone, which is surrounded by the most outer space where water is circulated for temperature control. A cross-section of the excimer photoreactor is illustrated in Figure 11(a):

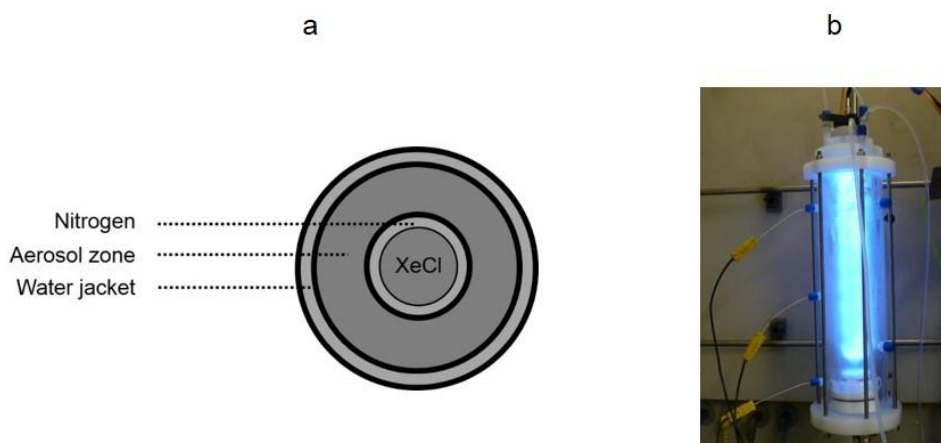


Figure 11 XeCl\* excimer photoreactor: (a) schematic cross-section view, (b) photo.

Effective irradiation length of this photoreactor is 32 cm and its radiant exitance  $10 \text{ mW cm}^{-2}$ . The average aerosol residence time can be varied between 15 and 60 s by applying different pressures at the nozzle inlet of the aerosol generator.

A second photoreactor consisting of a quartz glass tube and UV fluorescent tubes is employed as well. The quartz tube can be surrounded by 1 to 4 of such irradiation sources consisting of 2 to 3 tubes each. UV fluorescent tubes emit polychromatic radiation between

270 and 360 nm, but possess an emission maximum at 312 nm being comparable to the excimer source emitting at 308 nm. 6 UV fluorescent tubes being 41 cm long correspond approximately to  $5 \text{ mW cm}^{-2}$  irradiance. The quartz glass tube possessing an average aerosol residence time of about 1 min is 44 cm long and has an inner diameter of 52 mm. The aerosol residence time in this photoreactor can be changed either by nozzle inlet pressure or by using a shorter quartz glass tube. Figure 12 illustrates the setup for this photoreactor.



Figure 12 Photoreactor equipped with UV fluorescent tubes

Once polymeric particles are formed, the particle aerosol leaving the photoreactor is passed through a gas-washing bottle or a filter membrane. The former is performed via particle transfer from the aerosol into liquid via the surface area of bubbles. Usually, water is chosen as the liquid. However, this method is not effective regarding particle collection efficiency since the smaller particles follow the gas stream out of the washing bottle. By employing the latter method, nearly all of the particles can be collected on a PTFE filter membrane having an average pore diameter of 50 nm. A drawback of this collection method is the clogging of membrane with experimental time. Therefore, particle collection method strongly depends on the performed experiment and on the subsequent characterization techniques for the generated particles.

### **1.10 Polymer Reaction Engineering**

Polymerization kinetics for aerosol-photopolymerization is simulated with Predici<sup>®</sup> to estimate the required time for the sufficient conversion of monomer double bonds during photoreactor passage. Predici<sup>®</sup> is a simulation package for the modeling and dynamic simulation of macromolecular processes by using the Galerkin h-p method. It can rigorously treat e.g. complete molecular weight distributions in arbitrary polymerization processes, chain length-dependent reactions, copolymerization reactions, and heterogeneous systems. See Wulkow (Wulkow, 2008) for the mathematical details of this software.

A monofunctional monomer was chosen for the simulations, and the chain transfer step was neglected. The simulations were performed for a batch process lasting for 60 s of polymerization time. This batch reactor should represent a monomer droplet (of 150 nm

diameter) at isothermal conditions of 50 °C. Although the system in whole is heterogeneous, the polymerization of a single monomer droplet constitutes bulk polymerization. The kinetic coefficients were so chosen that the monomer is butyl acrylate, representing a “fast” propagating monomer. The initial species considered in the formulation were the dissolved photoinitiator and the monomer representing the main, continuous phase.

The termination rate coefficient of butyl acrylate is described dependent on monomer conversion according to the trend given by Buback (Buback, 1990). However, as the initial termination rate coefficient, a higher value of  $2 \times 10^8 \text{ L mol}^{-1} \text{ s}^{-1}$  is selected (Beuermann et al., 1996). Upon calculation of the ratio of initial values, a factor has been determined for multiplying the lower values given by Buback with this factor. Both combination and disproportionation rate coefficients are described in this way and are identical to each other. The initial propagation rate coefficient of butyl acrylate at 50 °C is selected to be  $2 \times 10^4 \text{ L mol}^{-1} \text{ s}^{-1}$  ( $20700 \text{ L mol}^{-1} \text{ s}^{-1}$  in Beuermann et al.) and a linear decrease with the conversion of monomer until becoming zero at complete conversion was assumed. The progress of these two coefficients is described as follows:

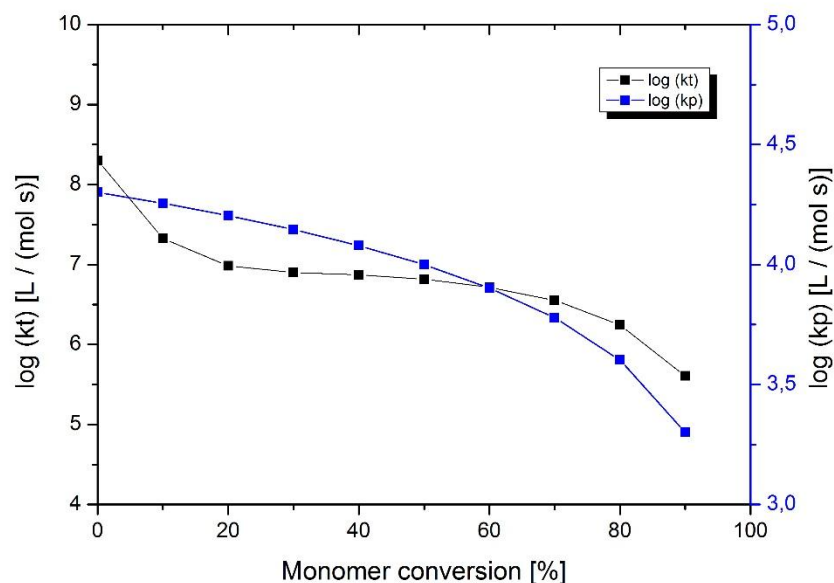


Figure 13 Termination and propagation rate coefficients as functions of butyl acrylate conversion.

Implementing the termination and propagation rate coefficients along with the initiation rate coefficient of  $0.03 \text{ s}^{-1}$  and an initiation efficiency of 1 (100 %), “standard” simulations have been performed. The obtained conversion profiles of the monomer butyl acrylate and the photoinitiator Irgacure 907 are illustrated below:

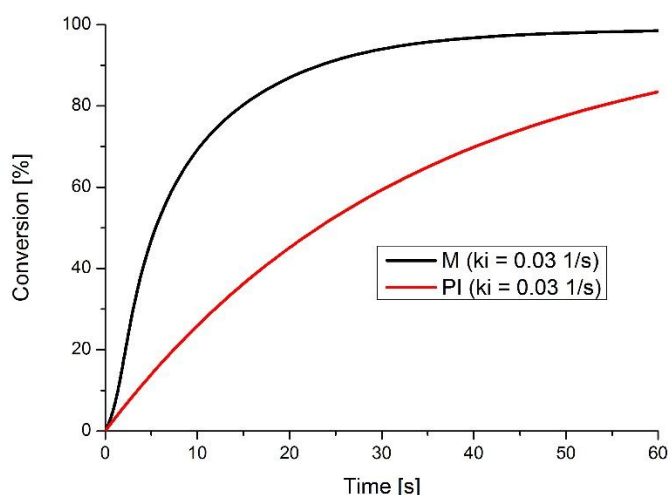


Figure 14 Monomer (M) and photoinitiator (PI) conversion profiles for butyl acrylate polymerization under “standard” conditions.

According to Figure 14, butyl acrylate can be converted to polymer very fast, practically within 40 s. In contrast, the photoinitiator dissociates at a rather constant rate. It dissociated more than 80 % after 1 min. This “standard” simulation resulted in the following dead polymer chain distributions:

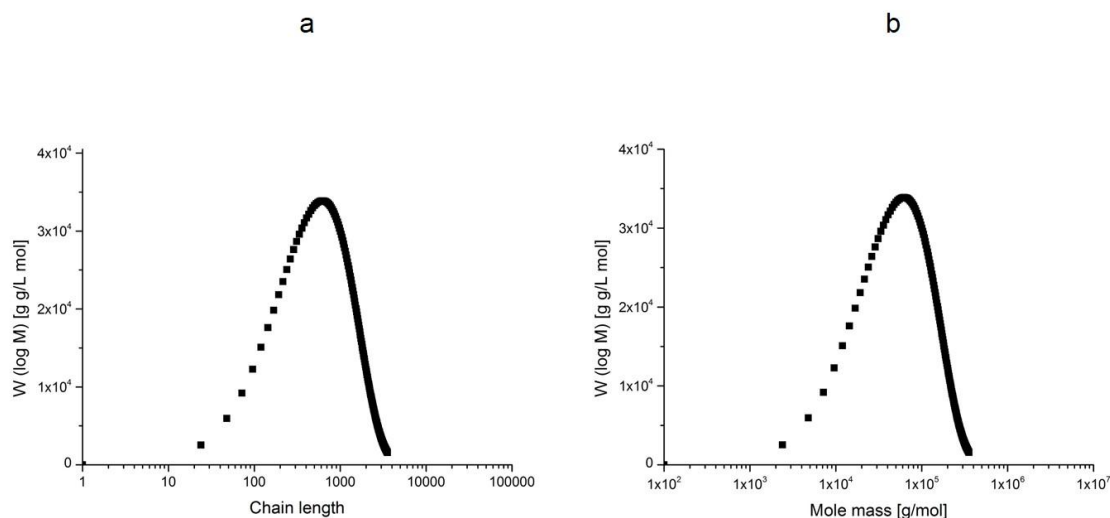


Figure 15 Polymer chain distributions: (a) chain length distribution, and (b) mole mass distribution.

The obtained polymer chains showed a broad distribution with a polydispersity of about 3.7.

For the illustration of the effect of initiation rate on the overall polymerization rate, the initiation rate coefficient of  $0.03 \text{ s}^{-1}$  was varied between two limits,  $0.001$  and  $0.5 \text{ s}^{-1}$ . The obtained photoinitiator (Irgacure 907) and monomer (butyl acrylate) conversion profiles are shown below:

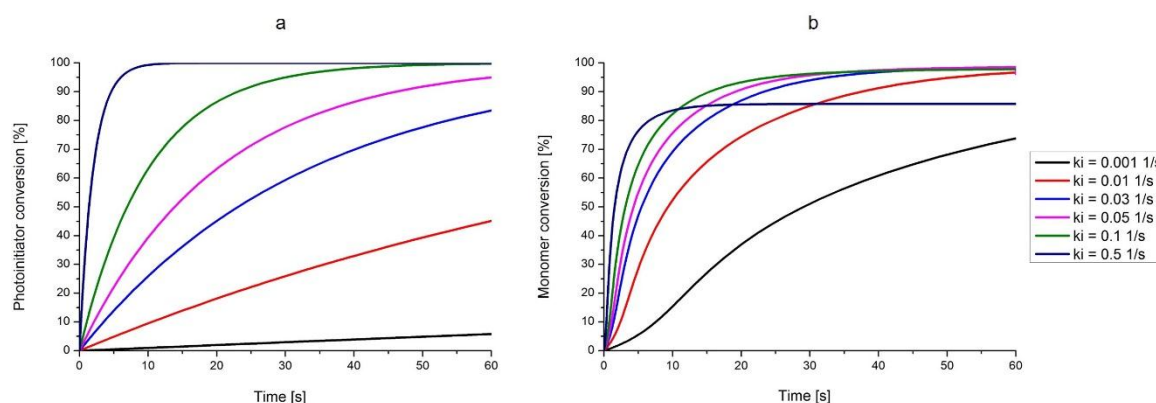


Figure 16 Conversion profiles of (a) photoinitiator and (b) monomer for different initiation rate coefficients.

The profiles for photoinitiator conversion in Figure 16(a) show that an irradiation time of 60 s results in total conversion if the initiation rate coefficient is higher than  $0.05 \text{ s}^{-1}$ . The monomer, in contrast, reaches practically total conversion even with an initiation rate coefficient of  $0.01 \text{ s}^{-1}$ . This is due to the “fast-propagating” nature of butyl acrylate. Regardless of the initiation rate, this monomer can polymerize within a short time. Whether fast or slow initiation takes place reflects itself on the final molecular weight distribution of the obtained poly(butyl acrylate) (PBA) as shown in the next figure:

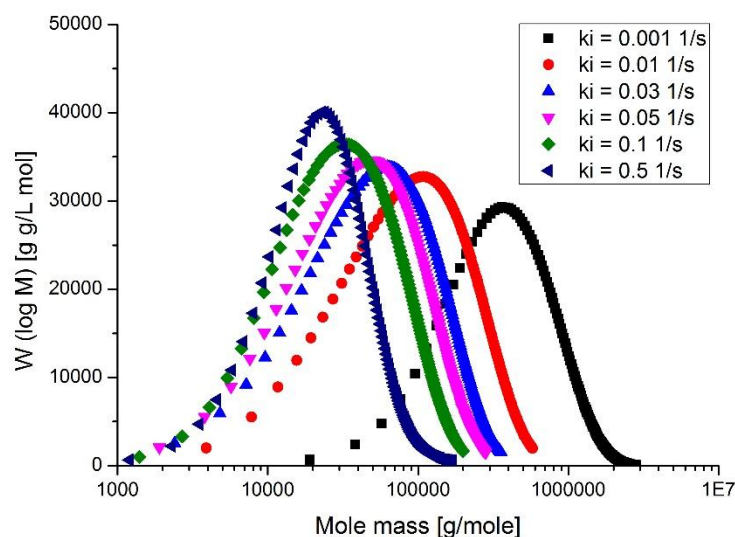


Figure 17 Polymer chain distribution as function of the initiation rate coefficient.

As expected, a smaller rate coefficient for initiation ( $0.01 \text{ s}^{-1}$  instead of  $0.05 \text{ s}^{-1}$ ) leads to a lower number of radicals generated per unit of time which results in longer polymer chains for complete conversion of butyl acrylate. However, even fast reacting monomers have their limits regarding complete conversion during certain time periods. If the initiation rate coefficient is considerably lower than  $0.01 \text{ s}^{-1}$ , e.g.  $0.001 \text{ s}^{-1}$ , less than 80 % of butyl acrylate will be polymerized after 1 min. Performing very high initiation rates via high initiation rate

coefficients such as  $0.5 \text{ s}^{-1}$  does not result in a complete conversion of the monomer as well. Such initiation rates can form radicals extremely fast, but only short dead chains will be formed so that no more photoinitiator is present for radical formation, leading to the presence of unreacted, rest monomer molecules which corresponds to lower overall monomer conversion. Therefore, a good agreement between the initiation and propagation rates is decisive and is a matter of optimization. Since not only the initiator concentration but also the irradiance of the UV source can be adjusted for obtaining the favored initiation rate, photoinitiated polymerization exhibits great power and potential for polymerization optimization.

Taking the “standard” value of  $0.03 \text{ s}^{-1}$  as the initiation rate coefficient, the initial propagation rate coefficient of the polymerization system was varied. Again a linear decrease with monomer conversion was assumed:

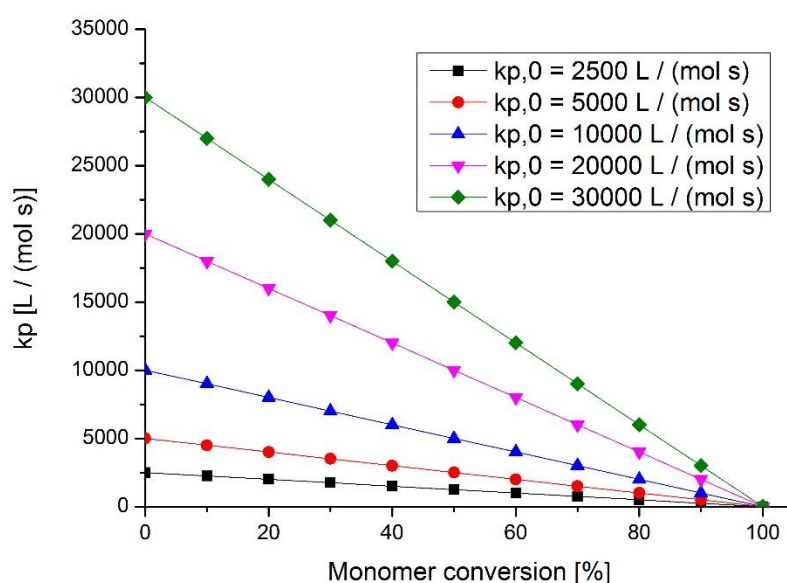


Figure 18 Selected initial propagation rate coefficients as function of monomer conversion.

Implementing the propagation rate coefficient profiles of Figure 18 resulted in monomer conversion profiles presented in Figure 19, illustrating the dependence of the monomer conversion profiles on the propagation rate coefficient.

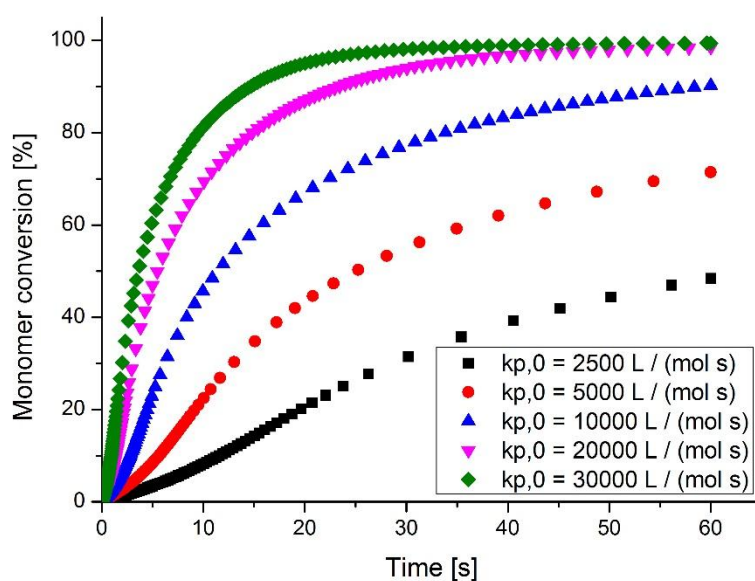


Figure 19 Monomer conversion profiles for different initial propagation rate coefficients.

In Figure 19, the curve represented by  $k_{p,0} = 2 \times 10^4 \text{ L mol}^{-1} \text{ s}^{-1}$  constitutes the “standard” monomer conversion profile as in Figure 16(b) with BA as the reference system, whereas the remaining curves are the simulations for faster or slower chain growth reactions. It is obvious that a minimum initial propagation rate coefficient of  $1 \times 10^4 \text{ L mol}^{-1} \text{ s}^{-1}$  is required for a monomer conversion of at least 80 % after 60 s of polymerization time. This example illustrates that not all kind of monofunctional monomer systems can be photopolymerized within a minute of aerosol residence time in the aerosol-photopolymerization setup with 1 min of irradiation time, but high optimization potential is hidden especially regarding the initiation step.

## 2. Research Proposal

Aerosol-photopolymerization was a research project within the broader research initiative IP3 JointLab, aiming at integrated processes for nanostructured functional materials. JointLab is incorporated in Karlsruhe at KIT with the support of BASF. IP3 stands for innovative products, intelligent particles, and integrated processes, highlighting the main foci of JointLab as integration of the know-hows of the involved research groups for the shared development of functional materials. Both organic and inorganic particles and their composites were of interest by either liquid or gas processing routes. Within this perspective, aerosol-photopolymerization represented a gas phase route for the generation of polymeric nanoparticles – polymer nanoparticles and hybrid nanoparticles.

Polymeric particles attract various industrial and research fields including the emerging applications such as optics and photonics, nanomedicine, and functional smart coatings. They have most often been prepared by techniques based on the liquid phase such as suspension polymerization or emulsion polymerization. Especially emulsion polymerization has been gaining more attractiveness for radical polymerization due to its capability of producing quasi-monodisperse particles in a wide size range. Various sophisticated particles such as composites or non-spherical particles have readily been prepared by this technique. Upon the employment of the special kinds of emulsion polymerization – miniemulsion or microemulsion polymerization – nanoscale polymeric particles can be synthesized. These techniques have a major drawback of surfactant usage which decreases the polymer purity. In addition, liquid-based techniques mostly require intensive downstream process steps regarding cost and time. Free radical polymerization reactions are frequently started via the decomposition of thermal initiators. This requires elevated temperatures disallowing processing of thermally sensitive materials such as biomolecules.

Aerosol-photopolymerization represents an alternative, novel technique for the generation of polymeric particles. It combines an aerosol-based process with photoinitiated polymerization and possesses characteristic advantages. Aerosols are attractive for continuous processing leading to highly pure materials and eliminate downstream steps. The advantages of photoinitiated polymerization are also numerous. Photopolymerization is capable of instantaneously starting the chain reactions and facilitates the treatment of thermally sensitive materials via operation at ambient temperature. Preventing higher temperatures both minimizes monomer evaporation which would be quite challenging in thermally initiated systems and thermodynamically favors the exothermic chain reactions.

Published work about the preparation of polymer microspheres by UV-initiated radical polymerization in aerosols had been available prior to this PhD thesis. Insofar, apart from fundamentals, there was a lack of detailed, comprehensive understanding of the process limiting the generation of precisely defined particle structures. A deeper understanding of the physical and chemical phenomena underlying the aerosol-photopolymerization could open pathways either for existing polymeric particles with improved properties or even could lead to novel, complex particulate matter.

Disregarding its potential as an effective unit operation, aerosol-photopolymerization is also flexible in terms of integration with various process units. The continuous aerosol processing

route enables the arrangement of photopolymerization step with other unit operations in series, or in other words, in flight. Such an integrated process can reduce operational time and cost. Furthermore, the contribution of each single process step can yield particles possessing tailor-made properties at the end. Also the aforementioned advantages of the photochemical technology make aerosol-photopolymerization flexible and attractive for integrated processes.

Integrated, continuous processes combining particle generation, surface modification, and integration within the polymeric material represent a challenge for the preparation of functional hybrid particles. Cross-cutting methods are needed for specific requirements of size, composition, porosity, functionality, and morphology of particles. Therefore, IP3 JointLab was aiming at integrated, aerosol-based processes for such materials - incorporation of drugs into a polymer matrix, coating of drugs with a polymer film to obtain nanocapsules, and generation of organic carrier particles for a subsequent coating. All these phenomena had not been adopted by aerosol-photopolymerization yet and a fundamental, detailed knowledge was missing.

This PhD project about aerosol-photopolymerization should seek for a deeper understanding of the process to prepare particles with favored properties. First of all, a photoreactor had to be designed and built. This reactor then had to be employed for the generation of spherical polymer particles. In a next step, composite (hybrid) particles were to be prepared which should rely on the basic knowledge to be gained in the previous step by pure polymer particle synthesis. Further particulate structures could be tried to be generated by the variation of formulation and process parameters. Finally, all the gained knowledge on the aerosol-photopolymerization would contribute for the application of integrated, aerosol-based processes to prepare tailor-made particles. Aside from process integration, there is also the possibility of presenting aerosol-photopolymerization as a versatile single-step process for the generation of different particle structures, representing the perspectives of this process and PhD thesis.

### **3. Patents, Publications & Manuscripts**

#### **Patent Applications**

- Patent Application 1:  
Aerosol Photopolymerization  
US 20130079482 A1  
Ertan Akgün, Wolfgang Gerlinger, Michael Wörner
- Patent Application 2:  
Finely Divided Particles of Core-Shell Structure  
US 20140061026 A1  
Ertan Akgün, Stephanie Sigmund, Wolfgang Gerlinger, Bernd Sachweh, Gerhard Kasper, Michael Wörner

#### **Journal Articles and Manuscripts**

1. Perspectives of Aerosol-Photopolymerization: Nanoscale Polymer Particles  
Ertan Akgün, Jürgen Hubbuch, Michael Wörner  
Chemical Engineering Science, 101, 248 (2013)
2. Perspectives of Aerosol-Photopolymerization: Organic-inorganic Hybrid Nanoparticles  
Ertan Akgün, Jürgen Hubbuch, Michael Wörner  
Colloid and Polymer Science, 292, 1241 (2014)
3. Perspectives of Aerosol-Photopolymerization: Nanostructured Polymeric Particles  
Ertan Akgün, Jürgen Hubbuch, Michael Wörner  
Macromolecular Materials and Engineering, 299, 11, 1316, 2014

4. Defined Polymer Shells on Nanoparticles via a Continuous Aerosol-Based Process

Ertan Akgün, Stephanie Sigmund, Jörg Meyer, Jürgen Hubbuch, Michael Wörner,  
Gerhard Kasper

Nanoparticle Research, 16, 2533, 2014

5. Cationic Aerosol-Photopolymerization

Ertan Akgün, Alex Muntean, Jürgen Hubbuch, Marco Sangermano, Michael Wörner

Macromolecular Materials and Engineering, DOI: 10.1002/mame.201400211

---

Patent Application 1

# Aerosol Photopolymerization

Ertan Akgün, Wolfgang Gerlinger, Michael Wörner

---

## Abstract

The present invention relates to a process for producing nanoparticles comprising at least one polymer and/or copolymer by providing an aerosol comprising droplets of at least one monomer and at least one photoinitiator in a gas stream, irradiating this aerosol stream with light such that the monomers present polymerize, and removing the nanoparticles formed from the gas stream, to nanoparticles producible by this process and to the use of these inventive nanoparticles in optical, electronic, chemical or biotechnological systems, or for active ingredient administration.

US 20130079482 A1

---

Patent Application 2

# Finely Divided Particles of Core-Shell Structure

Ertan Akgün, Stephanie Sigmund, Wolfgang Gerlinger, Bernd Sachweh,  
Gerhard Kasper, Michael Wörner

---

## Abstract

The invention provides a process for producing finely divided particles of core-shell structure where the shell comprises at least one polymer, said process comprising the steps of: i. providing a first aerosol stream of droplets in a carrier gas stream wherein the droplets comprise at least one monomer and charging droplets of the first aerosol with electric charge; ii. providing a second aerosol stream of solid particles in a carrier gas stream and charging the solid particles of the aerosol with an electric charge opposite to the electric charge on the droplets of the first aerosol stream; iii. mixing the first aerosol stream with the second aerosol stream to form a mixed aerosol stream; iv. initiating a polymerization of the monomers by irradiating this mixed aerosol stream with electromagnetic radiation. The invention also provides the finely divided particles of core-shell structure which are obtainable by this process.

US 201400611026 A1

---

# **Perspectives of Aerosol-Photopolymerization: Nanoscale Polymer Particles**

**Ertan Akgün, Jürgen Hubbuch, Michael Wörner\***

---

*Process Engineering in Life Sciences, Karlsruhe Institute of Technology*

*\* Corresponding author: Michael Wörner ([michael.woerner@kit.edu](mailto:michael.woerner@kit.edu))*

Chemical Engineering Science, 101, 248 (2013)

The final publication is available on:

<http://www.sciencedirect.com/science/article/pii/S000925091300417X>

## **Abstract**

Photoinitiated polymerization is employed to produce submicron polymer particles in aerosols. By ultraviolet (UV) irradiation of the aerosol monomer solution droplets, produced with the help of an atomizer, polymerization is initiated by free radical generation. The aerosol process allows the production of surfactant-free polymer particles without any solvent required, while photochemistry results in instantaneous formation of free radicals by cleavage of excited photoinitiator molecules. Furthermore, the initiation can take place independent of temperature, which provides polymerization at ambient temperature. A continuous experimental setup with a flow-through photoreactor is developed, which is characterized by a sub-minute aerosol residence time. The experiments reveal that spherical nanopolymers can be formed as 1-to-1 copy from the monomer droplets.

**Keywords:** Nanoparticle; Polymers; Aerosol; Photochemistry; Particle formation; Polymerization

## 1. Introduction

Polymeric (nano)particles have increasingly been raising interest for a number of applications ranging from optics and photonics to nanomedicine. They are used, for example, in combination with inorganic nanofillers for transparent polymers [1, 2], or in life sciences as controlled drug release agents [3]. Different production methods are available to obtain polymer particles. Emulsion polymerization is one of the most often established techniques, where the use of surfactants is required and mostly thermally initiated polymerization is applied. These surfactants may be incorporated in the polymer structure and decrease the product purity [4]. After polymerization in wet methods, the particles might have to be separated by downstream processes like centrifugation or filtration, washed and dried under vacuum [5]. These process operations consume time and cost.

Polymers as functional materials can also be prepared by photochemical technologies. The use of photons for polymer preparation goes back to the beginning of the 20<sup>th</sup> century, when *Klatte* converted vinyl chloride into PVC by light-induced polymerization [6]. Photoinitiated dispersion polymerization was successfully applied in aqueous alcohol media to produce submicron polymer particles on a lab-scale [7]. As an alternative to liquid process routes, polymer particles can also be produced by processes based on aerosols. Aerosol techniques avoid the need of surfactants and downstream processes, permitting integrated processes. Different aerosol-based methods were employed so far. Nebulization-polymerization was performed for producing micrometer-sized polystyrene particles. After nebulization of the liquid monomer to monomer droplets, the droplets were brought into contact with initiator vapor [8]. Esen and Schweiger [9] combined the aerosol technique with photopolymerization to produce micrometer-sized polymer particles. A multiacrylate monomer mixture containing photoinitiator and binding agents was dissolved in a volatile solvent and dispersed using a vibrating-orifice aerosol generator with the help of nitrogen gas. The generated aerosol droplets were irradiated with black light fluorescent strip lamps (wavelength  $\approx 360$  nm) to produce highly monodisperse spherical polymer particles with diameters between 5 and 50  $\mu\text{m}$  and smooth surfaces. In a similar work, where the aerosol generator was a modified vibrating-orifice aerosol generator, monodisperse polymer microspheres with diameters between 5 to 100  $\mu\text{m}$  were generated by photopolymerization via UV irradiation as well [10]. A drawback of the use of a vibrating-orifice aerosol generator is the limited droplet generation rate, leading to low polymer particle concentrations. The photopolymerization kinetics of a multiacrylate monomer droplet being a few micrometers in diameter was investigated on-line with Raman spectroscopy, revealing that a time period of nearly 100 s is required for the complete polymerization [11]. A number of publications can be found on the photopolymerization kinetics of very fast crosslinking reactions, where polymerization is completed within a few seconds [12-21].

In this work, photoinitiated free radical polymerization of submicron monomer droplets for the generation of spherical polymer nanoparticles is presented. The particles were produced from monomer solution droplets consisting of liquid monomer and dissolved photoinitiator. The size of the polymer particles can be pre-adjusted by the diameter of the monomer droplets since the polymerization process is restricted to the volume of each monomer droplet. No surfactants and any additional solvent were used for the preparation of the monomer droplet

aerosol, leading to highly pure polymer particles. The employed aerosol generator produces high concentrations of monomer droplets and has the potential of up-scale. The subsequent photoreactor of this continuous experimental setup can be operated with a sub-minute average aerosol residence time. Such a short reaction time necessitated fast overall polymerization kinetics. This can be accomplished by different combinations of initiation and propagation rates. The initiation rate in photochemical systems can be adjusted by photoinitiator concentration, photon exitance, and photophysical properties of the photoinitiator. Photochemistry also permits a continuous aerosol process. Fast propagating monomers could be polymerized with and without a crosslinker, but monomers exhibiting a low propagation rate coefficient required the addition of a crosslinker or a comonomer to accelerate the overall polymerization rate. A quasi-monochromatic UV excimer irradiation source [22] allowed instantaneous generation of free radicals and avoided the need of higher reaction temperatures, which would be required for thermally initiated systems. Lower reaction temperatures favor thermodynamically the polymerization process and lead to less droplet evaporation rates as well. Aerosol-photopolymerization also offers the potential of producing multicomponent materials.

## **2. Experimental**

### 2.1. Chemicals and Materials

Methyl methacrylate (MMA, Sigma-Aldrich, 99 % purity) and butyl acrylate (BA, Sigma-Aldrich, 99 % purity) were employed as monomers. Irgacure 907 (Methyl-1[4-(methylthio)phenyl]-2-morpholinopropan-1-one, Sigma-Aldrich, 98 % purity) and 1,6-hexanediol diacrylate (HDDA, Alfa Aesar, 99 % purity) were chosen as the photoinitiator and crosslinker, respectively. All chemicals were used as received except for copolymerization experiments. Pre-packed columns (Sigma-Aldrich) were used for inhibitor removal.

### 2.2. Process

The continuous experimental setup consists of two main components, an aerosol generator and a flow-through photoreactor, as depicted in Figure 1(a). The monomer solution was prepared by dissolving the photoinitiator (PI) in the liquid monomer (M) without using any additional solvent. The monomer solution was sprayed with nitrogen gas in an atomizer to generate the droplet aerosol. This droplet aerosol was passed through the photoreactor, where free radicals are generated upon UV irradiation for the polymerization process. The cylindrical flow-through photoreactor with negative irradiation geometry is in-house constructed and consists of concentric HSQ 300 quartz glass tubes. The cross-section of this photoreactor is schematically presented in Figure 1(b). The custom-made XeCl excimer irradiation source (Radium Lampenwerk, Wipperfürth, Germany) is placed in the center and surrounded by the inner quartz glass tube. The annular gap in between is flushed with nitrogen as cooling gas. Photopolymerization reactions take place in the annular gap between the inner and outer quartz tubes. A water jacket serves for the temperature control in the outer zone. The outer envelope is made of Plexiglas.

The aerosol generator consists of a two-component nozzle. Depending on the nozzle inlet pressure of nitrogen, which can be varied between 1 and 6 bars, the average aerosol residence time in the photoreactor can be varied between 15 and 60 s. In contrast, the time scale of aerosol generation lies within milliseconds. Therefore, the process residence time can be regarded as that in the photoreactor.

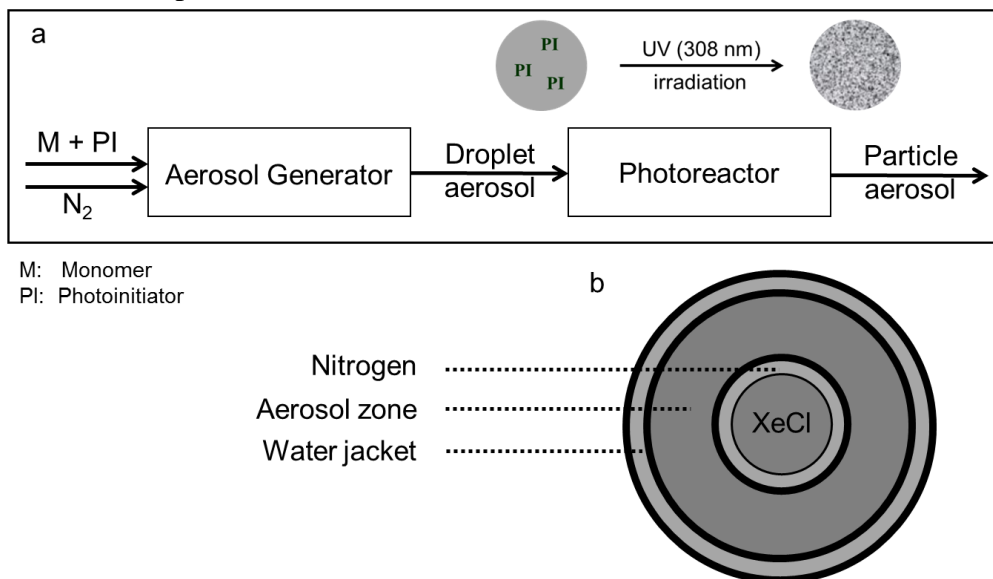


**Fig. 1.** (a) Scheme of the continuous experimental setup for aerosol-photopolymerization, (b) schematic cross-section view of the photoreactor.

The employed XeCl excimer irradiation source emits quasi-monochromatic at 308 nm (width of half height  $\approx 3$  nm) with a radiant exitance of  $10 \text{ mW/cm}^2$  at the envelope surface. The effective irradiation length of the photoreactor is 32 cm. Polymer particles leaving the photoreactor were collected either dry on a PTFE filter membrane with 50 nm average pore diameter or wet by transfer into water.

### 2.3. Particle characterization

For scanning electron microscopy images, Hitachi S-4500 and LEO 1530 were employed. The values of acceleration voltage can be found on the corresponding SEM images. A drop of the particle suspension was dropped onto a membrane (Whatman, Nucleopore Track-Etch Membrane, 200 nm pore width) or onto a silicium wafer. After drying, the particles were coated with a platinum-palladium mixture or platinum. Dry collected particles could be coated directly without the drying process. The coating thickness was 1-2 nm.

Fourier transform infrared spectrometry utilizing attenuated total reflectance (FTIR-ATR, Equinox 55, Bruker Optics) was employed for the determination of carbon-carbon double bond conversion of the monomer solution. The solution spectra were obtained by measuring a droplet of the corresponding monomer solution to be sprayed, and the polymer spectra after collecting the particles in the aerosol dry on a filter after aerosol-photopolymerization.

Scanning mobility particle sizer (SMPS consisting of electrostatic classifier 3080, differential mobility analyzer 3081, and condensation particle counter 3775, TSI Corp.) was used for the online characterization of droplet and particle size distributions in aerosols.

### 3. Results and Discussion

For the homopolymerization of methyl methacrylate, the monomer solution consisting of methyl methacrylate and photoinitiator did not result in successful photopolymerization. The aerosol residence time in the photoreactor was not long enough considering the low propagation rate coefficient of this monomer of about  $300 \text{ L mol}^{-1} \text{ s}^{-1}$  at room temperature [23]. Therefore, crosslinker or comonomer was required in order to polymerize methyl methacrylate. As a first strategy, a methyl methacrylate solution containing HDDA (1,6-hexanediol diacrylate) as crosslinker was prepared. In a typical recipe, the photoinitiator was 1 wt.% in methyl methacrylate and HDDA was 5 vol.% with respect to methyl methacrylate. Figure 2(a) shows a SEM image of HDDA crosslinked, agglomerated poly(methyl methacrylate) particles. Polymer particle aerosol leaving the photoreactor was either collected on a filter membrane or passed through an aqueous phase free of stabilizers, resulting in particle agglomeration. The nanoscale polymer particles were spherical and the aerosol process allowed the production of these particles without incorporation of impurities, e.g. surfactants.

Conversion of carbon-carbon double bond was analyzed by FTIR-ATR. The spectra of methyl methacrylate solution before aerosol generation and of crosslinked PMMA particles resulting from aerosol-photopolymerization are compared in Figure 2(b). The peaks in the range  $1700$  to  $1800 \text{ cm}^{-1}$  correspond to carbon-oxygen double bond valence vibration, which exist in the monomer solution and polymer particles. Carbon-carbon double bonds of acrylic monomers possess valence vibration between  $1620$  and  $1680 \text{ cm}^{-1}$ , clearly observed in the spectrum of methyl methacrylate monomer solution. The peak depleted in the spectrum of crosslinked PMMA particles, revealing a complete monomer conversion.

Irgacure 907 was chosen as the photoinitiator due to its strong UVB absorption characteristics matching the emission spectrum of the XeCl excimer irradiation source, resulting in high quantum yields [24]. Another decisive point concerning the photoinitiator selection was its solubility in the monomer. Hence, an oil-soluble photoinitiator is required. Blank experiments performed without any photoinitiator did not result in successful photopolymerization revealing that the presence of a photoinitiator is essential. The photoinitiator concentration of 1 wt.% was chosen according to literature recommendations [12] and led to monomer-free polymer particles by employing 5 wt.% HDDA as crosslinker, see above. Lower photoinitiator concentrations, e.g. 0.1 wt.%, resulted in similar spherical polymer particles containing rest monomer, detected by FTIR-ATR analysis. On the other hand, photoinitiator concentration of 5 wt.% resulted in completely polymerized particles, but slight deformations from spherical shape could be observed for a few particles by SEM analysis. In order to generate highly pure polymeric particles, 5 wt.% is a rather high photoinitiator concentration and not desired in the final product since initiator molecules (moieties) are potential impurities for polymers. Based on the experimental results for the photopolymerization of MMA, a photoinitiator concentration of 1 wt.% was selected for subsequent experiments, being aware that initiator type and concentration dependency have to be examined more in detail.

Experiments with HDDA-crosslinked MMA confirmed that 5 vol.-% crosslinker is required to polymerize the monomer droplets completely during photoreactor passage. Keeping the photoinitiator concentration at 1 wt.%, crosslinker concentration of 2 vol.% led to liquid rest monomer on the filter membrane, implying an insufficient overall polymerization rate. Incomplete polymerization was proved by FTIR-ATR measurements again. For HDDA concentrations of 10 and 20 vol.%, polymer particles were produced which showed complete acrylate conversion. In contrast, crosslinker concentration of 30 vol.% resulted in incomplete photopolymerization with rest monomer. This might be explained by the preferential fast crosslinking polymerization of HDDA while too much MMA molecules remained unpolymerized.

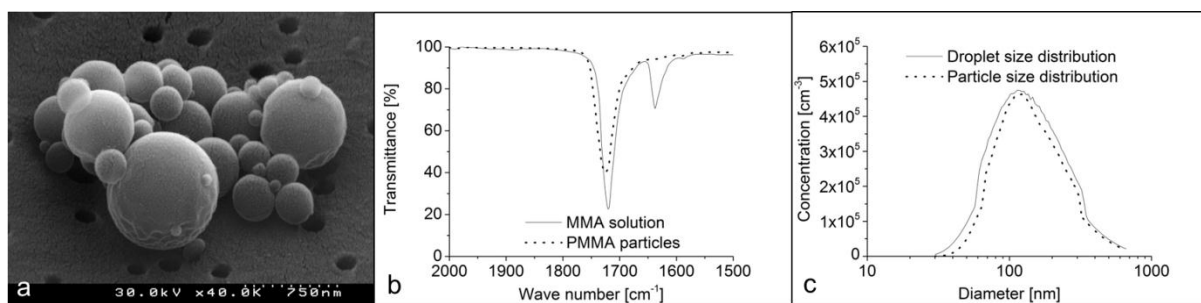


**Fig. 2.** (a) SEM image of PMMA particles produced by aerosol-photopolymerization, (b) FTIR-ATR spectra of MMA solution and PMMA particles, (c) particle size distributions of aerosol monomer droplets and PMMA particle aerosol.

The particle size distribution of HDDA crosslinked PMMA particles was measured on-line by a scanning mobility particle sizer (SMPS). The droplet size distribution before polymerization was also measured and compared to the particle size distribution after polymerization, see Figure 2(c). The one-to-one match of the two size distributions implies no significant droplet evaporation. Unfortunately, there is no information about the density of HDDA-crosslinked PMMA. Polymerization of pure MMA would lead to an approximate volume shrinkage of 20 %. The aerosol generator inlet pressure during SMPS analysis was 1 bar. Most of the polymer particles in the polydisperse aerosol were less than 300 nm in diameter, and a smaller fraction was larger than 500 nm. Total polymer particle concentration in the aerosol was measured to be  $1.7 \times 10^7 \text{ cm}^{-3}$ . The size distribution of polymer particles determined by SMPS analysis also matches well with the primary particle sizes obtained by SEM analysis. Droplet size (distribution) strongly depends on the monomer of choice, especially on its viscosity and surface tension. For a specific monomer solution, the droplet size can be adjusted e.g. by adding a highly volatile solvent to the monomer solution so that droplet sizes can be reduced via solvent evaporation before photopolymerization.

For the aerosol-photopolymerization of butyl acrylate, which is a highly reactive monomer possessing a high propagation rate coefficient of about  $15000 \text{ L mol}^{-1} \text{ s}^{-1}$  at room temperature [25], no addition of crosslinker was necessary. Spherical submicron polymer particles free of additives could be produced with and without crosslinker since the aerosol residence time in the photoreactor was long enough for the successful photopolymerization of this monomer. In

a typical recipe, butyl acrylate solution was prepared with 1 wt.% photoinitiator and no crosslinker. For SEM characterization, the poly(butyl acrylate) particles leaving the photoreactor were collected dry on a filter. A SEM image of the resulting PBA particles is presented in Figure 3(a). PBA possesses a glass transition temperature of about  $-49\text{ }^{\circ}\text{C}$ , which prevented these particles to be collected properly in liquids without any stabilizer due to their “sticky” character.

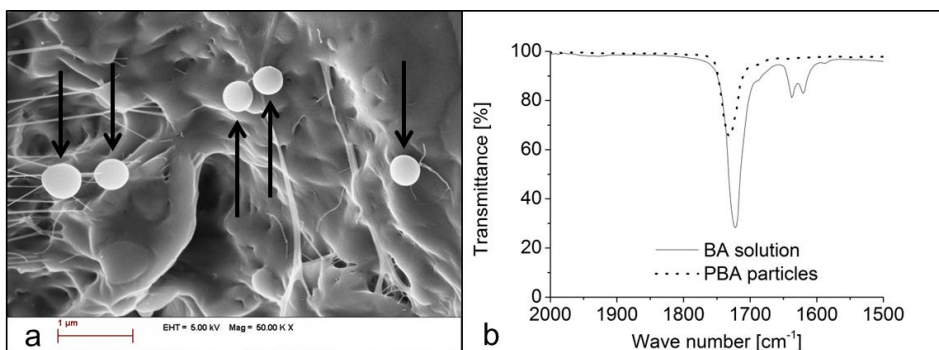


**Fig. 3.** (a) SEM image of PBA particles produced by aerosol-photopolymerization (indicated by arrows), (b) FTIR-ATR spectra of BA solution and PBA particles.

The FTIR spectra of butyl acrylate solution to be sprayed and PBA particles are compared in Figure 3(b). The two small peaks of the butyl acrylate monomer solution are characteristic for the butyl acrylate carbon-carbon double bond. The absence of an absorption peak between  $1600$  and  $1700\text{ cm}^{-1}$  for collected PBA particles revealed also for butyl acrylate a complete conversion to polymer particles.

Copolymer particles were also produced by aerosol-photopolymerization. The monomer combination served as an alternative strategy to increase the overall polymerization rate in the photoreactor. Equal volumes of methyl methacrylate and butyl acrylate were mixed. The concentration of photoinitiator was 1 wt.% in the monomer mixture and no crosslinker was employed. Methyl methacrylate, as the slow propagating monomer, could be successfully copolymerized with the fast propagating monomer butyl acrylate for the generation of poly(MMA-co-BA) copolymer particles. The resulting, in water collected particles, are visualized in Figure 4(a). As evidenced by FTIR analysis, Figure 4(b) depicts a complete conversion of monomers for the copolymerization system as well.

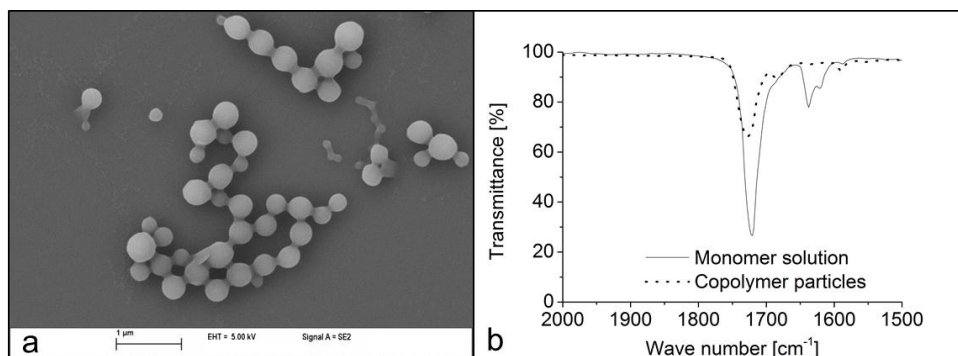


**Fig. 4.** (a) SEM image of poly(MMA-co-BA) particles produced by aerosol-photopolymerization, (b) FTIR-ATR spectra of monomer solution and copolymer particles.

Currently, the production rate of polymer particles via aerosol-photopolymerization is mainly limited by the relatively low droplet concentration. By photopolymerizing HDDA as the sole monomer using 1 wt.% photoinitiator, approximately 150 mg/h polymer could be generated with the presented experimental setup which has not been optimized yet. Scaling up aspects are going to be investigated more intensively in the next future. After optimizing the aerosol generation device and the photochemical reaction system, numbering up could be taken into consideration to increase the production rate further. However, our interest is more focused on nanostructured functional materials as highly attractive emerging products rather than on mass production of polymers. Aerosol-photopolymerization can serve as a fundamental part in integrated continuous aerosol-based processes for the generation of such multifunctional particles.

#### 4. Conclusions

To our knowledge, the production of nanoscale (submicron) spherical polymer particles by aerosol-photopolymerization has been presented for the first time. Utilizing photochemical techniques, instantaneous initiation of free radical chain reactions can be accomplished in the monomer droplets via UV irradiation. As a substantial advantage, polymerization reactions can be conducted at thermodynamically favored ambient temperatures, minimizing droplet evaporation and permitting 1-to-1 copies of monomer droplets to polymer particles. The aerosol-based process enables in combination with photochemical methods the realization of a continuous experimental setup. Compared to liquid routes, no surfactants are required, leading to highly pure materials. Furthermore, downstream processes may be avoided. Different strategies were developed to conduct photopolymerization of different monomers within the subminute aerosol residence time in the flow-through photoreactor. Fast propagating monomers can be polymerized with and without crosslinker. Even if the propagation rate coefficient of a monomer is not large enough, the overall polymerization rate can be increased by the addition of a crosslinker or a fast comonomer.

Aerosol generation and parameters affecting the photopolymerization kinetics should be investigated more in detail to increase the small production rate. Nevertheless, aerosol-photopolymerization bears great potential for integrated processes as a fast and flexible unit

operation for the generation of smart particles possessing multifunctional properties. To establish this, the generation of organic-inorganic hybrid nanoparticles by aerosol-photopolymerization is under progress by our team.

## Acknowledgements

This project is part of a joint initiative of KIT and BASF SE. Financial support by the ministry of science, research and the arts of Baden-Wuerttemberg (Az. 33-729.61-3) is gratefully acknowledged. We also wish to thank the Institute of Mechanical Process Engineering and Mechanics at KIT for providing the SMPS equipment.

## References

1. Althues, H., J. Henle, and S. Kaskel, *Functional inorganic nanofillers for transparent polymers*. Chemical Society Reviews, 2007. **36**(9): p. 1454-1465.
2. Khrenov, V., et al., *Surface functionalized ZnO particles designed for the use in transparent nanocomposites*. Macromolecular Chemistry and Physics, 2005. **206**(1): p. 95-101.
3. Shi, J., et al., *Nanotechnology in Drug Delivery and Tissue Engineering: From Discovery to Applications*. Nano Letters, 2010. **10**(9): p. 3223-3230.
4. Landfester, K., et al., *Miniemulsion polymerization with cationic and nonionic surfactants: A very efficient use of surfactants for heterophase polymerization*. Macromolecules, 1999. **32**(8): p. 2679-2683.
5. Huang, X.Y. and W.J. Brittain, *Synthesis and characterization of PMMA nanocomposites by suspension and emulsion polymerization*. Macromolecules, 2001. **34**(10): p. 3255-3260.
6. Braun, D., *PVC - Origin, growth, and future*. Journal of Vinyl & Additive Technology, 2001. **7**(4): p. 168-176.
7. Ye, Q., et al., *Formation of monodisperse polyacrylamide particles by radiation-induced dispersion polymerization. I. Synthesis and polymerization kinetics*. Journal of Applied Polymer Science, 2002. **86**(10): p. 2567-2573.
8. Shin, D.S., E.K. Oh, and S.G. Kim, *Preparation of polymer particles in aerosol-phase reaction*. Aerosol Science and Technology, 1996. **24**(4): p. 243-254.
9. Esen, C. and G. Schweiger, *Preparation of monodisperse polymer particles by photopolymerization*. Journal of Colloid and Interface Science, 1996. **179**(1): p. 276-280.

10. Gao, Z., E.A. Grulke, and A.K. Ray, *Synthesis of monodisperse polymer microspheres by photopolymerization of microdroplets*. Colloid and Polymer Science, 2007. **285**(8): p. 847-854.
11. Esen, C., T. Kaiser, and G. Schweiger, *Raman investigation of photopolymerization reactions of single optically levitated microparticles*. Applied Spectroscopy, 1996. **50**(7): p. 823-828.
12. Decker, C., *Kinetic study and new applications of UV radiation curing*. Macromolecular Rapid Communications, 2002. **23**(18): p. 1067-1093.
13. Decker, C., *Kinetic-study of light-induced polymerization by real-time UV and IR spectroscopy*. Journal of Polymer Science Part a-Polymer Chemistry, 1992. **30**(5): p. 913-928.
14. Decker, C., B. Elzaouk, and D. Decker, *Kinetic study of ultrafast photopolymerization reactions*. Journal of Macromolecular Science-Pure and Applied Chemistry, 1996. **A33**(2): p. 173-190.
15. Scherzer, T., R. Mehnert, and H. Lucht, *On-line monitoring of the acrylate conversion in UV photopolymerization by near-infrared reflection spectroscopy*. Macromolecular Symposia, 2004. **205**: p. 151-162.
16. Decker, C. and K. Moussa, *Kinetic investigation of photopolymerizations induced by laser-beams*. Makromolekulare Chemie-Macromolecular Chemistry and Physics, 1990. **191**(4): p. 963-979.
17. Andrzejewska, E., *Photopolymerization kinetics of multifunctional monomers*. Progress in Polymer Science, 2001. **26**(4): p. 605-665.
18. Bowman, C.N. and N.A. Peppas, *Coupling of kinetics and volume relaxation during polymerizations of multiacrylates and multimethacrylates*. Macromolecules, 1991. **24**(8): p. 1914-1920.
19. Kurdikar, D.L. and N.A. Peppas, *A kinetic-model for diffusion-controlled bulk cross-linking photopolymerizations*. Macromolecules, 1994. **27**(15): p. 4084-4092.
20. Anseth, K.S., C.M. Wang, and C.N. Bowman, *Kinetic evidence of reaction-diffusion during the polymerization of multi(meth)acrylate monomers*. Macromolecules, 1994. **27**(3): p. 650-655.
21. Kindernay, J., et al., *Effect of UV light source intensity and spectral distribution on the photopolymerisation reactions of a multifunctional acrylated monomer*. Journal of Photochemistry and Photobiology a-Chemistry, 2002. **151**(1-3): p. 229-236.
22. Kogelschatz, U., *Silent discharges for the generation of ultraviolet and vacuum ultraviolet excimer radiation*. Pure and Applied Chemistry, 1990. **62**(9): p. 1667-1674.

23. Beuermann, S., et al., *Critically evaluated rate coefficients for free-radical polymerization .2. Propagation rate coefficients for methyl methacrylate.* Macromolecular Chemistry and Physics, 1997. **198**(5): p. 1545-1560.
24. Scherzer, T. and U. Decker, *Kinetic investigations on UV-induced photopolymerization reactions by real-time FTIR-ATR spectroscopy: the efficiency of photoinitiators at 313 and 222 nm.* Nuclear Instruments & Methods in Physics Research Section B-Beam Interactions with Materials and Atoms, 1999. **151**(1-4): p. 306-312.
25. Lyons, R.A., et al., *Pulsed-laser polymerization measurements of the propagation rate coefficient for butyl acrylate.* Macromolecules, 1996. **29**(6): p. 1918-1927.

---

# Perspectives of Aerosol-Photopolymerization: Organic-Inorganic Hybrid Nanoparticles

Ertan Akgün, Jürgen Hubbuch, Michael Wörner\*

---

*Process Engineering in Life Sciences, Karlsruhe Institute of Technology*

\* Corresponding author: Michael Wörner ([michael.woerner@kit.edu](mailto:michael.woerner@kit.edu))

Colloid and Polymer Science, 292, 1241 (2014)

The final publication is available on:

<http://rd.springer.com/article/10.1007/s00396-014-3175-2#>

## **Abstract**

The technique of aerosol-photopolymerization is employed for the generation of organic-inorganic spherical polymer matrix nanocomposites (PMNCs). The loading amount of well-distributed ZnO nanoparticles in polymer networks is varied in a broad range up to 40 wt.-%. Similar hybrid particles are produced without the addition of a conventional photoinitiator by making use of the UV absorptivity of ZnO nanoparticles only. Highlights of the process are the continuous, aerosol-based setup with a flow-through photoreactor operated at ambient temperature and atmospheric pressure. Aerosol-photopolymerization possesses great potential of incorporating various materials *in situ* into a polymer matrix, resulting in hybrid materials for diverse applications. Furthermore, the process can be integrated with further unit operations for the design of smart materials.

**Keywords:** Hybrid materials; Nanocomposites; Photochemistry; Aerosols

## 1. Introduction

Integration of inorganic nanoparticles into polymeric materials may result in flexible, multifunctional composites exhibiting outstanding electrical, optical, and mechanical properties [1]. Unique combinations of material properties can be obtained for optoelectronic and magneto-optic applications [2]. Such hybrid materials possess promising (future) applications as functional smart coatings, fuel and solar cells, catalysts, sensors, separation materials for chemical and biotechnology [3], and imaging, treatment and drug delivery systems in medicine [4].

In traditional polymer composites, micron-sized particles or agglomerates cause light scattering hampering optical applications. On the other side, nanocomposites with particle dimensions small enough result in highly transparent materials [5, 6]. Such materials exhibit optical functions such as luminescence and UV-shielding while remaining transparent. The organic part of such hybrid materials enables cost-effective processing while the inorganic part fulfills specific functionality depending on the material.

A variety of methods exist for the synthesis of organic-inorganic hybrid materials. Some of them are more appropriate for the preparation of concentrated composites, and several are suitable regarding (the) process simplicity. Among other methods, composites can be generated by bulk chain polymerization [7, 8], by simple mixing or blending [9-11], and by more sophisticated methods leading to particulate products [12]. For the generation of organic-inorganic hybrid materials, the main challenge to be overcome is the absence of an integrated process combining particle generation, surface modification, and integration within the polymeric material [5]. Therefore, cross-cutting synthetic methods are required to achieve complex systems with specific requirements of size, composition, porosity, functionality, and morphology [13]. Most often, liquid-based processes are employed for the production of such materials. For nano- and microscale organic-inorganic hybrid particle synthesis, emulsion-based methods are applied most frequently [14, 15].

In this contribution, aerosol-photopolymerization is presented as an alternative route for the production of spherical organic-inorganic hybrid nanoparticles. The process has been introduced for the generation of highly pure nanoscale, spherical polymer particles [16]. As a step further, aerosol-photopolymerization was employed for the generation of submicron polymer-matrix nanocomposites (PMNCs), and zinc oxide has been chosen as the model inorganic compound. Apart from UV absorbance due to its bulk band-gap energy of about 3 eV [2], nanoscale ZnO particles possess physical and chemical properties like high chemical stability, low dielectric constant, large electromechanical coupling coefficient, high luminous transmittance, high catalytic activity, and intense infrared absorption [10]. Aerosol-photopolymerization can be conducted at ambient temperature and atmospheric pressure without using any solvent. It is possible to incorporate thermally sensitive materials into the monomer droplets. In fact, once the inorganic nanoparticles are stabilized in the monomer solution, any material could be incorporated into the monomer nanodroplets to be photopolymerized. Besides operation at ambient temperature, photopolymerization offers further numerous advantages over thermal systems as well. Photochemistry allows instantaneous generation of free radicals in the nanoscale monomer droplets, initiating the polymerization reactions. The possibility of tuning the initiation rate by the variation of

photoinitiator concentration, photon exitance, and photophysical properties of the photoinitiator is an excellent strategy for optimization. The aerosol-based experimental setup enables the implementation of a continuous process with a flow-through photoreactor. Furthermore, the aerosol route facilitates the realization of integrated processes by applying less downstream unit operations, saving time and cost for multifunctional hybrid nanoparticle synthesis.

## 2. Experimental Section

### 2.1 Materials

Methyl methacrylate (MMA, Sigma-Aldrich, 99 % purity) and butyl acrylate (BA, Sigma-Aldrich, 99 % purity) were used as monomers. Irgacure 907 (Methyl-1[4-(methylthio)phenyl]-2-morpholinopropan-1-one, Sigma-Aldrich, 98 % purity) and 1,6-hexanediol diacrylate (HDDA, Alfa Aesar, 99 % purity) were chosen as photoinitiator and crosslinker, respectively. Zinc oxide nanoparticles (Sigma-Aldrich, 40 wt.-% in ethanol, 30 nm average diameter and IBU-tec, 40 wt.-% in HDDA, 12 nm average diameter) and iron oxide nanoparticles (Sigma-Aldrich, 20 wt.-% in ethanol, 30 nm average diameter) were employed as the source of inorganic component of hybrid nanoparticles. All chemicals were used as received.

### 2.2 Process

The experimental setup consists of two main components, an aerosol generator and a photoreactor, and has been described [16]. The employed aerosol generator utilizes a two-stream nozzle which is based on the injection principle (ATM 220, Topas GmbH). Nozzle inlet pressure of this aerosol generator can be varied between 1 and 6 bars. 1 bar is the standard value for the experiments performed and corresponds to an average nitrogen volumetric flow rate of about  $1 \text{ L min}^{-1}$ . One of the photoreactors is equipped with a quasi-monochromatic XeCl excimer UV irradiation source emitting at 308 nm wavelength and possessing width of half height of about 3 nm. This UV source can be tuned up to a radiant exitance of  $10 \text{ mW cm}^{-2}$  (experimental standard value) at the envelope surface. The average aerosol residence time in the photoreactor corresponding to the nozzle inlet pressure of 1 bar is almost 1 min and can be reduced by increasing the aerosol volumetric flow rate via adjusting the nozzle inlet pressure of the aerosol generator. The reactor tube length is 425 mm and it is mounted in vertical alignment. An alternative photoreactor equipped with UV fluorescence tubes possesses the same average aerosol residence time as the excimer photoreactor. UV fluorescence tubes emit polychromatic UV radiation in the range 270-360 nm with a maximum at 312 nm. This photoreactor is built up by a cylindrical quartz glass tube (440 mm long, 52 mm inner diameter) surrounded by 6 UV fluorescence tubes (410 mm long) resulting in an irradiance of  $5 \text{ mW cm}^{-2}$  at the quartz glass tube surface. The aerosol residence time in this reactor can be varied by adjusting the nozzle inlet pressure of the aerosol generator or by selecting a shorter photoreactor tube.

A monomer formulation is required for the generation of the droplet aerosol. Such a formulation consists of at least one monomer, a photoinitiator, and inorganic nanoparticles. If such a formulation is not a commercial obtained one, it is prepared by dissolving the photoinitiator in the liquid monomer or monomer mixture, and adding the inorganic nanoparticles during stirring for obtaining a stable suspension called “monomer suspension”. Upon preparing a stable monomer suspension, it is sprayed with the help of nitrogen in the aerosol generator. Once the nitrogen-carried, nanoparticle-loaded monomer droplets are formed, they are passed through the photoreactor for the generation of organic-inorganic hybrid nanoparticles upon UV-initiated free radical polymerization. Fig. 1 illustrates schematically the process flow diagram. After droplet aerosol generation, photopolymerization of a single-phase (a) and a hybrid monomer droplet (b) result in a polymer nanoparticle (a) and in a hybrid nanoparticle (b), respectively. Since inorganic nanoparticles are brought into monomer droplets during the aerosol generation process, *in situ* aerosol-photopolymerization results in the formation of organic-inorganic hybrid nanoparticles which are in the form of polymer-matrix nanocomposites (PMNCs).

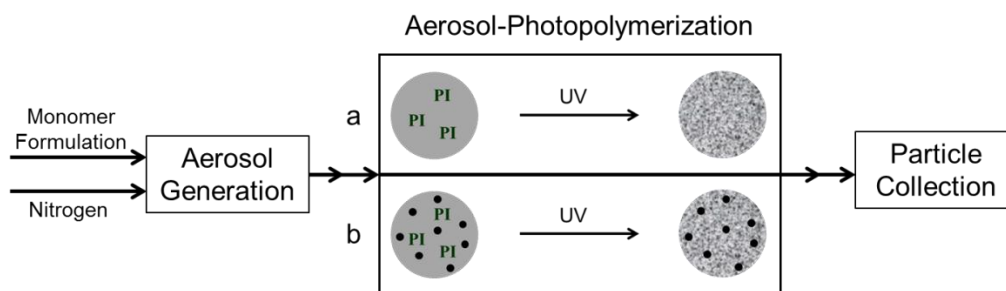


**Fig. 1.** Scheme of the process flow of aerosol-photopolymerization: (a) A monomer solution droplet containing the dissolved photoinitiator (PI) before photopolymerization and the produced polymer nanoparticle after photopolymerization. (b) A hybrid monomer suspension droplet containing the dissolved photoinitiator (PI) and nanoparticles (small spherical dots) before photopolymerization and the produced hybrid nanoparticle after photopolymerization.

Hybrid nanoparticles in aerosol leaving the photoreactor are collected either dry on a PTFE filter membrane with 50 nm average pore diameter or wet by transfer into a liquid for obtaining a suspension.

### 2.3 Particle Characterization

Transmission electron microscopy (TEM) was performed on a Philips CM 12 and a Zeiss TEM 912. The particles were brought on a TEM grid (Plano, S160-3, carbon film on 300 mesh Cu grid) directly from the aerosol phase.

Microtome cuts were prepared for the visualization of the inorganic nanoparticle distribution in the polymer matrices. The dry sample was embedded in acrylate dispersion for fixation, and the samples were cut at minus 140 °C into pieces of 100-150 nm thickness.

Fourier transform infrared spectroscopy (FTIR-ATR, Equinox 55, Bruker Optics) was employed for the examination of residual monomer in hybrid particles.

Scanning mobility particle sizer (SMPS consisting of electrostatic classifier 3080, differential mobility analyzer 3081, and condensation particle counter 3775, TSI Corp.) was used for the on-line measurement of droplet and particle size distributions in aerosols.

### **3. Results and Discussion**

#### *Variation of ZnO Nanoparticle Loading*

The generation of spherical nanoscale polymer particles by aerosol-photopolymerization has been introduced before [16]. In this work, inorganic nanoparticles were incorporated into the spherical polymer particles as a step further. The monomer formulations for hybrid particle generation were based on the results of the established technique for polymer particle production via aerosol-photopolymerization. Therefore, a typical recipe for the monomer system consisting of methyl methacrylate (MMA) and 1,6-hexanediol diacrylate (HDDA) contained 1 wt.-% Irgacure 907 in MMA and 10 vol.-% HDDA with respect to MMA. Zinc oxide has been chosen as the model inorganic compound and its loading in the formulation was varied. Organic-inorganic hybrid nanoparticles, specifically polymer-matrix nanocomposites (PMNCs), with varying loadings of zinc oxide nanoparticles were generated by aerosol-photopolymerization.

For the monomer system consisting of MMA and HDDA, the suspension with 40 wt.-% ZnO (30 nm mean diameter) in ethanol was used. Zinc oxide nanoparticles were mixed and suspended in the monomer solution for preparing the monomer suspension to be sprayed. The 40 wt.-% concentrated suspension of ZnO in ethanol enabled the addition of zinc oxide nanoparticles to the monomer solution while the added amount of ethanol was kept very low. Zinc oxide loadings in the hybrid nanoparticles were calculated according to zinc oxide concentration in the initial monomer suspensions. Fig. 2 illustrates TEM images of these hybrid particles with increasing concentration of zinc oxide nanoparticles indicated by the increase in darker proportion within the spheres. ZnO concentrations in the formulation were 0.6, 1.5, and 3.0 wt.-%. Since hybrid droplets were formed during spraying of the monomer suspension before photopolymerization, *in situ* generation of organic-inorganic hybrid nanoparticles in the photoreactor was realized. The average aerosol residence time in the photoreactor was 52 s. The size distribution of the hybrid particles was submicron and polydisperse, as it was for the nanoscale polymer particles generated by the same technique of aerosol-photopolymerization presented before [16]. A crosslinker concentration of 20 vol.-% resulted in similar hybrid nanoparticles. Alternative to hybrid particles consisting of HDDA-crosslinked PMMA as the polymeric part, aerosol-photopolymerization was also applied for polymerizing a butyl acrylate monomer suspension without employing a crosslinker.

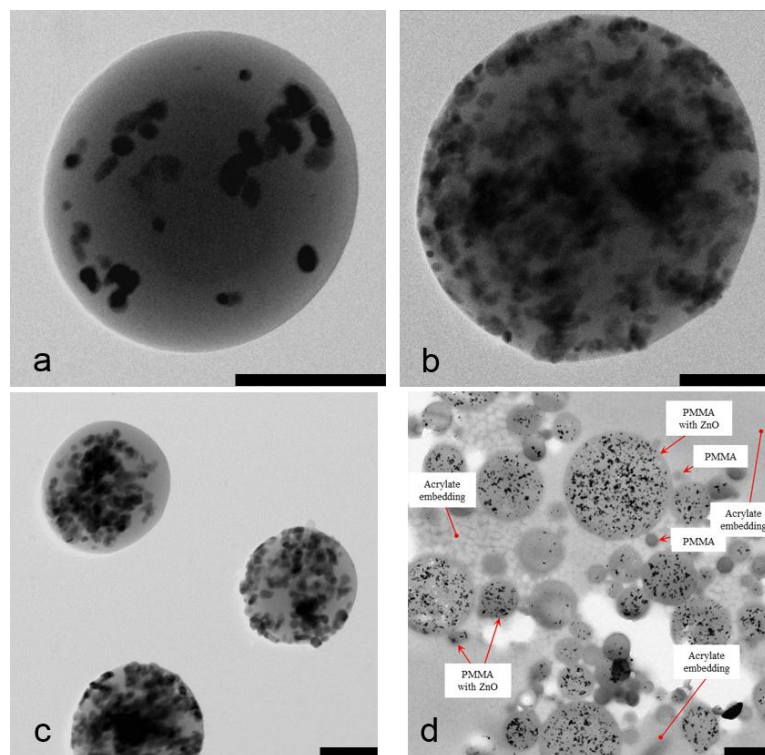


**Fig. 2.** TEM images of PMMA-ZnO hybrid nanoparticles with different loadings of ZnO generated by aerosol-photopolymerization: (a) 0.6 wt.-%, (b) 1.5 wt.-%, and (c) 3.0 wt.-%. The scale bars represent 200 nm. (d) TEM image of moderately-loaded (1.5 wt.-%) hybrid particles after microtoming. The scale bar represents 1  $\mu$ m.

TEM images of Fig. 2a-c are quite helpful to visualize the hybrid structure of the nanoparticles resulting from aerosol-photopolymerization, but they do not yield sufficient information about the distribution of zinc oxide nanoparticles within the polymer matrix or their location at the polymer surface. Therefore, microtome cuts of moderately-loaded hybrids with 1.5 wt.-% ZnO were prepared to visualize the location of inorganic nanoparticles with respect to the polymer matrix. The image shown in Fig. 2d represents PMNCs after microtoming. Although zinc oxide nanoparticles were well-distributed within the polymer matrices, some agglomerates can be observed. These might originate from the monomer suspension before spraying or might be secondary agglomerates which have developed during droplet formation by aerosol generation. Unfortunately, it is difficult to give a reliable number of ZnO nanoparticle fraction being individually present in the hybrid particles, especially for the considerably loaded ones. However, the particles prepared with ZnO in HDDA, as presented below, seem to contain a larger fraction of ZnO nanoparticles that did not agglomerate, which is explained by the different surface functionalization of the ZnO nanoparticle dispersions in HDDA and ethanol. As a consequence, the ZnO-loaded monomer formulation prepared by mixing the monomer solution with ZnO nanoparticles in ethanol is less stable and results in more agglomerates in the hybrid particles. Therefore, the preparation of a stable dispersion is crucial for the production of PMNCs with uniform particle distribution. Apart from agglomerates present, TEM analyses revealed basically uniform ZnO distributions in the nanocomposites. There is no evidence of ZnO nanoparticles accumulated at specific sites such

as on the surface or in the center of the polymeric particles. Nevertheless, SEM images of highly loaded (15 wt.-% ZnO), HDDA-crosslinked PMMA particles revealed ZnO nanoparticles at the surface or immediate vicinity of the polymer surface as well, as illustrated in Fig. 3a. The same polymer particles without ZnO are depicted in Fig. 3c and possess smoother surface characteristics than those where the inorganic nanoparticles were incorporated into polymers.

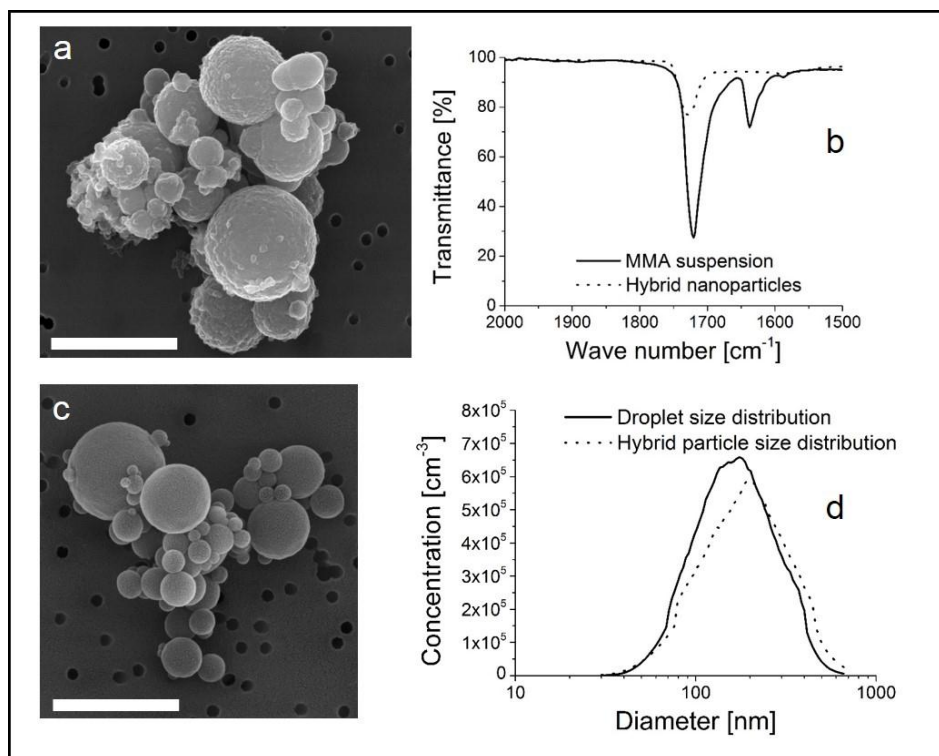


**Fig. 3.** (a) SEM image of PMMA-ZnO hybrid nanoparticles with 15 wt.% loading of ZnO generated by aerosol-photopolymerization, (b) FTIR-ATR spectra of the monomer suspension before spraying and hybrid nanoparticles, (c) SEM image of PMMA nanoparticles without ZnO incorporation generated by aerosol-photopolymerization, and (d) particle size distributions of monomer droplets and hybrid nanoparticles (SMPS analysis). The scale bars represent 1.5  $\mu\text{m}$ .

For the examination of residual monomer amount in hybrid nanoparticles, FTIR-ATR measurements were performed. The monomer spectrum was obtained by measuring the formulation to be sprayed (15 wt.-% ZnO) and that of the hybrid particles after collecting them on a filter membrane upon photoreactor passage. The results shown in Fig. 3b indicate practically no rest monomer in the hybrid particles due to the depletion of the carbon-carbon double bond valence vibration peak upon polymerization. Particle size distributions of the droplets and hybrid nanoparticles (0.6 wt.-% ZnO loading) in the aerosol before and after photopolymerization, respectively, were determined by SMPS analysis. In general, there is a match of these two size distributions, but not as good as for the measurements performed during development of the aerosol-photopolymerization technique for unloaded polymer

particle preparation revealing 1-to-1 copies [16]. Furthermore, the SMPS analysis of droplet aerosols is experimentally challenging.

Organic-inorganic PMNCs were synthesized with HDDA as the sole monomer as well. Hence, a highly crosslinked polymer network can be formed [17]. For these experiments, a commercial suspension of 40 wt.-% ZnO nanoparticles in HDDA was used. ZnO particles of this suspension were 12 nm in diameter. By diluting this HDDA-ZnO mixture with HDDA, variations in loading of polymer with ZnO were realized. Fig. 4a shows a particle with 10 wt.-% ZnO loading and the particles of Fig. 4b contain 40 wt.-% ZnO. Higher loadings might also be possible by this technique provided that the medium viscosity does not hinder proper spraying. Shim et al. [12] filled their PMMA-ZnO microspheres with 30 wt.-% ZnO *in situ* by suspension polymerization, and deformations from sphericity were observed after reaching a loading level of 50 wt.-%.

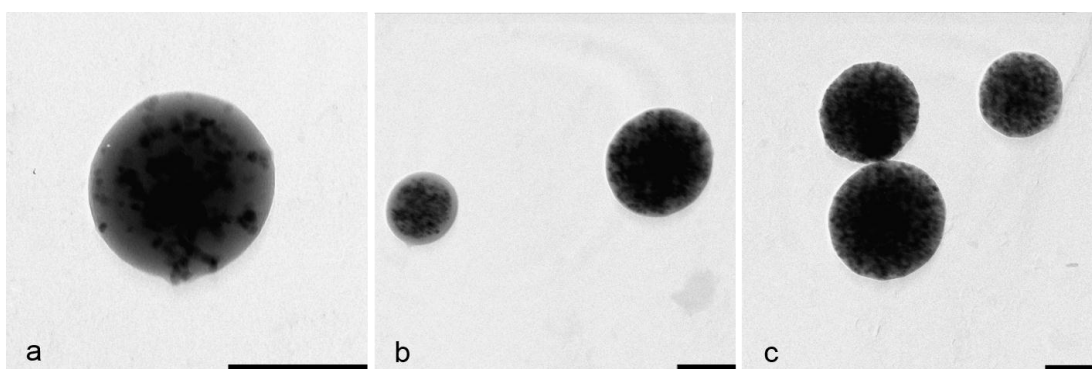


**Fig. 4.** PHDDA-ZnO hybrid nanoparticles containing generated by aerosol-photopolymerization: (a) 10 wt.-% ZnO, (b) 40 wt.-% ZnO, (c) 40 wt.-% ZnO without a conventional photoinitiator. The scale bars represent 200 nm.

The production rate of PHDDA particles loaded with 10 wt.-% ZnO was 180 mg/h when the average aerosol residence time was 52 s. However, the photopolymerization time required for HDDA was expected to be considerably shorter than 52 s. Multifunctional monomers such as HDDA can be converted to a three dimensional network within a few seconds by photopolymerization provided that a certain amount of photoinitiator and incident radiation exist in the system [18]. Indeed, decreasing the aerosol residence time from 52 to 21 s by shortening the photoreactor tube resulted in the same particles, confirming that this short residence time is enough for a complete photopolymerization of HDDA in the droplets consisting of Irgacure 907, HDDA, and ZnO nanoparticles. Moreover, this measure increased the production rate to about 300 mg/h.

#### *Semiconductor-Assisted (Induced) Photoinitiation*

Photopolymerization can also be performed without using a conventional photoinitiator like Irgacure 907. Semiconductors such as ZnO [19-21] and CdS [21] have been used to initiate polymerization reactions. Hoffman et al. [20] reported about photoinitiated polymerization of MMA in presence of quantum-sized ZnO colloids. They proposed an anionic initiation step followed by free radical propagation reactions. The possibility of employing semiconductors

as photoinitiators for radical polymerization reactions was discussed even earlier by means of MMA polymerization at ZnO surfaces [19].

For the generation of hybrid nanoparticles discussed so far in this work, the monomer suspensions were prepared by dissolving a conventional photoinitiator, Irgacure 907. For implementing photoinitiator-free photopolymerization in our aerosol-photopolymerization setup, Irgacure 907 was not added into the formulation to be sprayed for taking advantage of the photocatalytic activity of zinc oxide nanoparticles present in the aerosol monomer droplets upon spraying. Except the photoinitiator, the content of the monomer suspension was kept the same. Fig. 4c shows HDDA-crosslinked PMMA-ZnO hybrid nanoparticles produced by aerosol-photopolymerization without any conventional photoinitiator employed. ZnO loading was 40 wt.-% and the average aerosol residence time in the photoreactor was 52 s. It should be noticed that UV absorption measurements revealed that a suspension containing 40 wt.-% ZnO nanoparticles (30 nm) absorb in the range of the emission maxima of the irradiation sources (308-312 nm) about 20 times stronger than a solution with 1 wt.-% Irgacure 907. Nevertheless, hybrid nanoparticles with lower ZnO loadings of 5.8 and even 0.6 wt.-% could also be synthesized without using Irgacure 907.

Apart from the experiments where the crosslinker HDDA was employed as the monomer exclusively, PMMA-based ZnO hybrid particles could also be generated in the absence of a conventional photoinitiator by aerosol-photopolymerization of a MMA-HDDA monomer mixture. Similarly, butyl acrylate was photopolymerized for PBA-ZnO hybrid particle production without an added photoinitiator and without employing the crosslinker HDDA. It should be noticed that a blank experiment without ZnO did not yield polymer nanospheres under identical irradiation conditions. Alternative to ZnO, a monomer suspension consisting of Irgacure 907 and MMA-HDDA mixture prepared with 1.2 and 2.4 wt.-% Fe<sub>2</sub>O<sub>3</sub> as the inorganic content resulted in successful generation of hybrid nanoparticles. In contrast, no hybrid particles could be generated for the monomer formulation containing 1.2 wt.-% Fe<sub>2</sub>O<sub>3</sub> in the absence of Irgacure 907, revealing the difference in photocatalytic activities of zinc oxide and iron oxide nanoparticles for the initiation of free radical polymerization by UV irradiation.

## **4. Conclusions**

Organic-inorganic spherical hybrid nanoparticles have been produced via aerosol-photopolymerization. The inorganic content in the polymer particles could be varied in a considerable range up to 40 wt.-%. Well-distribution of ZnO nanoparticles within the polymer spheres resulted in polymer-matrix nanocomposites (PMNCs). Similar particles were generated without using a conventional photoinitiator by making use of the photocatalytic activity of ZnO nanoparticles. The process highlights are the continuous setup with a flow-through photoreactor operated at ambient temperature and atmospheric pressure.

Apart from its potential as a unit operation, aerosol-photopolymerization is also highly promising especially as a part of an integrated process where smart materials are aimed for diverse emerging applications. Its characteristic features like low (ambient) temperature processing and fast reactions permit a mild, continuous process which can be integrated into

complex units. By surface functionalization, almost any kind of organic or inorganic nanoparticles, nanoplatelets, nanorods etc. could be stabilized in a liquid which in the most ideal case would be the liquid monomer itself, and aerosol-photopolymerization can be employed for the *in situ* generation of hybrid nanoparticles with favored loading of the dispersed phase. This offers numerous material combinations depending on the desired functionality and application.

## Acknowledgements

This project is part of a joint initiative of KIT and BASF SE. Financial support by the Ministry of Science, Research and the Arts of Baden-Württemberg (Az. 33-729.61-3) is gratefully acknowledged. We thank to BASF for microtoming, Institute of Mechanical Process Engineering and Mechanics at KIT for providing the SMPS equipment, and Mr. Almstedt in our working group for his efforts on photoreactor construction.

## References

1. Balazs, A.C., T. Emrick, and T.P. Russell, *Nanoparticle polymer composites: Where two small worlds meet*. Science, 2006. **314**(5802): p. 1107-1110.
2. Li, S., et al., *Nanocomposites of polymer and inorganic nanoparticles for optical and magnetic applications*. Nano reviews, 2010. **1**.
3. Sanchez, C., et al., *Applications of hybrid organic-inorganic nanocomposites*. Journal of Materials Chemistry, 2005. **15**(35-36): p. 3559-3592.
4. Berry, C.C. and A.S.G. Curtis, *Functionalisation of magnetic nanoparticles for applications in biomedicine*. Journal of Physics D-Applied Physics, 2003. **36**(13): p. R198-R206.
5. Althues, H., J. Henle, and S. Kaskel, *Functional inorganic nanofillers for transparent polymers*. Chemical Society Reviews, 2007. **36**(9): p. 1454-1465.
6. Yuwono, A.H., et al., *Controlling the crystallinity and nonlinear optical properties of transparent TiO<sub>2</sub>-PMMA nanohybrids*. Journal of Materials Chemistry, 2004. **14**(20): p. 2978-2987.
7. Anzlovar, A., Z.C. Orel, and M. Zigon, *Poly(methyl methacrylate) composites prepared by in situ polymerization using organophillic nano-to-submicrometer zinc oxide particles*. European Polymer Journal, 2010. **46**(6): p. 1216-1224.
8. Demir, M.M., et al., *PMMA/zinc oxide nanocomposites prepared by in-situ bulk polymerization*. Macromolecular Rapid Communications, 2006. **27**(10): p. 763-770.

9. Khrenov, V., et al., *Surface functionalized ZnO particles designed for the use in transparent nanocomposites*. Macromolecular Chemistry and Physics, 2005. **206**(1): p. 95-101.
10. Xiong, M.N., et al., *Preparation and characterization of poly(styrene butylacrylate) latex/nano-ZnO nanocomposites*. Journal of Applied Polymer Science, 2003. **90**(7): p. 1923-1931.
11. Sun, D., N. Miyatake, and H.-J. Sue, *Transparent PMMA/ZnO nanocomposite films based on colloidal ZnO quantum dots*. Nanotechnology, 2007. **18**(21).
12. Shim, J.W., et al., *Zinc oxide/polymethylmethacrylate composite microspheres by in situ suspension polymerization and their morphological study*. Colloids and Surfaces a-Physicochemical and Engineering Aspects, 2002. **207**(1-3): p. 105-111.
13. Nicole, L., L. Rozes, and C. Sanchez, *Integrative Approaches to Hybrid Multifunctional Materials: From Multidisciplinary Research to Applied Technologies*. Advanced Materials, 2010. **22**(29): p. 3208-3214.
14. Hecht, L.L., et al., *Miniemulsions for the Production of Nanostructured Particles*. Chemical Engineering & Technology, 2012. **35**(9): p. 1670-1676.
15. Qi, D.-m., et al., *Preparation of acrylate polymer/silica nanocomposite particles with high silica encapsulation efficiency via miniemulsion polymerization*. Polymer, 2006. **47**(13): p. 4622-4629.
16. Akguen, E., J. Hubbuch, and M. Woerner, *Perspectives of aerosol-photopolymerization: Nanoscale polymer particles*. Chemical Engineering Science, 2013. **101**: p. 248-252.
17. Anseth, K.S., C.N. Bowman, and N.A. Peppas, *Polymerization kinetics and volume relaxation behavior of photopolymerized multifunctional monomers producing highly cross-linked networks*. Journal of Polymer Science Part a-Polymer Chemistry, 1994. **32**(1): p. 139-147.
18. Decker, C., *Kinetic study and new applications of UV radiation curing*. Macromolecular Rapid Communications, 2002. **23**(18): p. 1067-1093.
19. Kuriacose, J. and M.C. Markham, *Mechanism of photo-initiated polymerization of methyl methacrylate at zinc oxide surfaces*. Journal of Physical Chemistry, 1961. **65**(12): p. 2232-&.
20. Hoffman, A.J., et al., *Photoinitiated polymerization of methyl-methacrylate using Q-sized ZnO colloids*. Journal of Physical Chemistry, 1992. **96**(13): p. 5540-5546.

21. Hoffman, A.J., et al., *Q-sized CDS - Synthesis, characterization, and efficiency of photoinitiation of polymerization of several vinylic monomers*. Journal of Physical Chemistry, 1992. **96**(13): p. 5546-5552.

---

# Perspectives of Aerosol-Photopolymerization: Nanostructured Polymeric Particles

Ertan Akgün, Jürgen Hubbuch, Michael Wörner\*

---

*Process Engineering in Life Sciences, Karlsruhe Institute of Technology*

\* *Corresponding author: Michael Wörner ([michael.woerner@kit.edu](mailto:michael.woerner@kit.edu))*

Macromolecular Materials and Engineering, 299, 11, 1316, 2014

The final publication is available on:

<http://onlinelibrary.wiley.com/doi/10.1002/mame.201400032/abstract?deniedAccessCustomisedMessage=&userIsAuthenticated=false>

## **Abstract**

Nanostructured non-spherical (named nanocaps) and spherical porous particles (named mosaic nanoparticles) are generated by aerosol-photopolymerization. Nanocaps exhibit well-defined shapes independent of their diameter and are formed by employing a softening agent and a volatile non-solvent in the formulation, combining non-solvent evaporation and retarded gelation. Mosaic nanoparticles are produced by the addition of a non-volatile non-solvent into the monomer formulation, provoking phase separation. Both particle structures are generated in situ in the presence of zinc oxide nanoparticles. Similarly, they are loaded with caffeine for release experiments and feature potential for applications in emerging technologies such as optics, functionalized coatings and nanomedicine.

**Keywords:** Photopolymerization; Nanocomposites; Nanostructuring; Non-spherical nanoparticles; Porous particles

## **1. Introduction**

Besides crucial importance of spherical particles, a strong potential exists towards a broad range of applications of non-spherical particles [1]. The anisotropy of such nanostructured particles can be utilized for specific responses under electric [2] and magnetic [3] fields. They can pack more densely than their spherical counterparts [4] and might be employed in biotechnology [5], nanomedicine [6], structural materials [7], assembly into complex structures [8], three-dimensional photonic crystals [9], particle-cell interaction studies [10], and drug delivery [11]. Microfluidics is a well-established technique for the generation of micron-sized non-spherical particles [1, 12-18]. Alargova et al. [19] presented a technique which is also based on liquid-liquid dispersions for the production of rod-like microstructures. For submicron-sized anisotropic materials, miniemulsion-based methods can be employed. Florez et al. [10] discussed the effect of anisotropy for cellular particle uptake. First, they generated spherical nanoparticles via the miniemulsion process, and shape deformation was performed subsequently in a mechanical process. Yang et al. [20] reported on the formation of high-aspect-ratio ellipsoidal polymer nanoparticles of controlled diameter using miniemulsions. Staff et al. [21] reported also anisotropic nanoparticle generation via a miniemulsion method leading to semicrystalline polymers without defined shapes. Park et al. [22] employed two-step seeded emulsion polymerization for dumbbell-shaped polymer nanoparticles.

Nanostructured spherical or quasi-spherical particles are also of great industrial interest. They can be employed in energy conversion and storage devices [23], and sensors for improving biomolecular capture efficiency [24]. Lewandowski et al. [25] presented the synthesis of macroporous styrene-divinylbenzene copolymer particles by suspension polymerization and discussed the effect of porogen (non-solvent provoking pore formation) volume. Particles having larger pores could only be obtained after the amount of porogen reached a certain threshold value, which depended on the nature of the monomer. Different porogens were tested for controlling the porous morphology of poly(divinylbenzene) particles prepared by suspension polymerization [26]. Experiments with toluene resulted in particles having a large dry state area while oligomeric porogens led to particles with macropores. Sherrington [27] reports about gel-type resins and macroporous resins, and how they are formed. Comprehensive information about the synthesis, characterization, functionalization and applications of porous polymer particles is available by Gokmen and Du Prez. [28] They discuss e.g. about different porogen types for suspension polymerization, multistage methods and microfluidic tools. Wu et al. [29] reported about the preparation and design of porous polymers as well. Different methods such as layer-by-layer assembly or self-assembly are mentioned.

Particulate materials loaded with substances (encapsulation) are applied in a variety of areas such as pharmaceuticals, cosmetics, biotechnology, chemical production, electrical engineering, graphics, printing, and provide benefits in agrochemical formulations [30], cancer therapy [31], and cellular drug delivery [32]. Particle shape might have a strong impact on the performance of drug delivery systems [33]. Different methods exist for the preparation of drug-loaded polymeric nanoparticles such as emulsion polymerization, interfacial

polymerization, emulsification/solvent evaporation, solvent displacement and interfacial deposition [34].

The generation of non-spherical polymer particles (nanocaps) and nanostructured, porous polymer particles (mosaic particles) by aerosol-photopolymerization is presented in this contribution. The process has already been introduced for the generation of spherical, submicron polymer particles [35]. Nanocaps and mosaic particles are produced by photoinitiated free radical polymerization of submicron aerosol monomer droplets by using additional components in the formulation. Several strategies were employed to realize different nanostructures. A volatile solvent was used in combination with a soft-maker to generate nanocaps. For mosaic particle generation, a porogen (non-solvent) responsible for pore formation within the particles is essential. In contrast to nanocap generation, this porogen has to be non-volatile to prevent its evaporation to the carrier gas atmosphere.

The structure of nanocaps and mosaic particles could be changed to a certain extent by the variation of process and formulation parameters. In addition, hybrid nanocaps and hybrid mosaic particles were generated *in situ* by producing the caps and mosaic particles in the presence of zinc oxide nanoparticles. ZnO nanoparticles possess unique physical and chemical properties such as high chemical stability, low dielectric constant, large electromechanical coupling coefficient, high luminous transmittance, high catalytic activity, and intense infrared absorption [36]. The incorporation of such inorganic “nanofillers” can result e.g. in functional, transparent polymers [37] or in multifunctional, flexible composites with outstanding electrical, optical, and mechanical properties [38]. Hybrid mosaic particles were also generated without a conventional photoinitiator by making use of the photocatalytic activity of ZnO nanoparticles. Nanostructured polymeric particles were loaded *in situ* also with caffeine for release experiments. Their release profile was compared to that of spherical polymer particles loaded with caffeine also.

Photoinitiated polymerization enabled very high initiation rates which both contributes to the overall polymerization rate and plays a decisive role for nanostructuring. Moreover, the process of aerosol-photopolymerization can be driven at ambient temperature, which permits processing of temperature-sensitive materials. Aerosol-photopolymerization can be used as a single-step process or as a part of an integrated process for smart, functionalized nanoparticle generation for emerging applications.

## **2. Experimental Section**

### **2.1 Chemicals and Materials**

Methyl methacrylate (MMA, Sigma-Aldrich, 99 % purity) and butyl acrylate (BA, Sigma-Aldrich, 99 % purity) were employed as monomers. Irgacure 907 (Methyl-1[4-(methylthio)phenyl]-2-morpholinopropan-1-one, Sigma-Aldrich, 98 % purity) and 1,6-hexanediol diacrylate (HDDA, Alfa Aesar, 99 % purity) were chosen as the photoinitiator and crosslinker, respectively. Further materials involved are: Glycerol (Carl Roth GmbH Co. KG, > 99.5 purity), 2-ethylhexanol (Sigma-Aldrich, 99.6 % purity), absolute ethanol (Carl Roth GmbH Co. KG, > 99.9 purity), and zinc oxide nanoparticles (Sigma-Aldrich, 40 wt% in

ethanol, 30 nm average diameter and IBU-tec, 40 wt% in HDDA, 12 nm average diameter). Caffeine (Sigma-Aldrich, > 99 % purity) and ultrapure water (0.055  $\mu\text{S cm}^{-1}$ , Purelab Ultra) were used for caffeine release experiments from particles. All chemicals were used without further purification.

PTFE filter membranes with 50 nm average pore diameter were employed for dry particle collection from the aerosol. For caffeine release experiments, Spectra/Por<sup>®</sup> dialysis membranes (MWCO 25000) were used.

## 2.2 Setup

The continuous experimental setup consisting of two main components, an aerosol generator and a photoreactor in series, has been described before [35], and a schematic of the process flow is presented in **Figure 1**. The figure illustrates the generation of a droplet aerosol which is passed through the photoreactor where aerosol-photopolymerization converts the monomer droplets containing additives to nanostructured polymeric particles. In addition to the photoreactor equipped with a XeCl excimer UV irradiation source ( $\lambda_{\text{max}} = 308 \text{ nm}$ ) at the center, an alternative photoreactor with positive radiation geometry consisting of a cylindrical quartz glass tube (HSQ 300, 55 mm outer diameter, 490 mm length) surrounded by UV fluorescent tubes ( $\lambda_{\text{max}} = 312 \text{ nm}$ ) has been employed as well. Radiant exitance of the XeCl excimer irradiation source can be changed between 10 and 100% (100% corresponds to 10  $\text{mW cm}^{-2}$  at the envelope surface) by tuning the duty cycle, whereas radiant exitance for the photoreactor equipped with UV fluorescent irradiation sources (5  $\text{mW cm}^{-2}$  at the envelope surface for 3 tubes) is adjustable by varying the number of irradiation tubes.

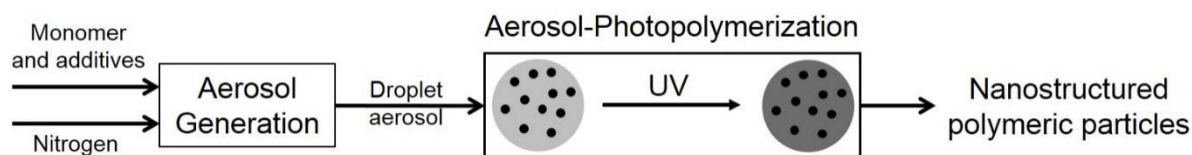


**Fig. 1.** Schematic of the process flow for aerosol-photopolymerization.

## 2.3 Characterization

Scanning electron microscopy (SEM) was performed on Hitachi S-4500 and LEO 1530. A droplet of the particle suspension was dropped onto a membrane (Whatman, Nucleopore Track-Etch Membrane, 200 nm pore width) or onto a silicon wafer. After drying, the particles were coated with a platinum-palladium mixture or platinum. Dry collected particles could be coated directly without the drying step. The coating thickness was 1-2 nm.

Transmission electron microscopy (TEM) was performed on a Philips CM 12 and a Zeiss TEM 912. The particles were brought on a TEM grid (Plano, S160-3, carbon film on 300 mesh grid). Particle collection was either dry from the aerosol phase onto a TEM grid or a

droplet of the suspension was brought onto a TEM grid after particle transfer from aerosol into water.

For microtoming, the dry sample was embedded in an acrylate dispersion for fixation, and the samples were cut at minus 140 °C. The pieces were 100-150 nm thick.

High pressure liquid chromatography analysis was used for the determination of caffeine concentration in water and glycerol concentration in ethanol employing an Agilent 1100 chromatographic system.

Scanning mobility particle sizer (SMPS, consisting of Electrostatic Classifier 3080, Differential Mobility Analyzer 3081, and Condensation Particle Counter 3775, TSI Corp.) was employed for the on-line measurement of particle size distributions in aerosols.

For BET characterization, the samples were first degased for 3h at 70 °C. Afterwards, the samples were filled up with helium at normal pressure and let to cool down to ambient temperature. Liquid nitrogen was used for the measurements during which an isothermal jacket served for the constant level of nitrogen.

### **3. Results and Discussion**

#### **3.1. Generation of Nanocaps**

After establishing the aerosol-photopolymerization process for the generation of spherical, nanoscale polymer particles [35], the same setup has been employed for the generation of nanostructured polymer particles. Both, nanocaps as non-spherical particles and mosaic particles as spherical, porous particles possessing nanostructured surface properties, were produced by this method.

The formulations for the production of spherical polymer particles did not require a solvent. The liquid monomer served as a solvent for the photoinitiator and crosslinker if added. More components were involved for nanocap synthesis. Apart from the monomer, crosslinker and photoinitiator, glycerol and a volatile solvent were employed for nanocap generation. For each experiment, two solutions were prepared and mixed to obtain the final solution to be sprayed via the aerosol generator. The first solution consisted of liquid monomer methyl methacrylate (MMA), photoinitiator (PI) Irgacure 907<sup>®</sup>, and the crosslinker 1,6-hexanediol diacrylate (HDDA). A second solution was prepared by dissolving glycerol in absolute ethanol. The two solutions were then mixed during stirring to obtain the final solution for the aerosol-photopolymerization experiments. Figure 2 illustrates SEM and TEM images of nanocaps produced. The particles were collected dry on a glass slides [Figure 2(a)] and wet in water containing no stabilizer [Figure 2(b)], which consequently leads to agglomeration. These nanocaps were generated by a formulation consisting of 5 wt% Irgacure 907 in MMA (1.4841 g Irgacure 907 / 30 mL MMA) and a HDDA amount of 10 vol% with respect to MMA (3 mL HDDA). Absolute ethanol was 31.6 wt% and glycerol 16.0 wt% in the final monomer formulation to be sprayed. This formulation was based on our preliminary results considering component solubility in ethanol (25 mL) and the intended use of glycerol (10 g) as a soft-maker [39]. The relatively high concentration of photoinitiator Irgacure 907 of 5 wt% was required to ensure a certain initiation rate, and HDDA amount was chosen such

that the overall polymerization rate would be sufficiently high for polymer formation during an aerosol mean residence time of about 1 min in the photoreactor. This solution to be sprayed is referred to as “standard formulation” for distinguishing in the following part from nanocaps synthesized with differing formulation compositions. The caps resulting from the “standard formulation” are named “standard nanocaps”.

MMA was polymerized in the presence of HDDA as a crosslinker during photopolymerization. Crosslinking affected the overall polymerization rate strongly so that the aerosol mean residence time during photoreactor passage was sufficient for the formation of stable, cap-shaped submicron particles. Due to the polydisperse droplet aerosol generation [35], the resulting particles possessed a polydisperse particle size distribution as well. All the particles possessed the same cap shape independent of their size, as visualized best by the agglomerate shown in Figure 2(b).

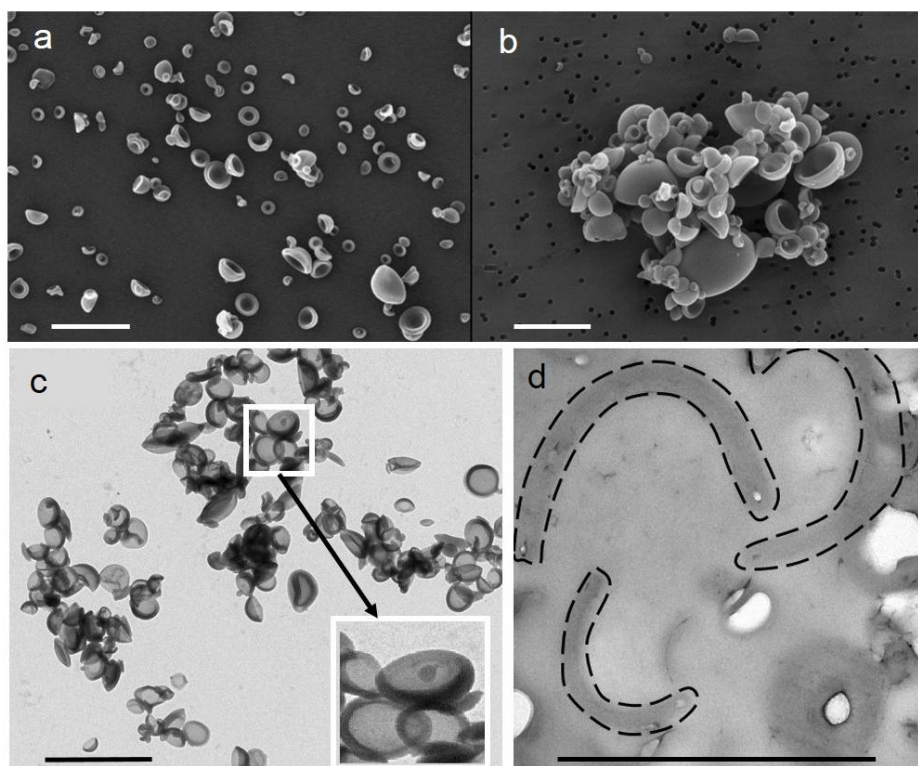


**Fig. 2.** Electron microscope images of “standard” nanocaps produced by aerosol-photopolymerization: (a) SEM image of nanocaps collected dry on glass, (b) SEM image of nanocaps collected wet in water, (c) TEM image of nanocaps collected wet in water, (d) TEM image of microtome cuts of nanocaps collected wet in water (dashed lines are drawn by us to focus on the longitudinal sliced pieces). The scale bars represent 2  $\mu\text{m}$ .

The selection of this MMA-HDDA monomer system was based on our previous results where different strategies were discussed for the polymer particle generation via aerosol-photopolymerization [35]. Depending on the crosslinking degree and monomer choice, various applications can be of interest such as polymer matrix preparation of adjusted mechanical stability or high swellability upon the use of different monomer ratios of the

comonomer system. Aerosol-photopolymerization can also be expanded for the generation of further polymeric matrices provided that a certain propagation rate coefficient is ensured, either by a highly reactive monomer or by a comonomer system possessing a high overall polymerization rate. Since the initiation rate can be varied by both the irradiance of the UV source and the photoinitiator concentration, there is the possibility of adjusting the overall polymerization rate.

The particle size distribution of nanocaps produced is polydisperse due to two-component nozzle employed in the aerosol generator. Figure 3 represents their distribution determined on-line in the aerosol phase via SMPS analysis. Being aware that the determined size distribution belongs to nanocaps which are non-spherical, it should be mentioned that the nanocap size distribution matches well to the size distribution of spherical nanoparticles produced with aerosol-photopolymerization as well [35]. Although monodisperse particles are usually favored for specific applications, the polydisperse character of the prepared nanocaps shows well that all of the particles in the produced size range possess indeed the same shapes disregarding their size. For monodisperse particles, there is the possibility of either generating monodisperse droplet aerosols with an appropriate aerosol generator or the polydisperse nanocaps can be classified “in flight” to quasi-monodisperse particles, e.g. by a differential mobility analyzer (DMA).

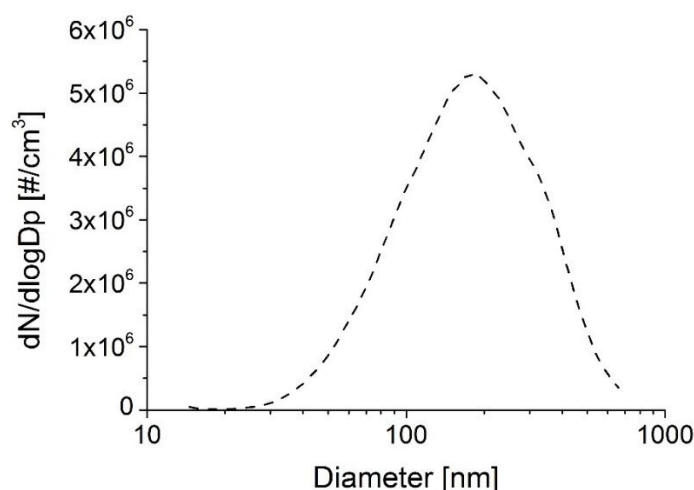


**Fig. 3.** Particle size distribution of “standard” nanocaps determined in the aerosol.

A TEM image of “standard nanocaps” collected in water is presented in Figure 2(c), and Figure 2(d) illustrates the same sample after microtoming. These cuts bear the idea that the nanocaps can be imagined as soccer balls from which the air has been sucked out leading to indentation. Upon a closer look at the image, a central line along the particle curvature can be observed, supporting the idea of controlled collapse of a polymeric shell.

For the formation of nanocaps by aerosol-photopolymerization, we propose a mechanism which is governed by the interplay of kinetic and thermodynamic phenomena. Spherical droplets are formed immediately after spraying the monomer solution. Such a droplet consisting of monomers and a highly evaporative solvent (e.g. ethanol), and photoinitiator and glycerol as the dissolved components, is homogeneous below the solubility limit of glycerol.

During the photoreactor passage, evaporation of the volatile solvent results in oversaturation of glycerol while (photo)polymerization leads to phase separation. Phase separation is thought to result in a polymer-rich phase within the outer sphere of the droplets whereas an ethanol-rich phase is concentrated in the inner part. Glycerol acts as a soft-maker for each sphere, enabling them to collapse in a controlled way before gelation results in a stable polymeric network. In other words, the presence of glycerol delays gelation during ethanol (non-solvent) evaporation. Polyols such as glycerol are plasticizers [39] that increase the plasticity or fluidity of a material for improved processing by enhancing flexibility and durability. They increase the free volume within the polymer chains and are responsible for lowering the glass transition temperature. In summary, the type of polymerization can be regarded as precipitation polymerization and the formation of caps can be described as an interplay between the rates of solvent evaporation and (photo)polymerization while glycerol acts as a softening agent enabling controlled collapse. This process bears great potential for the generation of various polymeric nanocaps regarding particle shape and properties by employing different plasticizers and solvents, optimization of polymerization initiation rate, polymerization kinetics, non-solvent evaporation rate, and the amount of plasticizer. Once photopolymerization occurs and the nanocaps containing glycerol are formed, they preserve their shapes even after glycerol extraction due to the already formed three dimensional molecular network within each particle. This was proven by suspending the dry collected nanocaps in ethanol and stirring at 25 °C for 70 h. HPLC measurements revealed glycerol extraction from nanocaps. About 60 % of the glycerol content of the original solution to be sprayed could be washed out in a single extraction step. The treated particles are visualized via SEM in Figure 4(a).

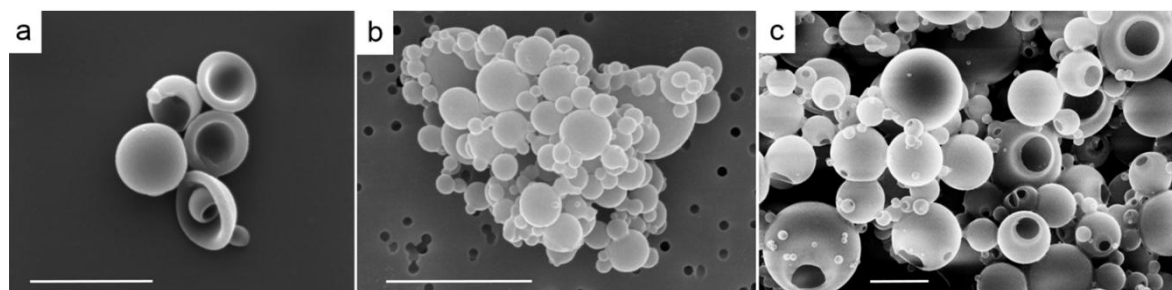


**Fig. 4.** SEM images of polymeric particles generated by aerosol-photopolymerization: (a) nanocaps after glycerol extraction, (b) spherical particles produced without employing glycerol, and (c) particles with HDDA as the sole monomer employed. The scale bars represent 2  $\mu\text{m}$ .

Formulations without glycerol resulted in spherical polymer particles, pointing out the necessity of a soft-maker to obtain cap-shaped structures. Figure 4(b) illustrates the resulting particles of the control experiment. The agglomerate consists of a number of spherical primary particles exclusively. Importance of the interplay between evaporation and photopolymerization can be illustrated by conducting the aerosol-photopolymerization experiments with the crosslinker HDDA as the sole monomer instead of using the established “standard” MMA-HDDA monomer mixture. Nanocaps were expected due to the presence of glycerol, however with varied shapes as a consequence of very fast crosslinking

polymerization reactions under consideration of the aforementioned mechanism proposed. As the SEM image of Figure 4(c) visualizes, the particles possess almost spherical shapes in contrast to standard nanocaps. However, all particles are nanostructured as evidenced by one lacuna in each sphere.

Further variations in formulation composition were also investigated to verify the proposed mechanism on cap formation. Increasing the glycerol concentration from 16.0 to 27.6 wt% (doubling glycerol mass in the solution to be sprayed) and decreasing it from 16.0 to 8.7 wt% (halving) led to caps too, but with slightly changed structures. Especially the larger caps from the experiment with less glycerol possessed more spherical shape in contrast to the “standard caps” where particles of all sizes had the same shape. Similarly, increasing the concentration of HDDA to 20 and 30 vol% with respect to methyl methacrylate resulted in caps having more spherical shapes as well. A possible explanation is the faster polymerization process which overcompensates the effect of ethanol (non-solvent) evaporation. The interim formation of nanocaps is suppressed by the fast development of a three dimensional polymer network. Therefore, a well-defined phase separation is a prerequisite for cap formation, in a way that polymer chains precipitate and stabilize the polymerizing droplet by accumulation in the outer sphere. The presence of glycerol contributes to moderate crosslinking and holds the polymeric shell elastic while ethanol evaporates. We conclude that all these concomitant processes account for cap formation. This complex mechanism depends on non-solvent evaporation, photoinitiation rate, overall polymerization rate, effect of retarded gelation, and phase separation via polymer formation.

Aerosol-photopolymerization experiments for nanocap generation were also conducted with different monomer and other volatile solvents. SEM images obtained after processing a formulation with the monomer butyl acrylate (BA) and ethanol as the solvent visualized “soft” poly(butyl acrylate) caps (not shown), most probably due to the sticky character of this polymer as a consequence of its low glass transition temperature. The glass transition temperature of PBA is -49 °C while that of PMMA is around 100 °C. 1-propanol and acetone were employed as alternative volatile solvents. The former possesses a higher and the latter a lower boiling point than ethanol. Basically, all experiments resulted in nanocaps without significant shape modifications.

Nanocaps consist of the polymeric part and glycerol if this is not removed from the caps afterwards. In order to bring more functionalities together, zinc oxide nanoparticles were incorporated into the nanocaps. ZnO has been chosen as a model inorganic compound with interesting properties as outlined in the Introduction. Therefore, combining multifunctionality with anisotropy (non-spherical particles, e.g. nanocaps) possesses potential applications for smart materials for emerging applications. A small amount of a commercial ZnO nanoparticle suspension (30 nm diameter, 40 wt% in ethanol) was added to the standard formulation for nanocap production. Zinc oxide nanoparticle concentrations in the formulation to be sprayed were 0.24, 0.70, and 1.40 wt%. The ZnO-loaded monomer formulation was sprayed by the aerosol generator. Afterwards, this generated droplet aerosol was passed through the photoreactor for *in situ* hybrid particle production via aerosol-photopolymerization. The resulting hybrid nanocaps possessed shapes like their non-hybrid pairs, as visualized in Figure 5(b). For comparison, spherical hybrid nanoparticles produced by the same technique of

aerosol-photopolymerization [40] is illustrated in Figure 5(a) as well. Neither glycerol nor ethanol were employed for spherical particle generation.

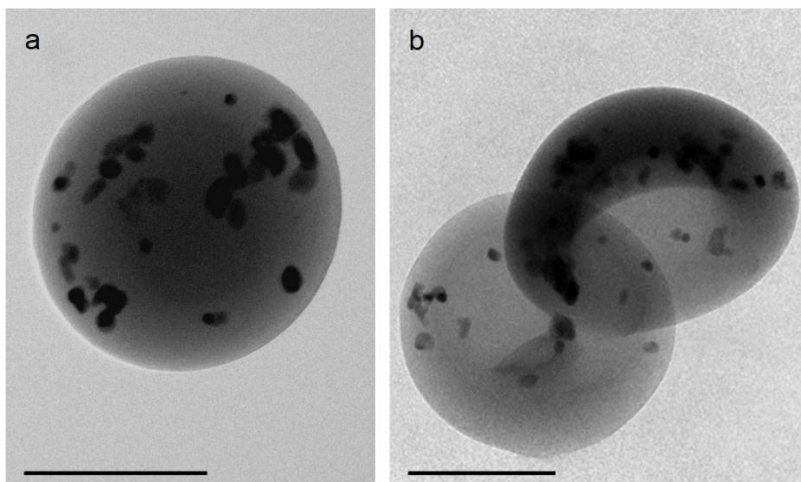


**Fig. 5.** TEM images of hybrid particles produced by aerosol-photopolymerization: (a) Spherical nanoparticles produced with 0.6 wt% ZnO in the formulation to be sprayed, (b) nanocaps produced with 0.7 wt% ZnO in the formulation to be sprayed. The scale bars represent 300 nm.

Unfortunately, no quantitative comparison has been done yet about the ZnO amounts in the prepared particles and formulations to be sprayed. Since the employed aerosol generator can spray particles having diameters up to 1-3  $\mu\text{m}$ , ZnO nanoparticles with 30 or 12 nm diameter are expected to follow the monomer stream practically free of inertia. This excludes a non-uniform spraying process and prevents ZnO accumulation within the formulation to be sprayed. Therefore, ZnO amount in both the formulation and generated particles is expected to be the same disregarding monomer evaporation during spraying and photoreactor passage.

We expect that aerosol-photopolymerization offers the generation of nanocaps with a variety of incorporated materials. Like in the case of zinc oxide, nanoparticles can be incorporated into the polymer matrix once they are homogeneously dispersed and stabilized in the monomer solution to be sprayed. Non-particulate substances which can be dissolved in the monomer solution can also be incorporated into the polymer matrix to create multiple functionalities. As an example, caffeine-loaded nanocaps were generated successfully by employing aerosol-photopolymerization. Also, spherical polymer nanoparticles loaded with caffeine were produced. For polymer particle loading and release, caffeine has been chosen as a non-toxic substance being a central nervous system stimulant for humans warding off drowsiness and restoring alertness. Due to its high recovery from molecularly imprinted polymers (MIPs) produced via free radical polymerization [41], it does not covalently bind to polymers and probably gets not modified. Therefore, polymer particles loaded with this substance via aerosol-photopolymerization represent a model system for controlled release experiments. A well-distribution of caffeine within the polymer particles is expected similar to the work of Mallikarjuna et al. [42] deducting molecularly dispersed distribution of the drug in the polymer matrix via free radical polymerization for *in situ* loading. SEM images of caffeine-loaded spheres and nanocaps are illustrated in Figure 6(a) and (b). After the particles

were collected dry on a filter membrane, 20 mg of caffeine-loaded polymer particles were placed into a dialysis membrane which was immersed in 200 mL water to determine the caffeine evolution in water with time. Both, nanocaps and spherical particles, were loaded *in situ* with caffeine upon spraying monomer formulations with 0.5 wt% caffeine. Since the nanocaps can be imagined in a first approximation as quasi-2-dimensional discs, they were expected to release caffeine faster than the spherical nanoparticles. HPLC analyses revealed contrary results. A faster caffeine release profile for spherical particles was obtained, as depicted in Figure 6(c). Also the total amount of caffeine released was higher from spherical polymers. Under the consideration of equally loaded particles, the different caffeine release behavior can be related to the presence of glycerol. It appears that glycerol is able to retain caffeine in the polymeric phase. This gives the idea of manipulating drug release behavior by the addition of auxiliaries.

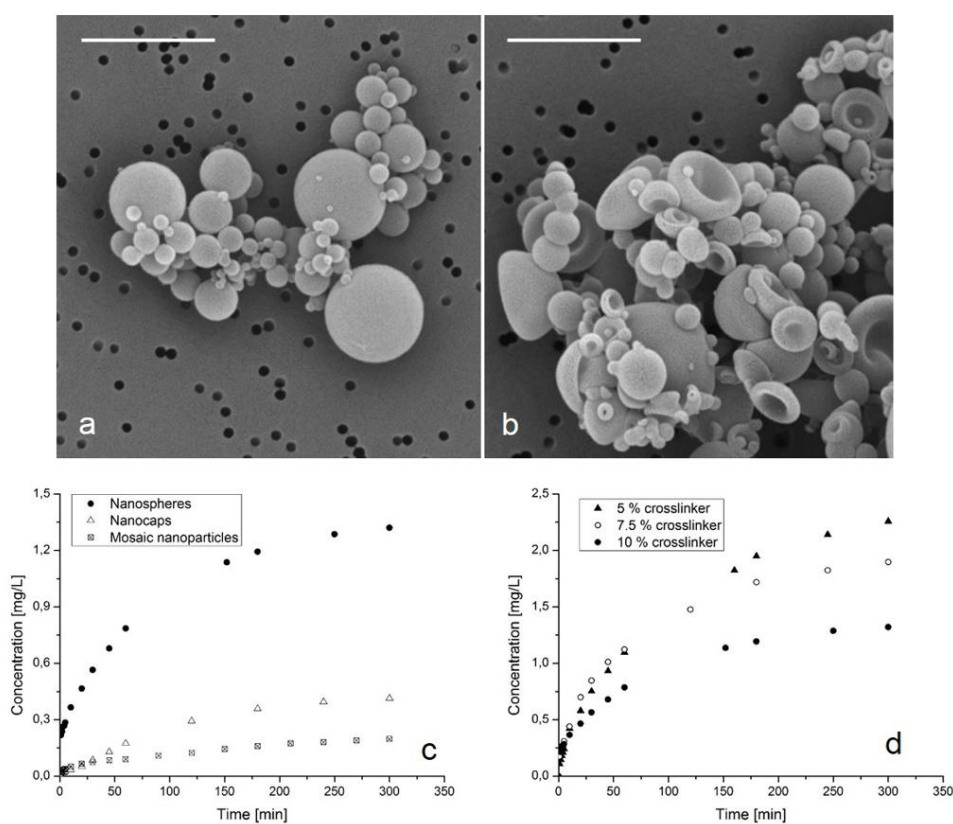


**Fig. 6.** Caffeine-loaded polymeric nanoparticles generated by aerosol-photopolymerization: (a) SEM image of spherical nanoparticles, (b) SEM image of nanocaps, (c) caffeine release profiles of nanocaps, nanospheres and mosaic nanoparticles, (d) caffeine release profiles of nanospheres with different crosslinking degrees. The scale bars represent 2 μm.

The degree of crosslinking in polymer particles can affect the duration of drug release [43]. Spherical PMMA particles loaded with caffeine but with different amounts of the crosslinker HDDA in the formulation to be sprayed were generated by aerosol-photopolymerization in order to compare their caffeine release profiles. Crosslinker amount is the volume percent of HDDA related to MMA. Figure 6(d) depicts the different release profiles. The higher the crosslinker amount, the slower the release of caffeine from the polymeric material. This is

explained by higher degrees of crosslinking, which corresponds to a smaller mesh size and retarded drug (caffeine) percolation through the polymer. This is in agreement with the observations of Rokhade et al. [44] who illustrated this by means of the controlled release of theophylline, which is a de-methylated (position 7) derivative of caffeine, and also with the observations of Mallikarjuna et al. [42] who demonstrated that drug release slows down with increasing amount of crosslinking agent.

### 3.2 Generation of Porous Nanoparticles (Mosaic Nanostructures)

Apart from non-spherical particles, spherical porous nanoparticles which we named mosaic particles were generated by aerosol-photopolymerization as well. The crosslinker HDDA was employed as the sole monomer in which the photoinitiator Irgacure 907 was dissolved. Only a single additional component was added to this monomer-photoinitiator mixture to introduce nanostructuring. In contrast to the experiments where nanocaps were formed, a non-volatile solvent instead of ethanol was employed. This non-solvent has to be miscible with the monomer solution before spraying but should be immiscible with the formed polymer afterwards.

Aerosol-photopolymerization experiments were conducted by employing a photoinitiator concentration of 1 wt% in a solution consisting of HDDA and Irgacure 907. Volume ratio of the crosslinker HDDA to the non-solvent 2-ethylhexanol in the formulation to be sprayed was varied first. Figure 7(a) illustrates a TEM image of particles produced with a 2-ethylhexanol-to-HDDA ratio of 1:6, leading to expected spherical particles. Such an amount of non-solvent is insufficient to provoke phase separation [27]. Increasing the volume ratio to 1:3 (non-solvent : monomer) still resulted in spherical particles possessing smooth surface properties, as visualized in Figure 7(b). Slightly structured particles (with moderate surface roughness) were obtained by spraying a formulation with a ratio of 2:3 [(Figure 7(c)] which can be regarded as a threshold value for surface nanostructuring, and by increasing this further to 1:1, nanostructured mosaic particles [(Figure 7(d)] were obtained after photoreactor passage. The particles look like consisting of an assembly of polymer globules interconnected to each other. The change of specific surface area with the volume ratio of non-solvent to the crosslinker monomer is illustrated in Table 1.

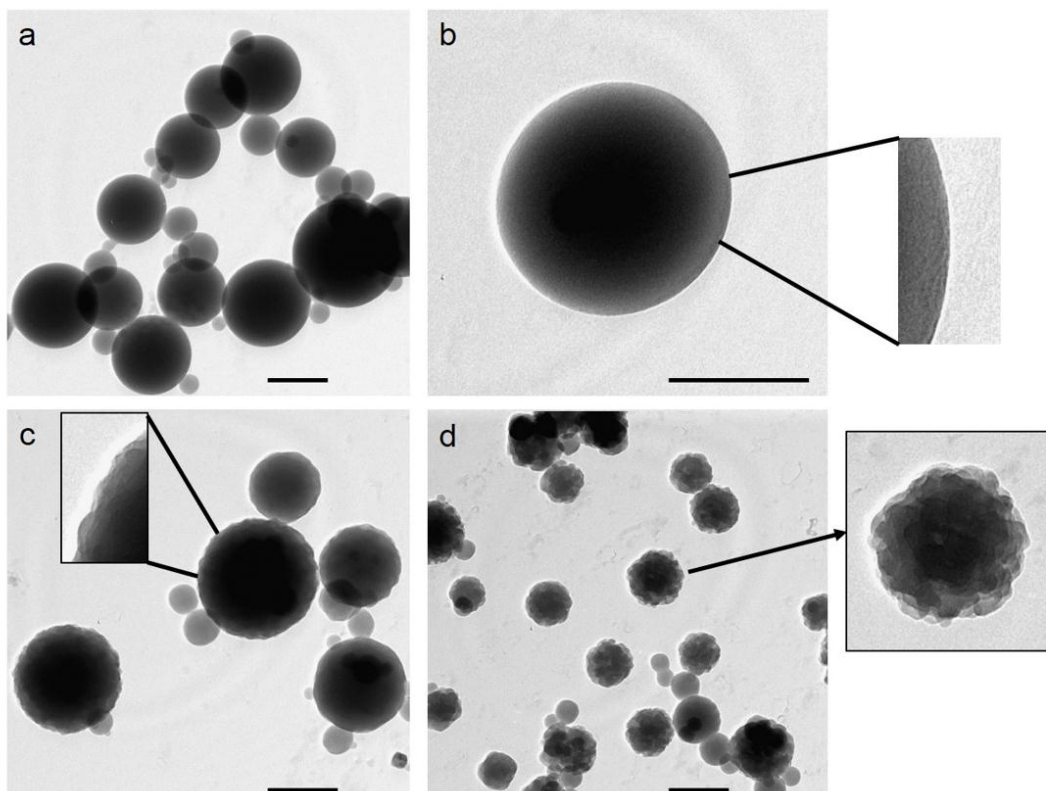


**Fig. 7.** TEM images of polymeric particles generated with varying volume ratios of 2-ethylhexanol to HDDA by aerosol-photopolymerization: (a) 1:6, (b) 1:3, (c) 2:3, (d) 1:1. The scale bars represent 200 nm.

The specific surface area of the spherical polymer particles produced with HDDA and photoinitiator in the formulation to be sprayed, but without any non-solvent (porogen), is practically the same as that of the particles prepared with a porogen-to-HDDA ratio of 1:6. A substantial increase in the specific surface area can be observed when the amount of porogen is further increased. Depending on their specific surface area and pore size distribution, mosaic particles might find applications e.g. as column material for separation techniques or as supports for active catalyst materials. Due to their nanostructured surface, they can be employed for obtaining controlled wetting properties for coatings industry, microelectronics, biotechnology, and medicine.

**Table 1.** Variation of specific surface area with porogen amount.

Volume ratio of 2-ethylhexanol to HDDA	Specific surface area
$\text{mL mL}^{-1}$	$\text{m}^2 \text{g}^{-1}$
0:6	3.6
1:6	3.5
2:6	7.1
3:6	19.0
6:6	34.9

An SEM image of the “mosaic particles” generated with the non-solvent 2-ethylhexanol (volume of non-solvent : volume of HDDA = 1:1) is depicted in Figure 8(a). The particles were collected in water where no stabilizing agent was employed, which resulted in physically loosely connected particles forming agglomerates. The nanostructured mosaic particles were obtained independent of their size within the size distribution produced by the aerosol generator, as in the case of polydisperse nanocaps.

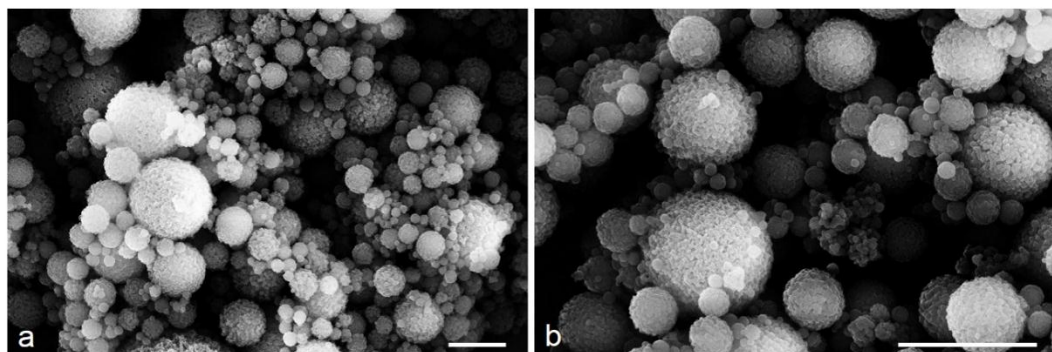


**Fig. 8.** SEM images of nanostructured mosaic particles generated with different non-solvents by aerosol-photopolymerization: (a) 2-ethylhexanol, (b) hexadecane. The scale bars represent 2  $\mu\text{m}$ .

As an alternative non-solvent to 2-ethylhexanol, hexadecane was tested by keeping the volume ratio of 1:1, required for phase separation, constant. Figure 8(b) shows the resulting porous particles looking quite similar to those generated with 2-ethylhexanol [(Fig. 8(a)]. This is in agreement with Sherrington [27] where the amount of non-solvent (porogen) is stated to be crucial. A phenomenon to be mentioned might be the effect of non-solvents on the polymerization rate. Morrison et al. [45] reported that solvents such as ethanol or methanol have no observable effects on the propagation rate coefficient ( $k_p$ ) of methyl methacrylate (MMA). They increased the solvent amount until phase separation took place. In our case, phase separation is required for pore/domain formation. Therefore, the amount of 2-ethylhexanol or hexadecane has to be considerable to adjust the onset of phase separation, which might indeed effect the polymerization rate. On the other hand, the employed monomer HDDA is a multifunctional monomer whose  $k_p$  is accordingly high [46] and might remain practically unaffected by the presence of a non-solvent.

Mosaic nanoparticles are composed of interconnected polymer globules which are proposed to originate from primary radicals upon photoinitiator cleavage. To verify this, photoinitiator concentration in the formulation to be sprayed was varied. The experiments were performed with the porogen 2-ethylhexanol (volume of non-solvent : volume of HDDA = 1:1) and photoinitiator concentrations of 9 and 0.11 wt%. Both of the experiments resulted in nanostructured particles, but with different morphologies as depicted in Figure 9. The particles produced with 9 wt% photoinitiator possess not as much macroporous voids as the ones generated with 0.11 wt% photoinitiator. This supports our hypothesis that photoinitiator cleavage starts the polymerization of each domain. Fewer photoinitiator molecules can start fewer number of chains, leading to larger globules among which larger voids are present within each particle. Therefore, by adjusting the number of initiating spots disregarding

termination and chain transfer reactions, particles with favored porosity or specific surface area can be obtained via manipulating the size of the globules in an assembly (particle). It is of importance to mention that a photoinitiator concentration of 9 wt% is relatively high and demonstrates an upper limit due to the formation of oligomeric species by chain termination. Similarly, a photoinitiator concentration of 0.11 wt% exhibits roughly a lower limit for the production of a stable polymeric assembly within the average aerosol residence time of about a minute.

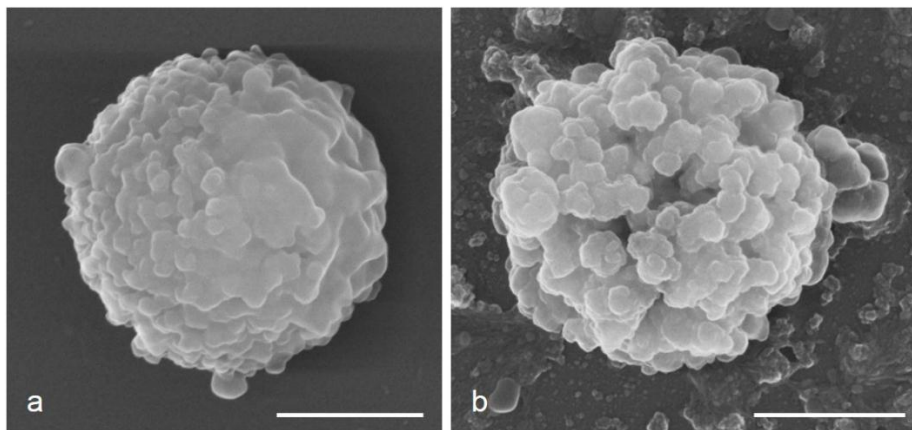


**Fig. 9.** SEM images of nanostructured mosaic particles generated with different photoinitiator concentrations in the formulation to be sprayed: (a) 9 wt%, (b) 0.11 wt%. The scale bars represent 500 nm.

Experiments performed with a monomer mixture consisting of MMA and HDDA (10 vol% with respect to MMA), and 2-ethylhexanol as the non-solvent (volume of non-solvent : volume of monomer = 1:1) did not result in “mosaic” particles, pointing out the importance of very fast crosslinking reactions. Therefore, it is not only the amount of non-solvent which contributes to the structured, mosaic particle formation. Nevertheless, higher amounts of HDDA in the MMA-HDDA mixture may lead to porous particles. Preliminary results on the aerosol-photopolymerization of butyl acrylate with HDDA (30 vol%) revealed nanostructured particles, which may be attributed to the high propagation rate coefficient of butyl acrylate [47] being in the order of the propagation rate coefficient of HDDA [48]. Copolymerization of monofunctional monomers and crosslinkers with regard to porous particle synthesis will be further investigated by our group. A formulation combining a crosslinking monomer only and a significant amount of non-solvent results in nanostructured particles by aerosol-photopolymerization. The large amount of non-solvent is required for fast phase separation and crosslinking reactions lead to a three dimensional polymer network formation in a monomer droplet within the corresponding time domain of aerosol-photopolymerization which is shorter than 1 min. It should be mentioned that photopolymerization of multifunctional monomers can occur even within a few seconds [49].

Caffeine-loaded porous mosaic particles were generated *in situ* by aerosol-photopolymerization. 0.5 wt% caffeine was dissolved in the formulation to be sprayed, and the release profile from the obtained particles was compared to that of spherical nanoparticles and

nanocaps. Figure 6(c) depicts a slower release from mosaic particles than from both nanocaps and spherical nanoparticles. However, mosaic particles are prepared by the crosslinker HDDA as the sole monomer. The delay of caffeine release may be attributed to suppressed percolation.

For a comprehensive understanding of the caffeine release profiles, glass transition temperatures of the three different structured particle collectives were compared. HDDA-crosslinked PMMA spheres possess a glass transition temperature of 98 °C, porous mosaic particles 94 °C, and nanocaps 91 °C. These close values suggest that not only the microstructure (crosslinking) of the particles, but also the macrostructure (nanoparticle geometry) and additives if employed can play a decisive role for drug release. While the slowest release profile belonging to mosaic particles can be explained by the use of the crosslinker monomer HDDA as the sole monomer, less crosslinked caps and spheres can be compared by means of glycerol. Although nanocaps have a higher surface-to-volume ratio in comparison to nanospheres, the presence of glycerol is expected to slow down the release rate of caffeine. Additives can contribute to the solubility of drugs within the polymer particle which would alter the release profile. Further research may help to clarify these issues more in detail, which is why we intensified collaborations with NMR research groups.

Since the release rate of caffeine from spherical nanoparticles, nanocaps, and mosaic nanoparticles can be varied by both the degree of crosslinking and particle structure, these can contribute to secondary functionalization of such particles. For instance, anisotropic particles like nanocaps could be employed for responses under flow conditions during which a specific cargo can be discharged. Substance-loaded porous particles might have attractive applications as well. Soaking of solutions into these particles can be manipulated via pore size adjustments, and the pre-incorporated materials within the porous particles could react or interact with the soaking substances.

As in the case of nanocaps, mosaic particles were also generated in the presence of zinc oxide nanoparticles. A formulation with 1 wt% Irgacure 907 and 1 wt% ZnO nanoparticles resulted in hybrid mosaic particles by aerosol-photopolymerization, as presented in Figure 10(a). The ratio of 2-ethylhexanol to HDDA was again 1:1. The inorganic nanoparticles were well-dispersed in the formulation to be sprayed and photopolymerization resulted in *in situ* generation of hybrid porous particles. Since any stable suspension consisting of crosslinker, photoinitiator, non-solvent, and nanoparticles can be processed by aerosol-photopolymerization, this technique bears great potential for the production of mosaic particles with a variety of material combinations.

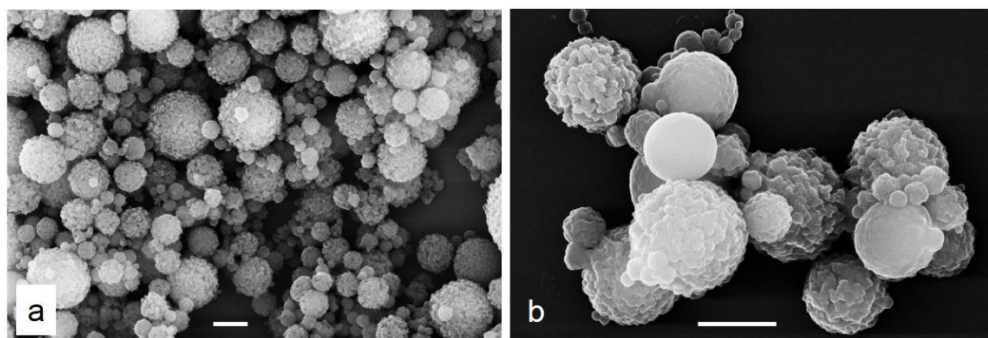


**Fig. 10.** SEM images of nanostructured mosaic particles generated in the presence of ZnO nanoparticles by aerosol-photopolymerization: (a) 1 wt% ZnO and 1 wt% Irgacure 907, (b) 1 wt% ZnO and without Irgacure 907. The scale bars represent 1  $\mu\text{m}$ .

Hybrid mosaic particles were also generated without employing the conventional photoinitiator Irgacure 907 in the formulation to be sprayed by making use of the photocatalytic activity of zinc oxide nanoparticles under UV irradiation. This represents a strategy for the preparation of particles containing less impurities considering photoinitiator residues. Zinc oxide nanoparticles were capable of starting photopolymerization reactions upon excitation.[40] Since the spray solutions of all experiments with ZnO as photoinitiator were containing alcohol (2-ethylhexanol as porogen), a mechanism is expected as proposed by Hoffman et al. [50] for MMA polymerization. They suggest that the reaction pathway appears to involve hole scavenging by the alcohol and anionic initiation via conduction band electrons followed by free radical propagation steps. In addition, it should be noticed that the oxidized alcohol (hole scavenger) might initiate the polymerization as well, either by addition to the vinyl double bond or by redox reaction with the monomer. Figure 10(b) shows an SEM image of hybrid mosaic particles produced without a conventional photoinitiator. The image visualizes that most of the particles are nanostructured and a few possess smoother surface characteristics. This observation might be explained by different initiation mechanisms on ZnO nanoparticles which can arise from non-uniform aerosol droplet trajectories. The control experiment with a formulation containing only HDDA and 2-ethylhexanol did not produce any particles, pointing out that ZnO nanoparticles are capable of initiating the polymerization reactions. Consequently, they are incorporated into the produced polymeric mosaic particles.

The production rate of aerosol-photopolymerization depends on the choice of substances and the adjusted process parameters. Though, 400  $\text{mg h}^{-1}$  can be given as an average, representative value for the preparation of nanostructured particles. However, aerosol-photopolymerization both as a unit operation which is fast and flexible and as a part of an integrated process chain, bears great potential for the generation of various nanostructures for emerging applications. Especially the integration of inorganic materials into nanostructured polymer particles possessing different shapes offers a wide spectrum of product application. The advantages of the aerosol processing route combined with photoinitiated aerosols are the generation of highly pure materials in a continuous process which can be conducted at ambient temperature.

## 4. Conclusions

To our best knowledge, the generation of nanoscale non-spherical polymer particles (nanocaps) and spherical porous polymer particles (mosaic nanoparticles) by aerosol-photopolymerization has been introduced for the first time. Both structures were synthesized independent of the particle size within the size distribution resulting from the aerosol generation process. Nanocap formation has been discussed on the basis of an interplay between the rates of photopolymerization and evaporation of the volatile solvent, and the onset of phase separation while glycerol acts as the softening agent. Variations in the solution to be sprayed resulted in structure modifications of the produced nanocaps. Aerosol-photopolymerization is unique for nanocap production due to the possibility of controlled non-solvent evaporation to the gas phase in a continuous process. Porous, mosaic nanoparticles have also been generated and discussed to result from an interplay between polymer network formation rate and onset of phase separation within the polymerizing droplets. The presence of a non-volatile non-solvent (porogen) is essential and its amount is crucial for phase separation. As the reactions proceed and polymeric domains are formed, they are crosslinked eventually to each other through the polymerization of the rest monomer dissolved in the porogen-rich phase.

Photochemistry in an aerosol-based system is shown to be a suitable tool for nanostructured particle synthesis via efficient and fast initiation reactions. It is a flexible and efficient tool for the polymerization within the time domain of aerosol-photopolymerization. Furthermore, the aerosol-based experimental setup can be driven as a continuous process at ambient temperature.

For the generation of multifunctional nanostructured particles, *in situ* hybridization of nanocaps and mosaic particles with zinc oxide nanoparticle as model compound was successfully tested. In addition, the conventional photoinitiator can be substituted by ZnO nanoparticles for the preparation of hybrid mosaic particles. Caffeine-loaded nanocaps and mosaic particles were also *in situ* generated to compare their caffeine release profiles with caffeine-loaded spherical nanoparticles which are also produced by aerosol-photopolymerization. The results give an insight of the effect of glycerol and crosslinking degree on the caffeine release behavior. Incorporation of ZnO or caffeine into nanostructured polymeric particles represents an example for combining different functionalities. The process of aerosol-photopolymerization offers authentic potential for the incorporation of further inorganic nanoparticles and molecularly dissolved compounds into the nanostructured polymeric particles to create smart materials.

## Acknowledgements

This project is part of a joint initiative of KIT and BASF SE. Financial support by the Ministry of Science, Research and the Arts of Baden-Wuerttemberg (Az. 33-729.61-3) is gratefully acknowledged. We thank Dr. Peter Weidler (Institute of Functional Interfaces, KIT) and Sabina Hug (Engler-Bunte Institute, Division Fuel Chemistry and Technology, KIT) for BET measurements, the Institute of Mechanical Process Engineering and Mechanics at KIT

for providing the SMPS equipment, Mr. Fotouhi and Mr. Zibat (Laboratory for Electron Microscopy, KIT) for TEM and SEM characterization, and Nina Merkel (Institute of Technical Thermodynamics and Refrigeration, KIT) for DSC measurements.

## References

1. Shum, H.C., et al., *Droplet Microfluidics for Fabrication of Non-Spherical Particles*. Macromolecular Rapid Communications, 2010. **31**(2): p. 108-118.
2. Gupta, S., et al., "*Self-corralling*" nanorods under an applied electric field. Nano Letters, 2006. **6**(9): p. 2066-2069.
3. Hwang, D.K., D. Dendukuri, and P.S. Doyle, *Microfluidic-based synthesis of non-spherical magnetic hydrogel microparticles*. Lab on a Chip, 2008. **8**(10): p. 1640-1647.
4. Donev, A., et al., *Improving the density of jammed disordered packings using ellipsoids*. Science, 2004. **303**(5660): p. 990-993.
5. Yoshida, M., K.-H. Roh, and J. Lahann, *Short-term biocompatibility of biphasic nanocolloids with potential use as anisotropic imaging probes*. Biomaterials, 2007. **28**(15): p. 2446-2456.
6. Tao, L., et al., *Shape-specific polymeric nanomedicine: emerging opportunities and challenges*. Experimental Biology and Medicine, 2011. **236**(1): p. 20-29.
7. Bonderer, L.J., A.R. Studart, and L.J. Gauckler, *Bioinspired design and assembly of platelet reinforced polymer films*. Science, 2008. **319**(5866): p. 1069-1073.
8. Glotzer, S.C. and M.J. Solomon, *Anisotropy of building blocks and their assembly into complex structures*. Nature Materials, 2007. **6**(8): p. 557-562.
9. Lu, Y., Y.D. Yin, and Y.N. Xia, *Three-dimensional photonic crystals with non-spherical colloids as building blocks*. Advanced Materials, 2001. **13**(6): p. 415-420.
10. Florez, L., et al., *How Shape Influences Uptake: Interactions of Anisotropic Polymer Nanoparticles and Human Mesenchymal Stem Cells*. Small, 2012. **8**(14): p. 2222-2230.
11. Sharma, G., et al., *Polymer particle shape independently influences binding and internalization by macrophages*. Journal of Controlled Release, 2010. **147**(3): p. 408-412.
12. Dendukuri, D., et al., *Controlled synthesis of nonspherical microparticles using microfluidics*. Langmuir, 2005. **21**(6): p. 2113-2116.

13. De Geest, B.G., et al., *Synthesis of monodisperse biodegradable microgels in microfluidic devices*. Langmuir, 2005. **21**(23): p. 10275-10279.
14. Jeong, W.J., et al., *Continuous fabrication of biocatalyst immobilized microparticles using photopolymerization and immiscible liquids in microfluidic systems*. Langmuir, 2005. **21**(9): p. 3738-3741.
15. Seo, M., et al., *Continuous microfluidic reactors for polymer particles*. Langmuir, 2005. **21**(25): p. 11614-11622.
16. Nie, Z.H., et al., *Polymer particles with various shapes and morphologies produced in continuous microfluidic reactors*. Journal of the American Chemical Society, 2005. **127**(22): p. 8058-8063.
17. Shepherd, R.F., et al., *Microfluidic assembly of homogeneous and janus colloid-filled hydrogel granules*. Langmuir, 2006. **22**(21): p. 8618-8622.
18. Dendukuri, D. and P.S. Doyle, *The Synthesis and Assembly of Polymeric Microparticles Using Microfluidics*. Advanced Materials, 2009. **21**(41): p. 4071-4086.
19. Alargova, R.G., et al., *Scalable synthesis of a new class of polymer microrods by a liquid - Liquid dispersion technique*. Advanced Materials, 2004. **16**(18): p. 1653-+.
20. Yang, Z.Q., et al., *Shape-memory nanoparticles from inherently non-spherical polymer colloids*. Nature Materials, 2005. **4**(6): p. 486-490.
21. Staff, R.H., et al., *Preparation and Characterization of Anisotropic Submicron Particles From Semicrystalline Polymers*. Macromolecular Chemistry and Physics, 2012. **213**(3): p. 351-358.
22. Park, J.-G., J.D. Forster, and E.R. Dufresne, *High-Yield Synthesis of Monodisperse Dumbbell-Shaped Polymer Nanoparticles*. Journal of the American Chemical Society, 2010. **132**(17): p. 5960-+.
23. Arico, A.S., et al., *Nanostructured materials for advanced energy conversion and storage devices*. Nature Materials, 2005. **4**(5): p. 366-377.
24. Bin, X., E.H. Sargent, and S.O. Kelley, *Nanostructuring of Sensors Determines the Efficiency of Biomolecular Capture*. Analytical Chemistry, 2010. **82**(14): p. 5928-5931.
25. Lewandowski, K., F. Svec, and J.M.J. Frechet, *Preparation of macroporous, monodisperse, functionalized styrene-divinylbenzene copolymer beads: Effect of the nature of the monomers and total porogen volume on the porous properties*. Journal of Applied Polymer Science, 1998. **67**(4): p. 597-607.

26. Macintyre, F.S. and D.C. Sherrington, *Control of porous morphology in suspension polymerized poly(divinylbenzene) resins using oligomeric porogens*. *Macromolecules*, 2004. **37**(20): p. 7628-7636.
27. Sherrington, D.C., *Preparation, structure and morphology of polymer supports*. *Chemical Communications*, 1998(21): p. 2275-2286.
28. Gokmen, M.T. and F.E. Du Prez, *Porous polymer particles-A comprehensive guide to synthesis, characterization, functionalization and applications*. *Progress in Polymer Science*, 2012. **37**(3): p. 365-405.
29. Wu, D., et al., *Design and Preparation of Porous Polymers*. *Chemical Reviews*, 2012. **112**(7): p. 3959-4015.
30. Hack, B., et al., *Advanced Agrochemical Formulations through Encapsulation Strategies?* *Chemie Ingenieur Technik*, 2012. **84**(3): p. 223-234.
31. Peer, D., et al., *Nanocarriers as an emerging platform for cancer therapy*. *Nature Nanotechnology*, 2007. **2**(12): p. 751-760.
32. Faraji, A.H. and P. Wipf, *Nanoparticles in cellular drug delivery*. *Bioorganic & Medicinal Chemistry*, 2009. **17**(8): p. 2950-2962.
33. Champion, J.A., Y.K. Katare, and S. Mitragotri, *Particle shape: A new design parameter for micro- and nanoscale drug delivery carriers*. *Journal of Controlled Release*, 2007. **121**(1-2): p. 3-9.
34. Reis, C.P., et al., *Nanoencapsulation I. Methods for preparation of drug-loaded polymeric nanoparticles*. *Nanomedicine-Nanotechnology Biology and Medicine*, 2006. **2**(1): p. 8-21.
35. Akguen, E., J. Hubbuch, and M. Woerner, *Perspectives of aerosol-photopolymerization: Nanoscale polymer particles*. *Chemical Engineering Science*, 2013. **101**: p. 248-252.
36. Xiong, M.N., et al., *Preparation and characterization of poly(styrene butylacrylate) latex/nano-ZnO nanocomposites*. *Journal of Applied Polymer Science*, 2003. **90**(7): p. 1923-1931.
37. Althues, H., J. Henle, and S. Kaskel, *Functional inorganic nanofillers for transparent polymers*. *Chemical Society Reviews*, 2007. **36**(9): p. 1454-1465.
38. Balazs, A.C., T. Emrick, and T.P. Russell, *Nanoparticle polymer composites: Where two small worlds meet*. *Science*, 2006. **314**(5802): p. 1107-1110.
39. Kesselring, A. and T. Koebnitz, *WO 2002006131 A1*. WO 2002006131 A1.

40. Akguen, E., J. Hubbuch, and M. Woerner, *Perspectives of Aerosol-Photopolymerization: Organic-inorganic hybrid nanoparticles*. Colloid Polym Sci, 2014. **292**: p. 1241-1247.
41. Villamena, F.A. and A.A. De La Cruz, *Caffeine selectivity of divinylbenzene crosslinked polymers in aqueous media*. Journal of Applied Polymer Science, 2001. **82**(1): p. 195-205.
42. Mallikarjuna, B., et al., *Development of Triprolidine-Hydrochloride-Loaded pH-Sensitive Poly(Acrylamide-co-Acrylamidoglycolic Acid) Co-Polymer Microspheres: In Vitro Release Studies*. Designed Monomers and Polymers, 2011. **14**(5): p. 445-459.
43. Kawaguchi, H., *Functional polymer microspheres*. Progress in Polymer Science, 2000. **25**(8): p. 1171-1210.
44. Rokhade, A.P., et al., *Novel interpenetrating polymer network microspheres of chitosan and methylcellulose for controlled release of theophylline*. Carbohydrate Polymers, 2007. **69**(4): p. 678-687.
45. Morrison, B.R., et al., *Solvent Effects on the Propagation Rate Coefficient for Free-Radical Polymerization*. Macromolecules, 1993. **26**(16): p. 4368-4372.
46. Tryson, G.R. and A.R. Shultz, *Calorimetric Study of Acrylate Photo-polymerization*. Journal of Polymer Science Part B-Polymer Physics, 1979. **17**(12): p. 2059-2075.
47. Beuermann, S., et al., *Determination of free-radical propagation rate coefficients of butyl, 2-ethylhexyl, and dodecyl acrylates by pulsed-laser polymerization*. Macromolecules, 1996. **29**(12): p. 4206-4215.
48. Lalevee, J., X. Allonas, and J.P. Fouassier, *Direct measurements of the addition and recombination of acrylate radicals: Access to propagation and termination rate constants?* Journal of Polymer Science Part a-Polymer Chemistry, 2006. **44**(11): p. 3577-3587.
49. Decker, C., *Light-induced crosslinking polymerization*. Polymer International, 2002. **51**(11): p. 1141-1150.
50. Hoffman, A.J., et al., *Photoinitiated Polymerization of Methyl-methacrylate Using Q-sized ZnO Colloids*. Journal of Physical Chemistry, 1992. **96**(13): p. 5540-5546.

---

# Defined Polymer Shells on Nanoparticles via a Continuous Aerosol-Based Process

Stephanie Sigmund<sup>1\* $\gamma$</sup> , Ertan Akgün<sup>2 $\gamma$</sup> , Jörg Meyer<sup>1</sup>, Jürgen Hubbuch<sup>2</sup>, Michael Wörner<sup>2\*</sup>, Gerhard Kasper<sup>1</sup>

---

*1: Mechanical Process Engineering and Mechanics, Karlsruhe Institute of Technology*

*2: Process Engineering in Life Sciences, Karlsruhe Institute of Technology*

*$\gamma$ : These authors contributed equally*

*\* Corresponding authors: Stephanie Sigmund ([stephanie.sigmund@kit.edu](mailto:stephanie.sigmund@kit.edu))*

*Michael Wörner ([michael.woerner@kit.edu](mailto:michael.woerner@kit.edu))*

Nanoparticle Research, 16, 2533, 2014

The final publication is available on:

<http://rd.springer.com/article/10.1007/s11051-014-2533-9#>

## **Abstract**

A continuous, aerosol-based process is described for the encapsulation of nanoparticles with a thin polymer shell. The process is essentially based on directed, binary collisions between gas-borne core particles and liquid monomer droplets carrying opposite electrical charges, followed by photo-initiated polymerization. Once the two streams are mixed together, the process runs to completion on a time scale of about 2 minutes or less, required for coagulation and polymerization.

Gold, silica, and sodium chloride nanoparticles were successfully coated by this technique with PHDDA (poly(hexanediol diacrylate)) and/or crosslinked PMMA (poly(methyl methacrylate)). It was found that all core materials as well as agglomerates were wettable at room temperature and that the spreading kinetics of the monomer were fast enough to cover the core particles uniformly within the time scale provided for coagulation. The shell thickness depends on the volume ratio between core particles and monomer droplets. This was demonstrated for a combination of monodisperse silica spheres ( $d = 241$  nm) and polydisperse methyl methacrylate (MMA) droplets, resulting in a theoretical shell thickness of 18 nm. There was very good agreement between measurements by TEM and electrical mobility spectroscopy. The results revealed that about 90 % or more of the core-shell structures were formed from 1:1 collisions between a core particle and a single monomer droplet.

**Keywords:** Surface coating; Electrostatically enhanced coagulation; Aerosol processing; Photopolymerization

## 1. Introduction

Numerous applications for nanostructured polymer composites have evolved during the past decade to obtain materials with interesting combinations of electrical, optical, mechanical or chemical functions [1]. Of special interest are core-shell structures, mostly composed of an inorganic core particle encapsulated by a polymeric shell. The polymer shell may act as a kind of spacer to prevent agglomeration of the core particles and thus loss of functionality [2]; it may preserve the mechanical and chemical stability of the core [3], may encapsulate the core particles completely to reduce their toxicity, to create vehicles for diagnostic purposes [4] or for medical treatment [5, 6]. Certain other applications actually require an empty core to obtain thermal insulators, gloss enhancers [7], drug carriers or dye dispersants [6].

Core-shell structures with an outer polymer layer are most often prepared in the liquid phase via emulsion polymerization [8, 9]. Hollow shells can be obtained in the same way, by first encapsulating template particles and then leaching out the core [10]. Various aerosol-based process routes have also been described, including chemical vapor deposition (CVD) to form inorganic shell structures via metal-organic precursors, to deposit organic layers such as PMMA onto inorganic particles in a low-pressure microwave plasma [2], or by photoinduced CVD using various carbon-containing precursors [11]. One can also deposit thin liquid layers onto gas-borne particles via physical vapor deposition [12] in preparation for subsequent polymerization. Each of these process routes has advantages and drawbacks. Emulsion polymerization most often employs surfactants and post-processing with costly separation techniques while CVD requires suitable precursors with decomposition kinetics to match the substrate material. On the other hand, physical vapor condensation leaves behind a significant amount of vapor in the carrier gas which may lead to downstream problems. In addition, wettability of the core particles is known to play a critical role during physical vapor deposition [13].

Here, we present yet another process route to coat nanoparticles with a very thin polymer shell. It is based on an electrostatic technique to cover substrate particles with a defined layer of liquid monomer, which is then solidified “in flight” by photopolymerization. For this purpose, separate streams of gas-borne substrate particles and monomer droplets – both submicron and of defined size - are at first charged electrically with opposite polarities and then mixed. In the combined aerosol stream, bipolar coagulation causes rapid preferential collisions between substrate particles and droplets, thereby forming a monomer layer of defined thickness around each substrate particle which is then polymerized by UV irradiation. By adjusting the volume ratio between substrate particles and monomer droplets, one can in principle generate core-shell structures of defined but variable shell thickness. The entire process operates continuously in the aerosol phase; it runs to completion on time scales of about a minute, is largely independent of the substrate material (with the exception of wettability, which is not a major limitation), and the carrier gas is not loaded with large amounts of monomer vapor.

The underlying theory of coagulation between aerosols of opposite or like electrical charge is not at all new (e.g. [14, 15]). Selective agglomeration between oppositely charged aerosol particles has been used e.g. to achieve stoichiometric combination of two substances which

triggers chemical reactions inside the combined droplets [16], to obtain doublets composed of two different solids [17], and most recently to “decorate” carrier particle surfaces evenly with a large number of catalytically active nanoparticles [18]. Photochemistry on aerosol particles has also been explored before, e.g. to functionalize their surface [19], to generate polymer nanoparticles from monomer droplets [20], and to prepare organic-inorganic polymer matrix nanocomposites from pre-mixed particle-monomer suspensions [21]. Widmann et al. [22] succeeded in creating a polymer shell on individual, levitated particles in an electrodynamic balance.

Despite all this prior work, it was challenging whether a continuous coating process would actually work as described above. Continuous, integrated processes in the aerosol phase are always challenging in practice because different “desirable” and “undesirable” kinetics have to be matched, including electrical charging of nanoparticles vs. particles losses in the charger, charge selective vs. purely Brownian coagulation, sufficiently fast spriting of a viscous liquid on solid core particles of different materials, potential evaporation of monomer during mixing, and finally the kinetics of aerosol-photopolymerization. This article provides details on the process sequence. Different core-shell combinations including HDDA-crosslinked PMMA and PHDDA on silica, gold, and sodium chloride are presented. Monodisperse silica particles were used to perform accurate measurements of the shell thickness and to compare these data with the theoretical shell thickness.

## **2. Experimental**

### **2.1 Particle Materials**

Three core particle materials were used for coating experiments, namely silica, gold and sodium chloride. Silica and gold particles were aerosolized from commercial suspensions with a concentration of about 1 mg/ml each. Silica particles were spherical and highly monodisperse with a manufacturer-stated size range of 235 nm  $\pm$  10 nm (Microparticles GmbH) and a measured mean mobility size of 241 nm in the aerosol. Gold particles were polydisperse with an approximate size of 100 nm (Postnova Analytics) and not perfectly spherical. Sodium chloride particles were generated by spraying a solution of 3,75 g/l sodium chloride in water, resulting in a mean mobility equivalent diameter of 65 nm.

The monomers selected as shell materials were methyl methacrylate (MMA, Sigma-Aldrich, 99 % purity), a monofunctional monomer, and 1,6-hexanediol diacrylate (HDDA, Alfa Aesar, 99 % purity) which is multifunctional. The photoinitiator added to the monomer was Irgacure 907® (Methyl-1[4-(methylthio)phenyl]-2-morpholinopropan-1-one, Sigma-Aldrich, 98 % purity), dissolved in the monomer in a concentration of 1 wt.-%. All chemicals were used without further purification. The monomers methyl methacrylate and hexanediol diacrylate have viscosities of 0.6 mPa s (at 20 °C) and 9 mPa s (at 25°C), respectively.

## 2.2 Experimental Setup and Coating Process

The complete experimental setup is shown in Figure 1. The core particle aerosol was generated by atomization of the respective suspension or solution with a Collision-type aerosol generator (Topas GmbH) into a flow of 2 l/min pure nitrogen followed by a diffusion dryer (Topas GmbH) to remove water vapor. In parallel, a second Collision-type atomizer was used to generate monomer droplets in a carrier gas of nitrogen at a flow rate of 1 l/min. Immediately following the atomizer, this second aerosol was diluted in a by-pass diluter where part of the flow was split off, filtered and then returned to the main aerosol stream in order to adjust the concentration ratio between core particles and monomer droplets.

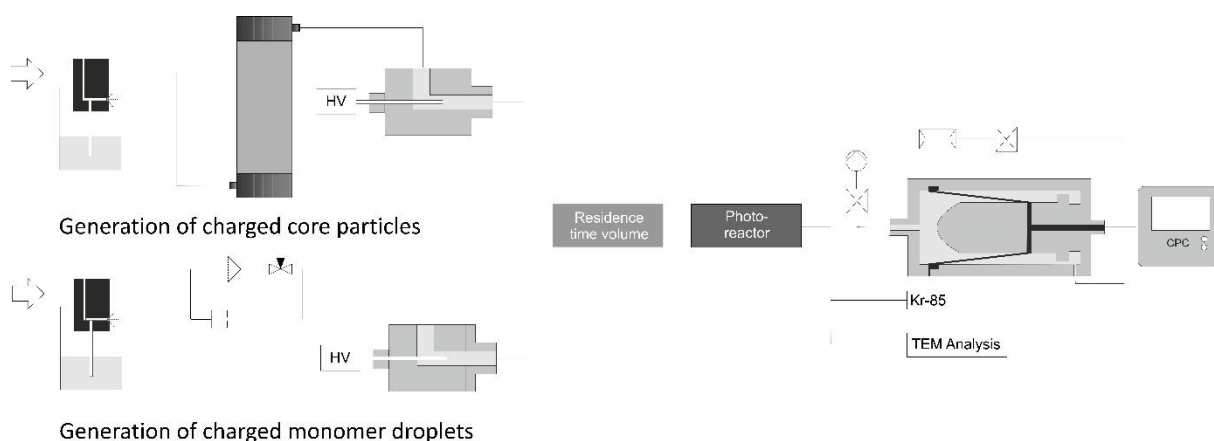


**Fig. 1.** Schematic of the experimental setup

The two aerosols then each passed through a high-voltage corona charger, built according to well-known design principles [23]. In this device, the discharge takes place between a needle-like HV electrode and a grounded annular counter-electrode, all enclosed in a PVC body (Fig. 2). The aerosol flows directly through the discharge zone where the concentration of unipolar ions is sufficient to impart a relatively high charge on the particles in a short time. This type of charger is easy to clean but known to have relatively high losses. However, this was immaterial for the present purposes.

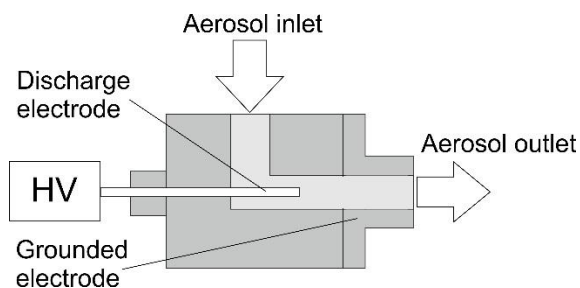


**Fig. 2.** Sketch of corona charger

The voltage applied to the discharge electrode was  $-5$  kV or  $+5$  kV, which imparted an average of  $+37$  elementary charge units to the carrier particles and about  $-15$  units to the droplets. The average charge was determined by comparing the physical diameters of the

respective particles - which were either known accurately (in case of silica) or measured separately as described below - with their mobility equivalent diameter distribution measured via conventional Scanning Mobility Particle Sizer (SMPS) technique but without prior particle neutralization. Note in this context that the droplets and particles entered the chargers with a negligible net charge.

These two aerosols were mixed immediately after charging and then introduced to a flow tube with an average residence time of 70 s (at 3 l/min) to allow bipolar coagulation. This amount of time was sufficient for the electrostatically enhanced coagulation to run to completion, according to an estimate made on the basis of well-known coagulation kinetic models (not discussed here in detail, for reference see e.g. [23] or [24]). For a mixture of uncharged particles and droplets on the other hand, the residence time of 70 s does not produce a measurable amount of coagulation, as confirmed by independent experiments.

Once a monomer droplet comes into contact with a core particle, the liquid spreads evenly around the core particle and forms a sphere-like meniscus, provided the core is wettable and the monomer viscosity low enough to permit complete coating within the time frame of the experiment. These assumptions are revisited in the results section. However, it can be said at this point, that all core particle materials used for this study were enclosed completely and uniformly after 70 s of residence time, and that the coagulation kinetics was therefore most likely the rate-determining step. For more viscous monomers, this would have to be reconfirmed, or the process step would need to be run at an elevated temperature which may increase monomer evaporation rate. The experiments described here were all performed at room temperature.

Monomer-coated particles were finally introduced to the photoreactor for aerosol-photopolymerization, a flow reactor where UV irradiation generates free radicals upon photoinitiated cleavage of photoinitiator molecules, thus permitting free radical polymerization to take place. The photoreactor consists of a cylindrical quartz glass tube (440 mm long, 52 mm inner diameter) surrounded by 6 UV fluorescent tubes (each 410 mm long) which produce a combined irradiance of about 5 mW/cm<sup>2</sup> measured at the surface of the quartz tube. This radiation is polychromatic with wavelengths between 270 and 360 nm and a maximum at 312 nm. The average aerosol residence time in the photoreactor was 20 or 60 s depending on the aerosol volumetric flow rate adjusted according to the monomer used.

Since the monomer droplet size distribution resulting from atomization was not known a priori, it was measured by electrical mobility spectrometry (SMPS). Preliminary experiments had raised some concern that the semi-volatile droplets may decrease in size while passing through the mobility spectrometer due to mixing with completely monomer-free sheath air. The droplets were therefore solidified first by polymerization in the photoreactor. An additional concern was the potential for some droplet evaporation during the mixing and in the residence time volume. Comparative size measurements were therefore performed before and after the residence time volume. For this purpose, monomer droplets were mixed with 2 l/min of particle-free air to simulate the addition of the core particle aerosol. No significant change in mean size was observed however. Figure 3 shows the size distribution of monomer droplets measured via the usual SMPS technique after neutralization. The size distribution is roughly log-normal with a median of 170 nm and a geometrical standard deviation of 1.9. This gives a count mean mobility equivalent diameter of 195 nm.

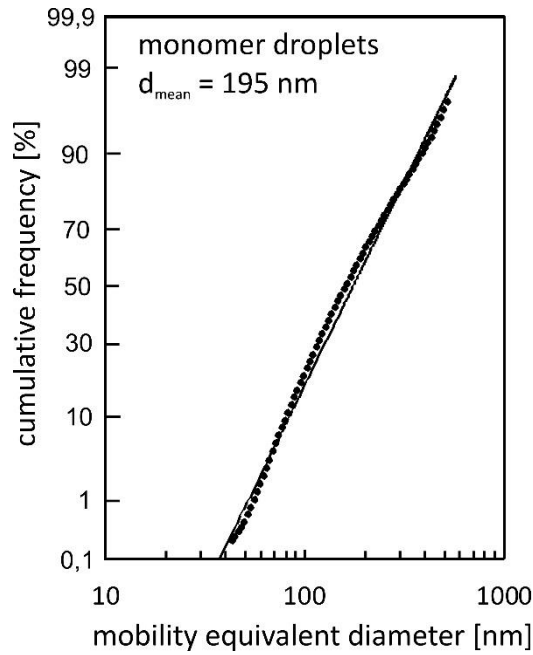


**Fig. 3.** Cumulative size distribution of monomer droplets directly after the nebulizer

If the mean particle sizes of core particles  $d_{\text{core}}$  and monomer droplets  $d_{\text{drop}}$  are known, one can readily calculate the resulting diameter of the coated particle:

$$d_{\text{hybrid}} = \sqrt[3]{d_{\text{drop}}^3 + d_{\text{core}}^3} \quad (1)$$

For example, when 241 nm silica particles are coated with 195 nm droplets, the resulting diameter of the hybrid particle should be 277 nm provided that one core particle is covered by only one monomer droplet. For two monomer droplets, the size would grow to 306 nm. Note that we have used the count mean sizes for this exercise, based on the argument that the most frequently occurring core-shell particle size is determined by the size classes of core particles and droplets which collide most frequently – i.e. those with the highest number concentration. The SMPS measurement technique was employed to determine the thickness of the polymer shell by comparing the mean sizes before and after the photoreactor assuming that the shell thickness corresponds to that of the liquid monomer. In addition, the layer thickness was also measured by transmission electron microscopy after collecting encapsulated particles onto carbon-coated copper grids.

### 3. Results and Discussion

#### 3.1 Encapsulation of Spherical Monodisperse Silica Particles

For the first experiments, silica core particles possessing spherical and highly monodisperse properties were employed, thus permitting a relatively accurate determination of the coating thickness according to Eq. (1). Silica particles had a mobility equivalent diameter of  $241 \text{ nm} \pm 4 \%$  and carried a mean charge of +37 units at a number concentration of  $3 \cdot 10^3$  particles per  $\text{cm}^3$  at the point of mixing. The monomer droplets consisted of HDDA with 1 wt.-% of

photoinitiator dissolved in it. Their count mean size was 195 nm, with a mean charge of -15 units, at a concentration about 3 times that of the core particles. After passing the residence time volume, the aerosol was polymerized within 20 s in the photoreactor.

Figure 4 shows the size distributions of the two aerosols before and after mixing (and photopolymerization). Before mixing (Figure 4a), the monomer droplet size distribution is evidently much wider than that of the silica particles. (The multiple peaks of the silica particles correspond to single, double and triple charged particles in the mobility spectrum. Relevant for the current discussion is the peak corresponding to 241 nm.) After mixing and passing the residence time volume (Figure 4b), a double peak appears with a maximum at 270 nm and another one at 195 nm. (For the third peak around 30 nm see below.) The peak at 270 nm agrees well with the value of 277 nm expected according to Eq. 1. It can therefore be assigned to core-shell particles resulting from a 1:1 combination of core particles and monomer droplets. The resulting shell thickness after polymerization is about 15 nm.

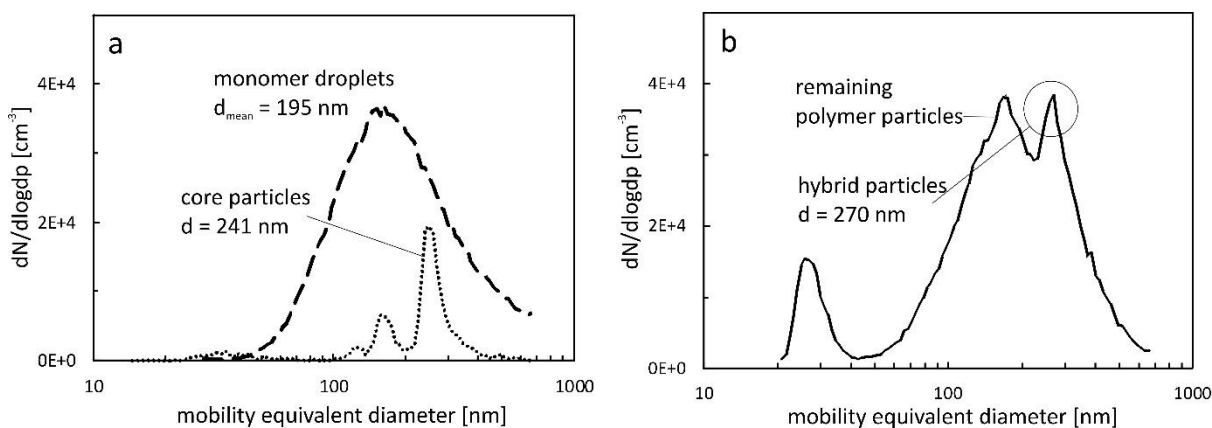


**Fig. 4.** Size distribution of oppositely charged core particles and monomer droplets before (a) and after mixing (b); these mobility based spectra were obtained after electrical neutralization of the aerosols

The second peak around 195 nm corresponds to monomer droplets which did not find a collision partner. The appearance of this second maximum is not entirely surprising, given that the initial droplet concentration exceeded that of the substrate particles by a factor of three. Unexpected was the absence of a peak around 306 nm, where core-shell particles formed with two monomer droplets per core particle should appear. However, one has to keep in mind that 306 nm is still within the one-sigma range of combinations between monomer droplets and core particles. Returning to Figure 3, a value around 270 nm for the diameter corresponding to the 84 percentile of the monomer droplet size distribution can be observed, which gives a combined diameter around 322 nm according to Eq. 1. One can thus estimate that the number of 1-core+2-droplet particles must be significantly less than about 10% of the 1-core+1-droplet particles. Apparently, coagulation rate between droplets and silica particles decreases sufficiently after the first collision to become undetectable in the measurements even though the silica particles still carry about half of their original charge.

The size distribution in Figure 4b shows a third peak around 30 nm which is far too small to be associated with any of the modes expected from the coating process. Instead, this mode may

contain particles formed by reaction of monomer vapor with ozone generated by the corona discharge. The formation of secondary organic particles via this route is well known [23]. It underlines that the optimization of the charger would be a critical step toward industrialization of this coating process.

Figure 5 provides a visual impression of a silica core particle encapsulated by a polymer layer. It was obtained by transmission electron microscopy from a sample of particles collected via impaction onto carbon-coated copper grids. A population of 60 randomly selected core-shell particles was analyzed on TEM grids in order to determine the geometrical particle size distribution (Figure 5a). The distribution is reasonably well represented by a monomodal log-normal function with a median diameter of 270 nm and a geometric standard deviation of 1.1. This results in a calculated count mean diameter of 270 nm, which is in good agreement with SMPS measurements and the calculated hybrid particle size.

The TEM images were also analyzed for the presence of larger core-shell particles formed by collision of a core particle with two monomer droplets, which should appear around 306 nm in the particle size spectrum as indicated in Figure 5a. The resulting shell thickness of 33 nm would be readily distinguishable in a TEM sample. However, as before in the SMPS spectra, no significant population with such a thick polymer layer was found. Based on the sample size, this fraction cannot represent more than a few percent of the total population revealing the significance of 1:1 coagulation.

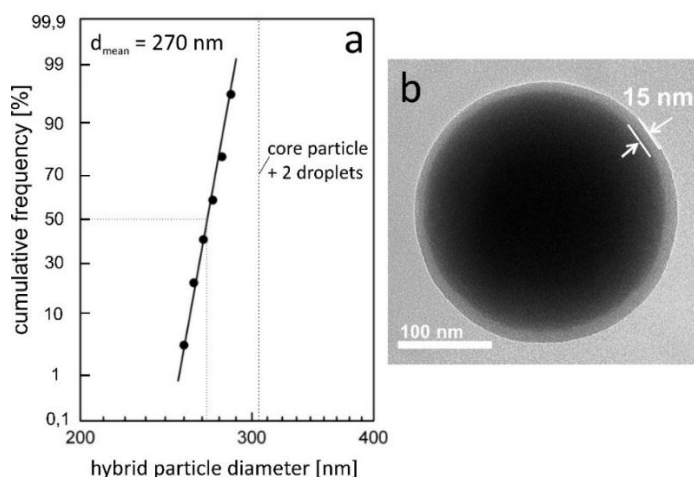


**Fig. 5.** (a) Cumulative size distribution of core-shell particles determined from transmission electron micrographs; (b) TEM image represents a typical particle

### 3.2 Encapsulation of Other Materials and Non-spherical Geometries

A feasibility study of the process of charge-controlled particle encapsulation requires tests with a few combinations of particulate materials and monomers in order to obtain a first estimate of the influence of wettability and non-ideal particle structures. The experimental procedures remained basically the same as before: Core particle and monomer aerosols were generated and charged separately, mixed and left to coagulate for 70 s, and finally irradiated for 20 or 60 s in the photoreactor depending on the monomer type. The resulting structures were investigated qualitatively by transmission electron microscopy analysis mainly for the

uniformity of coating. Quantitative measurements of the shell thickness were not considered meaningful due to the polydispersity of both populations.

*Polydisperse gold particles* with an average size of about 100 nm were generated from an aqueous suspension and then encapsulated using MMA (methyl methacrylate) containing 10 vol.-% HDDA (hexanediol diacrylate) with respect to MMA as crosslinking agent and 1 wt.-% photoinitiator (Irgacure 907) in MMA to enable polymerization within the time frame of 60 s in the photoreactor. The TEM images showed different degrees of polymer surface coverage, of which three characteristic images are represented in Figure 6. While most gold particles were uniformly enclosed by a polymer shell as in Figure 6c, some were not completely centered (Figure 6b), while a few rare particles were only partly enclosed. In Figure 6a only about 2/3 of the particle surface had been covered by liquid monomer prior to photopolymerization. However, the contact angle between monomer and particle surface was well below 90°. These images might represent “late” collisions in the residence time volume with insufficient time for spreading of the monomer. The monomers used appear to wet the gold particles completely and generally produce spherical and even HDDA-crosslinked PMMA shells as shown in Figure 6c. This confirms the observations by Zhang et al. (2004).

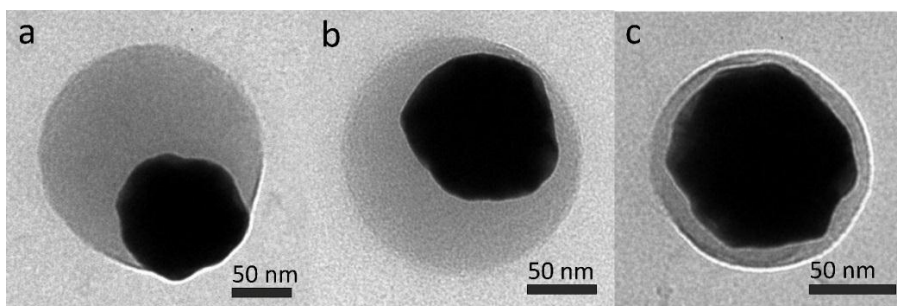


**Fig. 6.** Polymer encapsulated gold particles photopolymerized after different states of surface wetting

*Polydisperse sodium chloride particles* with a mean diameter of 65 nm were formed by atomization of a NaCl solution and coated with HDDA containing 1 wt.-% photoinitiator. The monomer shell was polymerized within 20 s in the photoreactor. A micrograph of sodium chloride encapsulated by PHDDA (poly(hexanediol diacrylate)) is shown in Figure 7a.

*Silica agglomerates* were formed by letting the primary spheres coagulate before initiating the charging process, and then coated with monomer consisting of MMA with 10 vol.-% HDDA with respect to MMA and 1 wt.-% photoinitiator in MMA. The polymerization time in the photoreactor was 60 s. Figure 7b shows an agglomerate of 3 primary spheres encapsulated in HDDA-crosslinked PMMA. According to a rough estimate, the shell in this particular instance must have also been formed from a single droplet, and is therefore much thinner than the 15 nm observed for a single core particle. Apparently, the monomer spreads fast enough around the entire agglomerate at room temperature to form a uniform layer.

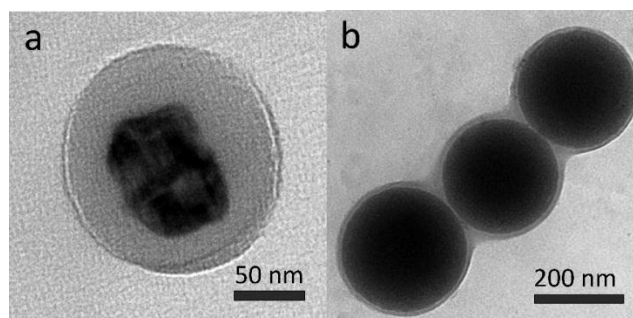


**Fig. 7.** Polymer-encapsulated particles of different core materials and/or shape: (a) sodium chloride and (b) silica agglomerate

The uniformity of the polymer shell observed in practically all cases suggests that all these core particle materials were completely wettable, that the monomer viscosities were sufficiently low at room temperature to allow for a uniform spread (with the exception of very “late” collisions), and that the surface tension had formed the expected minimum surface. Interestingly, the core particles were mostly positioned at the center of the droplets as far as electron microscopy could tell. Indirectly, this implies that the coagulation kinetics were the rate-determining step. This would have to be reconfirmed for more viscous monomers, or the process step would need to be run at elevated temperatures. However, this would increase monomer evaporation rate which could enhance secondary nucleation.

#### 4. Conclusions

A continuous process has been described for the encapsulation of wettable nanoparticles with a thin polymer shell. The process is essentially based on selective collisions between gas-borne, oppositely charged core particles and monomer droplets with a subsequent photo-initiated polymerization. Once the two streams of charged aerosols were mixed together at concentrations  $\leq 10^5$  particles per  $\text{cm}^3$  and particle charge levels on the order of 20 e, particles and droplets collide and monomer wets the surface to form a liquid shell within a time scale of 70 s. Photopolymerization of the liquid shell requires 60 s or less.

Using the presented technique, gold, silica, and sodium chloride nanoparticles were successfully encapsulated with thin layers of PHDDA and HDDA-crosslinked PMMA. It was found that all material surfaces as well as all kind of particle structures were wettable at room temperature and that the spreading kinetics of the monomers were fast enough to cover the core particles uniformly within the time scale provided for coagulation.

The shell thickness depends on the size of core particles and monomer droplets. For spherical, monodisperse silica core particles ( $d = 241$  nm), the coating thickness was determined in combination with polydisperse HDDA droplets ( $d_{\text{mean}} = 195$  nm), resulting in a theoretical shell thickness of about 18 nm. The measurements by TEM and electrical mobility spectroscopy revealed very good agreement. At concentrations and particle charge levels used in these experiments, an estimated 90% or more of the core-shell structures were formed by 1:1 combinations of core particles and monomer droplets.

To summarize, the process of charge-controlled encapsulation of arbitrary core materials with various polymers is thus effective and versatile.

## Acknowledgements

This project is part of the JointLab IP3, a joint initiative of KIT and BASF. Financial support by the Ministry of Science, Research and the Arts of the State of Baden-Württemberg (Az. 33-729.61-3) is gratefully acknowledged.

## References

1. Balazs, A.C., T. Emrick, and T.P. Russell, *Nanoparticle polymer composites: Where two small worlds meet*. Science, 2006. **314**(5802): p. 1107-1110.
2. Vollath, D., D.V. Szabo, and J. Fuchs, *Synthesis and properties of ceramic - Polymer composites*. Nanostructured Materials, 1999. **12**(1-4): p. 433-438.
3. Athanassiou, E.K., R.N. Grass, and W.J. Stark, *Large-scale production of carbon-coated copper nanoparticles for sensor applications*. Nanotechnology, 2006. **17**(6): p. 1668-1673.
4. Haag, R., *Supramolecular drug-delivery systems based on polymeric core-shell architectures*. Angewandte Chemie-International Edition, 2004. **43**(3): p. 278-282.
5. El-Sayed, I.H., X.H. Huang, and M.A. El-Sayed, *Surface plasmon resonance scattering and absorption of anti-EGFR antibody conjugated gold nanoparticles in cancer diagnostics: Applications in oral cancer*. Nano Letters, 2005. **5**(5): p. 829-834.
6. Emmerich, O., et al., *Molecular boxes based on hollow organosilicon micronetworks*. Advanced Materials, 1999. **11**(15): p. 1299-+.
7. Kobayashi, H., E. Miyanaga, and M. Okubo, *Studies on suspension and emulsion - Part 295. Preparation of multihollow polymer particles by seeded emulsion polymerization using seed particles with incorporated nonionic emulsifier - Part CCXCV of the series "Studies on Suspension and Emulsion"*. Langmuir, 2007. **23**(17): p. 8703-8708.
8. Landfester, K., et al., *Miniemulsion polymerization with cationic and nonionic surfactants: A very efficient use of surfactants for heterophase polymerization*. Macromolecules, 1999. **32**(8): p. 2679-2683.
9. Mahdavian, A.R., Y. Sarrafi, and M. Shabankareh, *Nanocomposite particles with core-shell morphology III: preparation and characterization of nano Al<sub>2</sub>O<sub>3</sub>-poly(styrene-methyl methacrylate) particles via miniemulsion polymerization*. Polymer Bulletin, 2009. **63**(3): p. 329-340.
10. Fu, G.-D., et al., *Hollow polymeric nanostructures-Synthesis, morphology and function*. Progress in Polymer Science, 2011. **36**(1): p. 127-167.
11. Zhang, B., et al., *Growth of coatings on nanoparticles by photoinduced chemical vapor deposition*. Journal of Nanoparticle Research, 2008. **10**(1): p. 173-178.

12. Seipenbusch, M., et al., *Determination of coating thickness of DEHS on submicron particles by means of low pressure impaction*. Chemical Engineering & Technology, 2002. **25**(1): p. 77-82.
13. Zhang, L., M.B. Ranade, and J.W. Gentry, *Formation of organic coating on ultrafine silver particles using a gas-phase process*. Journal of Aerosol Science, 2004. **35**(4): p. 457-471.
14. Zebel, G., *Zur Theorie des Verhaltens elektrisch geladener Aerosole*. Kolloid-Zeitschrift, 1958. **157**: p. 35-50.
15. Kasper, G., *Electrostatic dispersion of homopolar charged aerosols*. Journal of Colloid and Interface Science, 1981. **81**(1): p. 32-40.
16. Borra, J.P., et al., *Bipolar coagulation for powder production: Micro-mixing inside droplets*. Journal of Aerosol Science, 1999. **30**(7): p. 945-958.
17. Maisels, A., et al., *Synthesis of tailored composite nanoparticles in the gas phase*. Applied Physics Letters, 2000. **77**(26): p. 4431-4433.
18. Sigmund, S., et al., *An Aerosol-Based Process for Electrostatic Coating of Particle Surfaces with Nanoparticles*. Aerosol Science and Technology, 2014. **48**(2): p. 142-149.
19. Salas Vicente, J., et al., *VUV-photochemical functionalization of polystyrene aerosols*. Basics and Applications of Photo-polymerization Reactions, 2010. **3**: p. 47-65.
20. Akguen, E., J. Hubbuch, and M. Woerner, *Perspectives of aerosol-photopolymerization: Nanoscale polymer particles*. Chemical Engineering Science, 2013. **101**: p. 248-252.
21. Akguen, E., J. Hubbuch, and M. Woerner, *Perspectives of Aerosol-Photopolymerization: Organic-inorganic hybrid nanoparticles*. Colloid Polym Sci, 2014.
22. Widmann, J.F., et al., *Encapsulation of levitated microparticles*. Journal of Colloid and Interface Science, 1998. **199**(2): p. 197-205.
23. Whitby, K.T., *Generator for producing high concentrations of small ions*. Review of Scientific Instruments, 1961. **32**(12): p. 1351-&.
24. Fuchs, N.A., *The mechanics of aerosols*. 1964.
25. Zaikov, G., S. Rakovsky, and M. Anachkov, *Ozone and its reactions with diene rubbers*. Chemistry and Chemical Technology, 2012. **6**(3): p. 307-319.

---

# Cationic Aerosol-Photopolymerization

Ertan Akgün<sup>1</sup>, Alex Muntean<sup>1</sup>, Jürgen Hubbuch<sup>1</sup>, Marco Sangermano<sup>2\*</sup>,  
Michael Wörner<sup>1\*</sup>

---

*1: Process Engineering in Life Sciences, Karlsruhe Institute of Technology*

*2: Department of Applied Science and Technology, Politecnico di Torino*

*\* Corresponding authors: Marco Sangermano ([marco.sangermano@polito.it](mailto:marco.sangermano@polito.it))*

*Michael Wörner ([michael.woerner@kit.edu](mailto:michael.woerner@kit.edu))*

Macromolecular Materials and Engineering, DOI: 10.1002/mame.201400211

The final publication is available on:

<http://onlinelibrary.wiley.com/doi/10.1002/mame.201400211/abstract?deniedAccessCustomisedMessage=&userIsAuthenticated=false>

## **Abstract**

Photoinitiated polymerization in aerosols is employed for the preparation of spherical polymer particles via cationic polymerization. The UV irradiation of aerosol monomer droplets starts the cationic curing process without the employment of any solvent or additives such as stabilizers, resulting in highly pure polymers. Crosslinked polymer spheres with a high gel content are obtained by processing vinyl ether and epoxy monomers via this aerosol-photopolymerization technique, which exhibits great potential for the development of multifunctional materials.

**Keywords:** Cationic photopolymerization; Aerosol processing; Particle formation

## 1. Introduction

Polymer micro- and nanoparticles are widely attractive from a scientific and industrial point of view, especially in the form of polymer-filler composites, ranging from transparent polymers [1] and magneto-optical applications [2] to biotechnology [3] and controlled drug release agents [4]. The recent research has allowed the development of many different synthetic procedures to prepare polymer particles with a wide range of properties under controlled conditions [5]. These particulate systems are characterized by a size ranging from a few nanometers to micron-sized dimension.

The proposed methods reported in literature for the preparation of polymeric particles include two main steps [6]. First, the preparation of an emulsified system, and the second step is the synthesis of polymer particles. This second step is achieved either by the precipitation or the gelation of a polymer, or by polymerization of monomers; it is also possible to obtain polymer particles at the time of emulsification. Suitable emulsified systems can be emulsions, mini-emulsions, nano-emulsions and micro-emulsions where surfactants are used frequently and decrease product purity [7]. Employing these emulsions suffers from additional drawbacks such as time and cost consumption. In fact, after wet polymerization, the particles might have to be separated by downstream processes such as centrifugation or filtration followed by washing and drying steps [8].

As an appealing alternative to liquid processes, aerosol techniques can be used for polymer particle production as well. Different aerosol-based methods have been proposed so far: micrometer-sized polystyrene particles were obtained by aerosol-polymerization via contact of monomer droplets with initiator vapor [9] and aerosol-photopolymerization of acrylic formulations was proposed by Esen et al. for the generation of microspheres of diameters within 5 to 100  $\mu\text{m}$  [10, 11]. Similar results were obtained with the same technique by Gao et al. [12]. Smaller polymer particles were generated by Akguen et al. [13], who also reported on the preparation of acrylic organic-inorganic hybrid particles via aerosol-photopolymerization in which ZnO nanoparticles were well distributed resulting in polymer-matrix nanocomposites [14]. While radical aerosol-photopolymerization seems therefore to be a well-established technique and cationic photopolymerization itself well-known as well [15], we could find, to the best of our search, only one report regarding the cationic photopolymerization in aerosols. Starting from a bis-epoxy silicone monomer in the presence of a diaryliodonium salt photoinitiator and a template, silicone microbeads were prepared [16]. It was found that photopolymerization occurred fast enough to polymerize the droplets of an aerosol spray in flight.

In this work, for the first time, we report a preliminary investigation of the reactivity of epoxy monomer and vinyl ether as cationically UV-curable monomers via aerosol-photopolymerization. Spherical polymer particles were produced from monomer solution droplets consisting of liquid monomer and dissolved cationic photoinitiator. No surfactants and any additional solvent were used for the formation of the monomer droplets and polymer particles obtained afterwards.

## 2. Experimental

### 2.1 Materials

The monomers tri(ethylene glycol) divinyl ether (DVE2), cyclohexene oxide (CY) and 3,4-epoxycyclohexylmethyl 3,4-epoxycyclohexanecarboxylate (CE), and the cationic photoinitiator triarylsulfonium hexafluoroantimonate were purchased from Sigma-Aldrich and used without any purification.

### 2.2 Aerosol-photopolymerization

Two main components are involved for the continuous experimental setup of aerosol-photopolymerization. A Collision-type aerosol generator sprays the monomer solution, which is prepared by dissolving the photoinitiator in the liquid monomer without the addition of any solvent, and a flow-through photoreactor is responsible for the conversion of gas-carried monomer droplets to gas-carried polymer particles. The photoreactor consists of a cylindrical quartz glass tube (440 mm long, 52 mm inner diameter) surrounded by 6 UV fluorescent tubes (410 mm long each) emitting polychromatic UV radiation between 270 and 360 nm, with a maximum at 312 nm. The irradiance at the quartz surface is approximately  $5 \text{ mW cm}^{-2}$ . The average aerosol residence time in this photoreactor can be varied by varying the nozzle inlet pressure of the aerosol generator or by selecting a shorter quartz glass tube. The experiments reported in this contribution were performed at an average aerosol residence time of about 50 s in the photoreactor.

The monomer solution is sprayed with nitrogen gas in the aerosol generator to generate the droplet aerosol. This droplet aerosol is passed through the photoreactor where reactive species are generated upon UV irradiation for the polymerization process. Polymer particles leaving the photoreactor were collected dry at the exit of the quartz tube onto PTFE filter membranes with 50 nm average pore diameter.

### 2.3 Particle Characterization

Fourier transform infrared spectroscopy utilizing attenuated total reflectance (FTIR-ATR, Thermo-Nicolet 5700, Bruker Optics) was employed for the determination of carbon-carbon double bond or epoxy group conversion. The solution spectra were obtained by measuring a droplet of the corresponding monomer solution to be sprayed, and the polymer spectra after dry particle collection upon aerosol-photopolymerization.

The gel content of the crosslinked polymer powder was determined by measuring the weight loss after 24 h of monomer extraction with chloroform at room temperature according to the standard test method ASTM D2765-84.

DSC measurements of UV-crosslinked powder were performed using a Mettler DSC 30 apparatus equipped with a low-temperature probe and a heating rate of  $10 \text{ }^\circ\text{C min}^{-1}$ .

For scanning electron microscopy imaging, LEO 1530 was employed. Dry collected particles were brought onto a silicium wafer and coated with platinum being 1–2 nm in thickness.

### 3. Results and Discussion

As a first step, the vinyl ether (DVE2) monomer was investigated taking into account its high reactivity towards cationic UV curing process as well as its low viscosity. 1 wt.-% of cationic photoinitiator was added to the monomer on the basis of previous investigations [17]. Polymer particles in the aerosol leaving the photoreactor were collected at a production rate of almost  $300 \text{ mg h}^{-1}$ , which could be increased above  $300 \text{ mg h}^{-1}$  upon dissolving 2 wt.-% of the same photoinitiator. This value is comparable to the production rate for particles obtained via free radical initiated aerosol-photopolymerization [18]. Vinyl ether double bond conversion was measured via FTIR-ATR analysis after collecting the polymer powder. The spectra of DVE2 before aerosol generation and of poly(DVE2) particles resulting from aerosol-photopolymerization are compared in Figure 1. The disappearance of the typical vinyl ether bands centered at around  $1620 \text{ cm}^{-1}$  indicates the completeness of the photopolymerization reaction during the residence time of the aerosol in the photoreactor. The polymeric particles were fully crosslinked, resulting in a gel content of 100% and a glass transition temperature ( $T_g$ ) of about  $38 \text{ }^\circ\text{C}$  as illustrated in Figure 2.

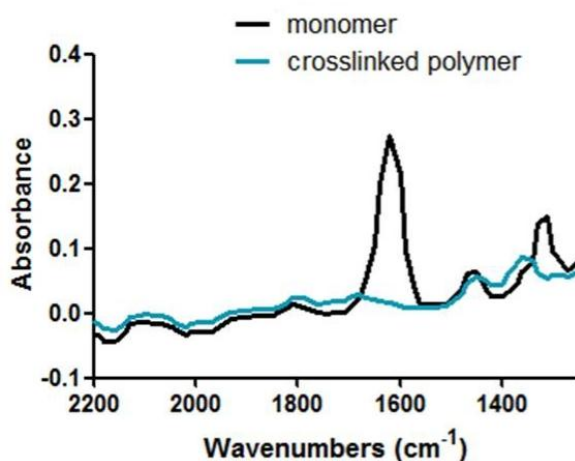


**Fig. 1.** FTIR-ATR spectra (shown only between  $1300\text{-}2100 \text{ cm}^{-1}$  of spectral range) of DVE2 before aerosol generation and of crosslinked poly(DVE2) particles resulting from cationic aerosol-photopolymerization.

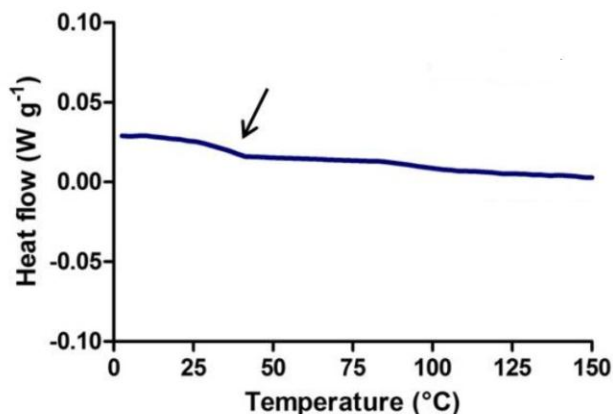


**Fig. 2.** DSC trace of the crosslinked poly(DVE2) particles produced by cationic aerosol-photopolymerization.

The morphology of the prepared particles was investigated by SEM. Figure 3 presents the images of dry collected, crosslinked poly(DVE2) particles possessing smooth surface characteristics.

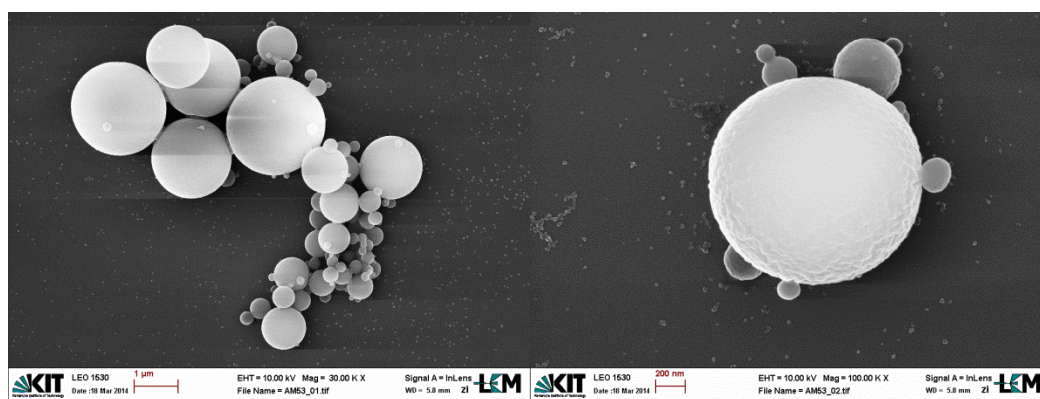


**Fig. 3.** SEM images of crosslinked poly(DVE2) particles produced by cationic aerosol-photopolymerization.

Investigation of the cationic aerosol-photopolymerization process was pursued using the 3,4-epoxycyclohexylmethyl 3,4-epoxycyclohexanecarboxylate (CE) as photocurable monomer. Because of its higher viscosity compared to divinyl ether monomer, the epoxy monomer was mixed with 50 vol.-% of cyclohexene oxide (CY). The monofunctional monomer CY will both strongly reduce the viscosity of the dicycloaliphatic epoxy resin and accelerate the cationic UV curing process by a strong delay of vitrification during network build-up. The spectra of CE/CY 50:50 formulation before aerosol generation and of crosslinked polymer particles resulting from aerosol-photopolymerization are compared in Figure 4. The complete disappearance of the typical epoxy bands centered around 800 cm<sup>-1</sup> is evident, indicating practically complete conversion of the photopolymerization medium. Also in this case completely crosslinked polymer particles with a gel content of 100% and a T<sub>g</sub> value of about 42 °C were achieved. The low T<sub>g</sub> value for the epoxy crosslinked particles is due to the high content of the monofunctional monomer which was used to adjust the

viscosity of the formulation and to delay vitrification in order to obtain fully cured polymeric particles. As a drawback, the crosslinking density is reduced and a low  $T_g$  value is obtained in comparison to the pure epoxy system.

The morphology of the achieved particles was characterized by SEM analysis. Figure 5 shows the images of dry collected, crosslinked polymer particles.

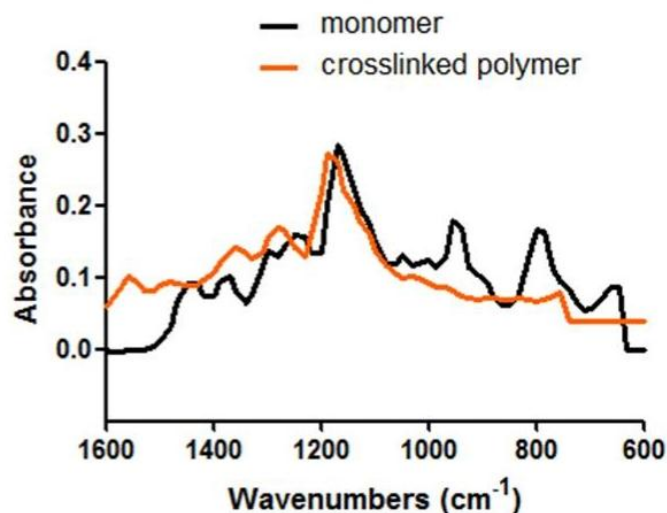


Figure 4: FTIR-ATR spectra of the CE/CY 50:50 formulation before aerosol generation and of crosslinked particles resulting from cationic aerosol-photopolymerization.

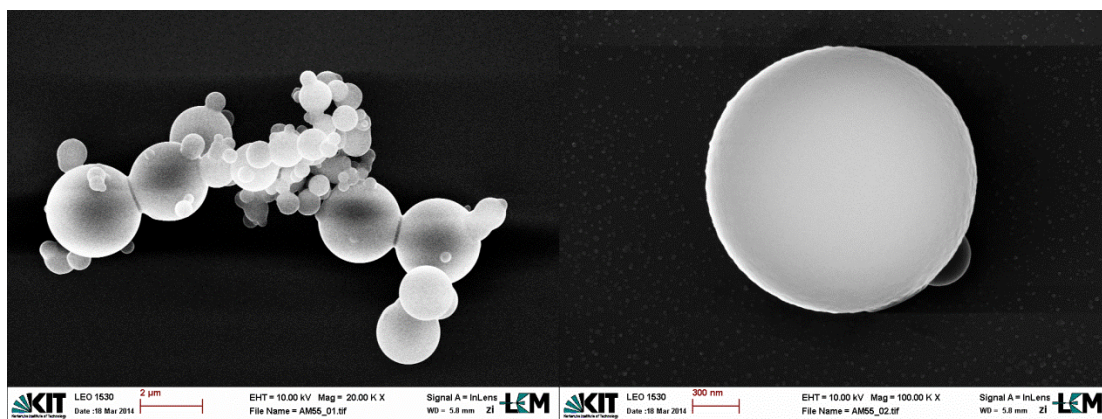


Figure 5: SEM images of crosslinked particles obtained from the CE/CY 50:50 formulation produced by cationic aerosol-photopolymerization.

#### 4. Conclusions

We report the very first preliminary results of cationic aerosol-photopolymerization of vinyl ether and epoxy monomer systems. This is an interesting alternative to the production of

polymer particles via liquid processing routes and free radical initiated photopolymerization. We have demonstrated the very fast UV curing process allowing the complete crosslinking of both vinyl ether and epoxy monomer during the residence time of the droplets in the photoreactor. While the high reactivity of DVE2 monomer is well known and its low viscosity is suitable for aerosol applications, epoxy monomer was mixed with 50 vol.-% of cycloaliphatic epoxy resin in order to reduce the monomer formulation viscosity, enhance the rate of photopolymerization, and to induce a complete epoxy group conversion delaying vitrification.

We could get fully crosslinked polymeric particles with high gel content values and glass transition temperature tunable as a function of the starting formulation. SEM images of the dry collected polymer particles revealed the formation of homogeneous, micrometer-round particles with smooth surfaces.

We have demonstrated the potential of cationic aerosol-photopolymerization as a fast and flexible generation technique which could be further investigated for the generation of smart polymeric particles such as polymer-matrix nanocomposites and nanostructured particles obtained by free radical initiated aerosol-photopolymerization.

## Acknowledgements

Alexander von Humboldt Foundation is gratefully acknowledged for financial support of one of the authors (M.S.).

## References

1. Althues, H., J. Henle, and S. Kaskel, *Functional inorganic nanofillers for transparent polymers*. Chemical Society Reviews, 2007. **36**(9): p. 1454-1465.
2. Li, S., et al., *Nanocomposites of polymer and inorganic nanoparticles for optical and magnetic applications*. Nano reviews, 2010. **1**.
3. Sanchez, C., et al., *Applications of hybrid organic-inorganic nanocomposites*. Journal of Materials Chemistry, 2005. **15**(35-36): p. 3559-3592.
4. Shi, J., et al., *Nanotechnology in Drug Delivery and Tissue Engineering: From Discovery to Applications*. Nano Letters, 2010. **10**(9): p. 3223-3230.
5. Braunecker, W.A. and K. Matyjaszewski, *Controlled/living radical polymerization: Features, developments and perspectives (vol 32, pg 93, 2007)*. Progress in Polymer Science, 2008. **33**(1): p. 165-165.
6. Vauthier, C. and K. Bouchemal, *Methods for the Preparation and Manufacture of Polymeric Nanoparticles*. Pharmaceutical Research, 2009. **26**(5): p. 1025-1058.

7. Landfester, K., et al., *Miniemulsion polymerization with cationic and nonionic surfactants: A very efficient use of surfactants for heterophase polymerization*. *Macromolecules*, 1999. **32**(8): p. 2679-2683.
8. Huang, X.Y. and W.J. Brittain, *Synthesis and characterization of PMMA nanocomposites by suspension and emulsion polymerization*. *Macromolecules*, 2001. **34**(10): p. 3255-3260.
9. Shin, D.S., E.K. Oh, and S.G. Kim, *Preparation of polymer particles in aerosol-phase reaction*. *Aerosol Science and Technology*, 1996. **24**(4): p. 243-254.
10. Esen, C. and G. Schweiger, *Preparation of monodisperse polymer particles by photopolymerization*. *Journal of Colloid and Interface Science*, 1996. **179**(1): p. 276-280.
11. Esen, C., T. Kaiser, and G. Schweiger, *Raman investigation of photopolymerization reactions of single optically levitated microparticles*. *Applied Spectroscopy*, 1996. **50**(7): p. 823-828.
12. Gao, Z., E.A. Grulke, and A.K. Ray, *Synthesis of monodisperse polymer microspheres by photopolymerization of microdroplets*. *Colloid and Polymer Science*, 2007. **285**(8): p. 847-854.
13. Akguen, E., J. Hubbuch, and M. Woerner, *Perspectives of aerosol-photopolymerization: Nanoscale polymer particles*. *Chemical Engineering Science*, 2013. **101**: p. 248-252.
14. Akguen, E., J. Hubbuch, and M. Woerner, *Perspectives of Aerosol-Photopolymerization: Organic-inorganic hybrid nanoparticles*. *Colloid Polym Sci*, 2014.
15. Decker, C. and K. Moussa, *Kinetic-study of the cationic photopolymerization of epoxy monomers*. *Journal of Polymer Science Part a-Polymer Chemistry*, 1990. **28**(12): p. 3429-3443.
16. Vorderbruggen, M.A., et al., *Use of cationic aerosol photopolymerization to form silicone microbeads in the presence of molecular templates (vol 8, pg 1106, 1996)*. *Chemistry of Materials*, 1999. **11**(5): p. 1398-1398.
17. Sangermano, M., et al., *Cationic photopolymerization of vinyl ether systems: influence of the presence of hydrogen donor additives*. *European Polymer Journal*, 1999. **35**(4): p. 639-645.
18. Akguen, E., J. Hubbuch, and M. Woerner, *Perspectives of aerosol-photopolymerization: Nanostructured polymeric particles*. *Macromolecular Materials and Engineering*, 2014. DOI: 10.2002/mame.201400032.

## 4. Conclusions & Outlook

This PhD thesis presents a spectrum of various polymeric particles generated via the process of aerosol-photopolymerization. Spherical polymer nanoparticles, spherical organic-inorganic polymer-matrix nanocomposites, non-spherical nanocaps, and spherical porous particles were successfully produced and have been published in the first three papers within the concept of “Perspectives of Aerosol-Photopolymerization” to introduce this relatively young technique as a promising tool. In addition, core-shell nanoparticles were prepared by an integrated aerosol-based process as well. These particles have been discussed in the fourth paper resulting from this thesis.

As a first step, polymer nanoparticles were generated as a proof of concept for the experimental setup upon photoreactor construction. Molecularly crosslinked and non-crosslinked polymer particles were obtained by aerosol-photopolymerization. A major observation was the necessity of a minimum monomer propagation rate coefficient due to the short aerosol residence time in the photoreactor of about 1 min. Although this limited the monomer selection, slow-propagating monofunctional monomers still could be polymerized in the presence of faster copolymerization partners. Multifunctional monomers or fast-propagating monofunctional monomers were able to homopolymerize within the limited polymerization time. The resulting polymer particles served as a proof of concept and demonstrated the potential of aerosol-photopolymerization.

More complex particle structures were formed by spraying monomer formulations with specific additives. Inorganic nanoparticles suspended in the monomer solution were used for the preparation of organic-inorganic hybrid nanoparticles. Upon the employment of the same experimental setup and procedure, hybrid monomer droplets were obtained by aerosol generation, and these droplets were photopolymerized into hybrid polymeric particles online in the subsequent photoreactor. Hybrid particles were composed of inorganic content and the same polymer as produced in the “proof of concept” step.

Apart from the spherical particle shape resulting naturally due to in-flight polymerization of aerosol droplets, non-spherical polymeric particles which we named “nanocaps” were synthesized by aerosol-photopolymerization too. Specific additives were employed in the monomer solution to realize concomitant processes which are assigned as evaporation of a volatile solvent and retardation of gelation via a softening agent during the course of photopolymerization. Hybrid nanocaps were also prepared similar to hybrid spheres. Disregarding the polydisperse size distribution, every particle size within the atomization range of the aerosol generator possessed the shape of a “cap”. All of the particle structures up to this point – spherical polymers, spherical hybrids, and nanocaps – have been summarized within the first patent application “aerosol photopolymerization”.

Porous spherical polymer particles possessing rough surface characteristics, which we named mosaic nanoparticles, were prepared with the help of a porogen. This solvent had to be miscible with the liquid monomer but immiscible with the polymer formed afterwards. Furthermore, it had to be low volatile in comparison to the solvent employed for nanocap generation. As for the spheres and caps, mosaic particles were produced in the presence of ZnO nanoparticles as well. These particles, along with the nanocaps, can be found in the third

paper where nanostructured particle synthesis by aerosol-photopolymerization has been presented.

Organic-inorganic hybrid nanoparticles with ZnO as the inorganic part represented polymer-matrix nanocomposites (PMNCs) containing nanofillers distributed in the polymer matrix of spheres and caps. Similar PMNCs, but with molecularly dispersed distribution of the inorganic content in the polymer matrix, were also produced by employing caffeine. Caffeine-loaded spheres, caps, and mosaic particles were synthesized by aerosol-photopolymerization, and drug release experiments were performed. Release kinetics not only depended on the degree of molecular crosslinking in the polymer particles, but also on the particle shape offering controlled drug release.

Apart from composites where a number of inorganic nanoparticles are distributed within the polymer matrix, polymer spheres containing a single inorganic core were also successfully produced. These core-shell structures resulted from an integrated process – bipolar coagulation with subsequent photopolymerization – all in an aerosol-based process. Two aerosol streams, one with monomer droplets and the other one with core particles to be encapsulated as the dispersed phase, were electrostatically charged with opposite signs and mixed. A certain coagulation time for this aerosol allowed 1-to-1 bipolar coagulation of monomer droplets and core particles. Once each core particle got wetted and encapsulated by the liquid monomer, aerosol-photopolymerization solidified the liquid layer to a solid polymer shell around each core particle. The coagulation process, which is based on electrostatic effects, allowed the coagulation of various combinations of monomer droplets and core particles provided that the core material can be wetted by the liquid monomer. The synthesis of these core-shell particles has been submitted as a patent which is the second patent application resulting from this PhD thesis.

The entire particle structures of this work were produced by both an excimer photoreactor and a simpler photoreactor equipped with UV fluorescent tubes. The latest results verified that this process is not only suitable for radical photopolymerization but also cationic photopolymerization as presented in the last manuscript. Aside from the experimental work which constituted the main part of this thesis, simulations were performed to estimate the time for complete monomer conversion under different conditions. The photopolymerization reactions occurring within the monomer droplets were simulated by selecting suitable kinetic parameters and varying them within certain ranges.

The obtained widespread particle structures prepared by aerosol-photopolymerization illustrate the power of this technique. By selecting the proper particle type along with the “correct” material combination, multifunctional smart materials can be obtained. Aerosol-photopolymerization has been proven to be a promising tool for specialty material preparation. Its scale-up issues and particle production for direct applications as specific products should be considered for future work.

## 5. References

- Akguen, E., Hubbuch, J., Woerner, M., 2013. Perspectives of aerosol-photopolymerization: Nanoscale polymer particles. *Chemical Engineering Science* 101, 248-252.
- Akguen, E., Hubbuch, J., Woerner, M., 2014. Perspectives of Aerosol-Photopolymerization: Organic-inorganic hybrid nanoparticles. *Colloid Polym Sci.* 292, 1241-1247.
- Akguen, E., Hubbuch, J., Woerner, M., 2014. Perspectives of Aerosol-Photopolymerization: Nanostructured polymeric particles. *Macromolecular Materials and Engineering*. DOI: 10.2002/mame.201400032.
- Alargova, R.G., Bhatt, K.H., Paunov, V.N., Velev, O.D., 2004. Scalable synthesis of a new class of polymer microrods by a liquid - Liquid dispersion technique. *Advanced Materials* 16, 1653-+.
- Althues, H., Henle, J., Kaskel, S., 2007. Functional inorganic nanofillers for transparent polymers. *Chemical Society Reviews* 36, 1454-1465.
- Andrzejewska, E., 2001. Photopolymerization kinetics of multifunctional monomers. *Progress in Polymer Science* 26, 605-665.
- Anseth, K.S., Anderson, K.J., Bowman, C.N., 1996. Radical concentrations, environments, and reactivities during crosslinking polymerizations. *Macromolecular Chemistry and Physics* 197, 833-848.
- Anseth, K.S., Bowman, C.N., Peppas, N.A., 1994. Polymerization Kinetics and Volume Relaxation Behavior of Photopolymerized Multifunctional Monomers Producing Highly Cross-linked Networks. *Journal of Polymer Science Part a-Polymer Chemistry* 32, 139-147.
- Anseth, K.S., Kline, L.M., Walker, T.A., Anderson, K.J., Bowman, C.N., 1995. Reaction-kinetics and Volume Relaxation During Polymerizations of Multiethylene Glycol Dimethacrylates. *Macromolecules* 28, 2491-2499.
- Anseth, K.S., Wang, C.M., Bowman, C.N., 1994. Kinetic evidence of reaction-diffusion during the polymerization of multi(meth)acrylate monomers. *Macromolecules* 27, 650-655.
- Anzlovar, A., Orel, Z.C., Zigon, M., 2010. Poly(methyl methacrylate) composites prepared by in situ polymerization using organophilic nano-to-submicrometer zinc oxide particles. *European Polymer Journal* 46, 1216-1224.
- Arico, A.S., Bruce, P., Scrosati, B., Tarascon, J.M., Van Schalkwijk, W., 2005. Nanostructured materials for advanced energy conversion and storage devices. *Nature Materials* 4, 366-377.
- Athanassiou, E.K., Grass, R.N., Stark, W.J., 2006. Large-scale production of carbon-coated copper nanoparticles for sensor applications. *Nanotechnology* 17, 1668-1673.

- Balazs, A.C., Emrick, T., Russell, T.P., 2006. Nanoparticle polymer composites: Where two small worlds meet. *Science* 314, 1107-1110.
- Berglund, R.N., Liu, B.Y.H., 1973. Generation of Monodisperse Aerosol Standards. *Environmental Science & Technology* 7, 147-153.
- Berry, C.C., Curtis, A.S.G., 2003. Functionalisation of magnetic nanoparticles for applications in biomedicine. *Journal of Physics D-Applied Physics* 36, R198-R206.
- Berthelot, D., Gaudechon, H., 1910. *Compt. Rend.* 150, 1169.
- Beuermann, S., Buback, M., Davis, T.P., Gilbert, R.G., Hutchinson, R.A., Olaj, O.F., Russell, G.T., Schweer, J., vanHerk, A.M., 1997. Critically evaluated rate coefficients for free-radical polymerization. 2. Propagation rate coefficients for methyl methacrylate. *Macromolecular Chemistry and Physics* 198, 1545-1560.
- Beuermann, S., Paquet, D.A., McMinn, J.H., Hutchinson, R.A., 1996. Determination of free-radical propagation rate coefficients of butyl, 2-ethylhexyl, and dodecyl acrylates by pulsed-laser polymerization. *Macromolecules* 29, 4206-4215.
- Bin, X., Sargent, E.H., Kelley, S.O., 2010. Nanostructuring of Sensors Determines the Efficiency of Biomolecular Capture. *Analytical Chemistry* 82, 5928-5931.
- Biskos, G., Vons, V., Yurteri, C.U., Schmidt-Ott, A., 2008. Generation and Sizing of Particles for Aerosol-Based Nanotechnology. *Kona Powder and Particle Journal* 26, 13-35.
- Bonderer, L.J., Studart, A.R., Gauckler, L.J., 2008. Bioinspired design and assembly of platelet reinforced polymer films. *Science* 319, 1069-1073.
- Borra, J.P., Camelot, D., Chou, K.L., Kooyman, P.J., Marijnissen, J.C.M., Scarlett, B., 1999. Bipolar coagulation for powder production: Micro-mixing inside droplets. *Journal of Aerosol Science* 30, 945-958.
- Bowman, C.N., Kloxin, C.J., 2008. Toward an Enhanced Understanding and Implementation of Photopolymerization Reactions. *Aiche Journal* 54, 2775-2795.
- Bowman, C.N., Peppas, N.A., 1991. Coupling of kinetics and volume relaxation during polymerization of multiacrylates and multimethacrylates. *Macromolecules* 24, 1914-1920.
- Braun, D., 2001. PVC - Origin, growth, and future. *Journal of Vinyl & Additive Technology* 7, 168-176.
- Braunecker, W.A., Matyjaszewski, K., 2008. Controlled/living radical polymerization: Features, developments and perspectives (vol 32, pg 93, 2007). *Progress in Polymer Science* 33, 165-165.

- Buback, M., 1990. Free-radical Polymerization up to High Conversion- A General Kinetic Treatment. *Makromolekulare Chemie-Macromolecular Chemistry and Physics* 191, 1575-1587.
- Buback, M., Gilbert, R.G., Hutchinson, R.A., Klumperman, B., Kuchta, F.D., Manders, B.G., Odriscoll, K.F., Russell, G.T., Schweer, J., 1995. Critically Evaluated Rate Coefficients for Free-radical Polymerization.1. Propagation Rate Coefficient for Styrene. *Macromolecular Chemistry and Physics* 196, 3267-3280.
- Casari, W., 2010. Color switching in nanocomposites comprising inorganic nanoparticles dispersed in a polymer matrix. *Journal of Materials Chemistry* 20, 5582-5592.
- Champion, J.A., Katare, Y.K., Mitragotri, S., 2007. Particle shape: A new design parameter for micro- and nanoscale drug delivery carriers. *Journal of Controlled Release* 121, 3-9.
- Crivello, J.V., Reichmanis, E., 2014. Photopolymer Materials and Processes for Advanced Technologies. *Chemistry of Materials* 26, 533-548.
- De Geest, B.G., Urbanski, J.P., Thorsen, T., Demeester, J., De Smedt, S.C., 2005. Synthesis of monodisperse biodegradable microgels in microfluidic devices. *Langmuir* 21, 10275-10279.
- Decker, C., 1992. Kinetic-study of light-induced polymerization by real-time UV and IR spectroscopy. *Journal of Polymer Science Part a-Polymer Chemistry* 30, 913-928.
- Decker, C., 1996. Photoinitiated crosslinking polymerisation. *Progress in Polymer Science* 21, 593-650.
- Decker, C., 2002. Kinetic study and new applications of UV radiation curing. *Macromolecular Rapid Communications* 23, 1067-1093.
- Decker, C., 2002. Light-induced crosslinking polymerization. *Polymer International* 51, 1141-1150.
- Decker, C., Bianchi, C., Decker, D., Morel, F., 2001. Photoinitiated polymerization of vinyl ether-based systems. *Progress in Organic Coatings* 42, 253-266.
- Decker, C., Elzaouk, B., Decker, D., 1996. Kinetic study of ultrafast photopolymerization reactions. *Journal of Macromolecular Science-Pure and Applied Chemistry* A33, 173-190.
- Decker, C., Moussa, K., 1990. Kinetic investigation of photopolymerizations induced by laser-beams. *Makromolekulare Chemie-Macromolecular Chemistry and Physics* 191, 963-979.
- Decker, C., Moussa, K., 1990. Kinetic Investigation of Photopolymerizations Induced by Laser-beams. *Makromolekulare Chemie-Macromolecular Chemistry and Physics* 191, 963-979.

- Decker, C., Moussa, K., 1990. Kinetic-study of the Cationic Photopolymerization of Epoxy Monomers. *Journal of Polymer Science Part a-Polymer Chemistry* 28, 3429-3443.
- Demir, M.M., Memesa, M., Castignolles, P., Wegner, G., 2006. PMMA/zinc oxide nanocomposites prepared by in-situ bulk polymerization. *Macromolecular Rapid Communications* 27, 763-770.
- Dendukuri, D., Doyle, P.S., 2009. The Synthesis and Assembly of Polymeric Microparticles Using Microfluidics. *Advanced Materials* 21, 4071-4086.
- Dendukuri, D., Tsoi, K., Hatton, T.A., Doyle, P.S., 2005. Controlled synthesis of nonspherical microparticles using microfluidics. *Langmuir* 21, 2113-2116.
- Donev, A., Cisse, I., Sachs, D., Variano, E., Stillinger, F.H., Connelly, R., Torquato, S., Chaikin, P.M., 2004. Improving the density of jammed disordered packings using ellipsoids. *Science* 303, 990-993.
- Elliott, J.E., Bowman, C.N., 2001. Monomer functionality and polymer network formation. *Macromolecules* 34, 4642-4649.
- El-Sayed, I.H., Huang, X.H., El-Sayed, M.A., 2005. Surface plasmon resonance scattering and absorption of anti-EGFR antibody conjugated gold nanoparticles in cancer diagnostics: Applications in oral cancer. *Nano Letters* 5, 829-834.
- Emmerich, O., Hugenberg, N., Schmidt, M., Sheiko, S.S., Baumann, F., Deubzer, B., Weis, J., Ebenhoch, J., 1999. Molecular boxes based on hollow organosilicon micronetworks. *Advanced Materials* 11, 1299-+.
- Esen, C., Kaiser, T., Schweiger, G., 1996. Raman investigation of photopolymerization reactions of single optically levitated microparticles. *Applied Spectroscopy* 50, 823-828.
- Esen, C., Schweiger, G., 1996. Preparation of monodisperse polymer particles by photopolymerization. *Journal of Colloid and Interface Science* 179, 276-280.
- Faraji, A.H., Wipf, P., 2009. Nanoparticles in cellular drug delivery. *Bioorganic & Medicinal Chemistry* 17, 2950-2962.
- Florez, L., Herrmann, C., Cramer, J.M., Hauser, C.P., Koynov, K., Landfester, K., Crespy, D., Mailaender, V., 2012. How Shape Influences Uptake: Interactions of Anisotropic Polymer Nanoparticles and Human Mesenchymal Stem Cells. *Small* 8, 2222-2230.
- Fu, G.-D., Li, G.L., Neoh, K.G., Kang, E.T., 2011. Hollow polymeric nanostructures-Synthesis, morphology and function. *Progress in Polymer Science* 36, 127-167.
- Fuchs, N.A., 1964. The mechanics of aerosols.
- Gao, Z., Grulke, E.A., Ray, A.K., 2007. Synthesis of monodisperse polymer microspheres by photopolymerization of microdroplets. *Colloid and Polymer Science* 285, 847-854.

- Glotzer, S.C., Solomon, M.J., 2007. Anisotropy of building blocks and their assembly into complex structures. *Nature Materials* 6, 557-562.
- Gokmen, M.T., Du Prez, F.E., 2012. Porous polymer particles-A comprehensive guide to synthesis, characterization, functionalization and applications. *Progress in Polymer Science* 37, 365-405.
- Gupta, S., Zhang, Q., Emrick, T., Russell, T.P., 2006. "Self-corralling" nanorods under an applied electric field. *Nano Letters* 6, 2066-2069.
- Haag, R., 2004. Supramolecular drug-delivery systems based on polymeric core-shell architectures. *Angewandte Chemie-International Edition* 43, 278-282.
- Hack, B., Egger, H., Uhlemann, J., Henriot, M., Wirth, W., Vermeer, A.W.P., Duff, D.G., 2012. Advanced Agrochemical Formulations through Encapsulation Strategies? *Chemie Ingenieur Technik* 84, 223-234.
- Hecht, L.L., Winkelmann, M., Wagner, C., Landfester, K., Gerlinger, W., Sachweh, B., Schuchmann, H.P., 2012. Miniemulsions for the Production of Nanostructured Particles. *Chemical Engineering & Technology* 35, 1670-1676.
- Hoffman, A.J., Mills, G., Yee, H., Hoffmann, M.R., 1992a. Q-sized CDS - Synthesis, Characterization, and Efficiency of Photoinitiation of Polymerization of Several Vinyllic Monomers. *Journal of Physical Chemistry* 96, 5546-5552.
- Hoffman, A.J., Yee, H., Mills, G., Hoffmann, M.R., 1992. Photoinitiated Polymerization of Methyl-methacrylate using Q-sized ZnO Colloids. *Journal of Physical Chemistry* 96, 5540-5546.
- Huang, X.Y., Brittain, W.J., 2001. Synthesis and characterization of PMMA nanocomposites by suspension and emulsion polymerization. *Macromolecules* 34, 3255-3260.
- Hwang, D.K., Dendukuri, D., Doyle, P.S., 2008. Microfluidic-based synthesis of non-spherical magnetic hydrogel microparticles. *Lab on a Chip* 8, 1640-1647.
- Jeong, W.J., Kim, J.Y., Choo, J., Lee, E.K., Han, C.S., Beebe, D.J., Seong, G.H., Lee, S.H., 2005. Continuous fabrication of biocatalyst immobilized microparticles using photopolymerization and immiscible liquids in microfluidic systems. *Langmuir* 21, 3738-3741.
- Johnson, P.M., Stansbury, J.W., Bowman, C.N., 2007. Alkyl chain length effects on copolymerization kinetics of a monoacrylate with hexanediol diacrylate. *Journal of Combinatorial Chemistry* 9, 1149-1156.

- Kasper, G., 1981. Electrostatic Dispersion of Homopolar Charged Aerosols. *Journal of Colloid and Interface Science* 81, 32-40.
- Kawaguchi, H., 2000. Functional polymer microspheres. *Progress in Polymer Science* 25, 1171-1210.
- Kesselring, A., Koeblitz, T., WO 2002006131 A1. WO 2002006131 A1.
- Khrenov, V., Klapper, M., Koch, M., Mullen, K., 2005. Surface functionalized ZnO particles designed for the use in transparent nanocomposites. *Macromolecular Chemistry and Physics* 206, 95-101.
- Kindernay, J., Blazkova, A., Ruda, J., Jancovicova, V., Jakubikova, Z., 2002. Effect of UV light source intensity and spectral distribution on the photopolymerisation reactions of a multifunctional acrylated monomer. *Journal of Photochemistry and Photobiology a-Chemistry* 151, 229-236.
- Kobayashi, H., Miyanaga, E., Okubo, M., 2007. Studies on suspension and emulsion - Part 295. Preparation of multihollow polymer particles by seeded emulsion polymerization using seed particles with incorporated nonionic emulsifier - Part CCXCV of the series "Studies on Suspension and Emulsion". *Langmuir* 23, 8703-8708.
- Kogelschatz, U., 1990. Silent discharges for the generation of ultraviolet and vacuum ultraviolet excimer radiation. *Pure and Applied Chemistry* 62, 1667-1674.
- Kurdikar, D.L., Peppas, N.A., 1994. A kinetic-model for diffusion-controlled bulk cross-linking photopolymerizations. *Macromolecules* 27, 4084-4092.
- Kuriacose, J., Markham, M.C., 1961. Mechanism of Photo-initiated Polymerization of Methyl Methacrylate at Zinc Oxide Surfaces. *Journal of Physical Chemistry* 65, 2232-&.
- Lalevee, J., Allonas, X., Fouassier, J.P., 2006. Direct measurements of the addition and recombination of acrylate radicals: Access to propagation and termination rate constants? *Journal of Polymer Science Part a-Polymer Chemistry* 44, 3577-3587.
- Lalevee, J., Allonas, X., Jradi, S., Fouassier, J.P., 2006. Role of the medium on the reactivity of cleavable photoinitiators in photopolymerization reactions. *Macromolecules* 39, 1872-1879.
- Landfester, K., Bechthold, N., Tiarks, F., Antonietti, M., 1999. Miniemulsion polymerization with cationic and nonionic surfactants: A very efficient use of surfactants for heterophase polymerization. *Macromolecules* 32, 2679-2683.
- Landfester, K., Bechthold, N., Tiarks, F., Antonietti, M., 1999. Miniemulsion polymerization with cationic and nonionic surfactants: A very efficient use of surfactants for heterophase polymerization. *Macromolecules* 32, 2679-2683.

- Lewandowski, K., Svec, F., Frechet, J.M.J., 1998. Preparation of macroporous, monodisperse, functionalized styrene-divinylbenzene copolymer beads: Effect of the nature of the monomers and total porogen volume on the porous properties. *Journal of Applied Polymer Science* 67, 597-607.
- Li, F.S., Zhou, S.X., You, B., Wu, L.M., 2006. Kinetic investigations on the UV-induced photopolymerization of nanocomposites by FTIR spectroscopy. *Journal of Applied Polymer Science* 99, 1429-1436.
- Li, S., Meng Lin, M., Toprak, M.S., Kim, D.K., Muhammed, M., 2010. Nanocomposites of polymer and inorganic nanoparticles for optical and magnetic applications. *Nano reviews* 1.
- Lovell, L.G., Berchtold, K.A., Elliott, J.E., Lu, H., Bowman, C.N., 2001. Understanding the kinetics and network formation of dimethacrylate dental resins. *Polymers for Advanced Technologies* 12, 335-345.
- Lovestead, T.M., Berchtold, K.A., Bowman, C.N., 2002. Modeling the effects of chain length on the termination kinetics in multivinyl photopolymerizations. *Macromolecular Theory and Simulations* 11, 729-738.
- Lovestead, T.M., Burdick, J.A., Anseth, K.S., Bowman, C.N., 2005. Understanding multivinyl monomer photopolymerization kinetics through modeling and GPC investigation of degradable networks. *Polymer* 46, 6226-6234.
- Lovestead, T.M., O'Brien, A.K., Bowman, C.N., 2003. Models of multivinyl free radical photopolymerization kinetics. *Journal of Photochemistry and Photobiology a-Chemistry* 159, 135-143.
- Lu, Y., Yin, Y.D., Xia, Y.N., 2001. Three-dimensional photonic crystals with non-spherical colloids as building blocks. *Advanced Materials* 13, 415-420.
- Lyons, R.A., Hutovic, J., Piton, M.C., Christie, D.I., Clay, P.A., Manders, B.G., Kable, S.H., Gilbert, R.G., 1996. Pulsed-laser polymerization measurements of the propagation rate coefficient for butyl acrylate. *Macromolecules* 29, 1918-1927.
- Macintyre, F.S., Sherrington, D.C., 2004. Control of porous morphology in suspension polymerized poly(divinylbenzene) resins using oligomeric porogens. *Macromolecules* 37, 7628-7636.
- Mahdavian, A.R., Sarrafi, Y., Shabankareh, M., 2009. Nanocomposite particles with core-shell morphology III: preparation and characterization of nano Al<sub>2</sub>O<sub>3</sub>-poly(styrene-methyl methacrylate) particles via miniemulsion polymerization. *Polymer Bulletin* 63, 329-340.
- Maisels, A., Kruis, F.E., Fissan, H., Rellinghaus, B., Zahres, H., 2000. Synthesis of tailored composite nanoparticles in the gas phase. *Applied Physics Letters* 77, 4431-4433.

- Mallikarjuna, B., Rao, K.M., Prasad, C.V., Rao, K.C., Subha, M.C.S., 2011. Development of Triprolidine-Hydrochloride-Loaded pH-Sensitive Poly(Acrylamide-co-Acrylamidoglycolic Acid) Co-Polymer Microspheres: In Vitro Release Studies. *Designed Monomers and Polymers* 14, 445-459.
- Michinaka, Y., Mitragotri, S., 2011. Delivery of polymeric particles into skin using needle-free liquid jet injectors. *Journal of Controlled Release* 153, 249-254.
- Minsk, L.M., Van Deusen, W.P., Robertson, M., 1954. Photosensitization of polymeric cinnamic acid esters, US2670285 A.
- Morrison, B.R., Piton, M.C., Winnik, M.A., Gilbert, R.G., Napper, D.H., 1993. Solvent Effects on the Propagation Rate Coefficient for Free-radical Polymerization. *Macromolecules* 26, 4368-4372.
- Nicole, L., Rozes, L., Sanchez, C., 2010. Integrative Approaches to Hybrid Multifunctional Materials: From Multidisciplinary Research to Applied Technologies. *Advanced Materials* 22, 3208-3214.
- Nie, Z.H., Xu, S.Q., Seo, M., Lewis, P.C., Kumacheva, E., 2005. Polymer particles with various shapes and morphologies produced in continuous microfluidic reactors. *Journal of the American Chemical Society* 127, 8058-8063.
- Odian, G., 2004. *Principles of Polymerization*.
- Oster, G., Yang, N.L., 1968. Photopolymerization of Vinyl Monomers. *Chemical Reviews* 68, 125-151.
- Park, J.-G., Forster, J.D., Dufresne, E.R., 2010. High-Yield Synthesis of Monodisperse Dumbbell-Shaped Polymer Nanoparticles. *Journal of the American Chemical Society* 132, 5960-+.
- Peer, D., Karp, J.M., Hong, S., FaroKhazad, O.C., Margalit, R., Langer, R., 2007. Nanocarriers as an emerging platform for cancer therapy. *Nature Nanotechnology* 2, 751-760.
- Peiffer, R.W., 1997. Applications of photopolymer technology, in: Scranton, A.B., Bowman, C.N., Peiffer, R.W. (Eds.), *Photopolymerization: Fundamentals and Applications*, pp. 1-14.
- Plambeck, J.L., 1956. Photographic preparation of relief images, US 2760863 A.
- Qi, D.-m., Bao, Y.-z., Weng, Z.-x., Huang, Z.-m., 2006. Preparation of acrylate polymer/silica nanocomposite particles with high silica encapsulation efficiency via miniemulsion polymerization. *Polymer* 47, 4622-4629.
- Reis, C.P., Neufeld, R.J., Ribeiro, A.J., Veiga, F., 2006. Nanoencapsulation I. Methods for preparation of drug-loaded polymeric nanoparticles. *Nanomedicine-Nanotechnology Biology and Medicine* 2, 8-21.

- Rokhade, A.P., Shelke, N.B., Patil, S.A., Aminabhavi, T.M., 2007. Novel interpenetrating polymer network microspheres of chitosan and methylcellulose for controlled release of theophylline. *Carbohydrate Polymers* 69, 678-687.
- Salas Vicente, J., López Gejo, J., Rothenbacher, S., Sarojiniamma, S., Gogritchiani, E., Miranda, M.A., Woerner, M., Oliveros, E., Kasper, G., Braun, A.M., 2010. VUV-photochemical functionalization of polystyrene aerosols. *Basics and Applications of Photopolymerization Reactions* 3, 47-65.
- Sanchez, C., Julian, B., Belleville, P., Popall, M., 2005. Applications of hybrid organic-inorganic nanocomposites. *Journal of Materials Chemistry* 15, 3559-3592.
- Sangermano, M., Malucelli, G., Morel, F., Decker, C., Priola, A., 1999. Cationic photopolymerization of vinyl ether systems: influence of the presence of hydrogen donor additives. *European Polymer Journal* 35, 639-645.
- Schenkel, A., Schaber, K., 1995. Growth of salt and acid aerosol-particles in humid air. *Journal of Aerosol Science* 26, 1029-1039.
- Scherzer, T., Decker, U., 1999. Kinetic investigations on UV-induced photopolymerization reactions by real-time FTIR-ATR spectroscopy: the efficiency of photoinitiators at 313 and 222 nm. *Nuclear Instruments & Methods in Physics Research Section B-Beam Interactions with Materials and Atoms* 151, 306-312.
- Scherzer, T., Mehnert, R., Lucht, H., 2004. On-line monitoring of the acrylate conversion in UV photopolymerization by near-infrared reflection spectroscopy. *Macromolecular Symposia* 205, 151-162.
- Seipenbusch, A., Weber, A.P., Schiel, A., Kasper, G., 2003. Influence of the gas atmosphere on restructuring and sintering kinetics of nickel and platinum aerosol nanoparticle agglomerates. *Journal of Aerosol Science* 34, 1699-1709.
- Seipenbusch, M., Heel, A., Weber, A.P., Kasper, G., 2002. Determination of coating thickness of DEHS on submicron particles by means of low pressure impaction. *Chemical Engineering & Technology* 25, 77-82.
- Seo, M., Nie, Z.H., Xu, S.Q., Mok, M., Lewis, P.C., Graham, R., Kumacheva, E., 2005. Continuous microfluidic reactors for polymer particles. *Langmuir* 21, 11614-11622.
- Sharma, G., Valenta, D.T., Altman, Y., Harvey, S., Xie, H., Mitragotri, S., Smith, J.W., 2010. Polymer particle shape independently influences binding and internalization by macrophages. *Journal of Controlled Release* 147, 408-412.
- Shepherd, R.F., Conrad, J.C., Rhodes, S.K., Link, D.R., Marquez, M., Weitz, D.A., Lewis, J.A., 2006. Microfluidic assembly of homogeneous and janus colloid-filled hydrogel granules. *Langmuir* 22, 8618-8622.

- Sherrington, D.C., 1998. Preparation, structure and morphology of polymer supports. *Chemical Communications*, 2275-2286.
- Shi, J., Votruba, A.R., Farokhzad, O.C., Langer, R., 2010. Nanotechnology in Drug Delivery and Tissue Engineering: From Discovery to Applications. *Nano Letters* 10, 3223-3230.
- Shim, J.W., Kim, J.W., Han, S.H., Chang, I.S., Kim, H.K., Kang, H.H., Lee, O.S., Suh, K.D., 2002. Zinc oxide/polymethylmethacrylate composite microspheres by in situ suspension polymerization and their morphological study. *Colloids and Surfaces a-Physicochemical and Engineering Aspects* 207, 105-111.
- Shin, D.S., Oh, E.K., Kim, S.G., 1996. Preparation of polymer particles in aerosol-phase reaction. *Aerosol Science and Technology* 24, 243-254.
- Shum, H.C., Abate, A.R., Lee, D., Studart, A.R., Wang, B., Chen, C.-H., Thiele, J., Shah, R.K., Krummel, A., Weitz, D.A., 2010. Droplet Microfluidics for Fabrication of Non-Spherical Particles. *Macromolecular Rapid Communications* 31, 108-118.
- Sigmund, S., Yu, M., Meyer, J., Kasper, G., 2014. An Aerosol-Based Process for Electrostatic Coating of Particle Surfaces with Nanoparticles. *Aerosol Science and Technology* 48, 142-149.
- Staff, R.H., Lieberwirth, I., Landfester, K., Crespy, D., 2012. Preparation and Characterization of Anisotropic Submicron Particles From Semicrystalline Polymers. *Macromolecular Chemistry and Physics* 213, 351-358.
- Sun, D., Miyatake, N., Sue, H.-J., 2007. Transparent PMMA/ZnO nanocomposite films based on colloidal ZnO quantum dots. *Nanotechnology* 18.
- Tao, L., Hu, W., Liu, Y., Huang, G., Sumer, B.D., Gao, J., 2011. Shape-specific polymeric nanomedicine: emerging opportunities and challenges. *Experimental Biology and Medicine* 236, 20-29.
- Tryson, G.R., Shultz, A.R., 1979. CALORIMETRIC STUDY OF ACRYLATE PHOTO-POLYMERIZATION. *Journal of Polymer Science Part B-Polymer Physics* 17, 2059-2075.
- van Vlerken, L.E., Amiji, M.M., 2006. Multi-functional polymeric nanoparticles for tumour-targeted drug delivery. *Expert opinion on drug delivery* 3, 205-216.
- Vauthier, C., Bouchemal, K., 2009. Methods for the Preparation and Manufacture of Polymeric Nanoparticles. *Pharmaceutical Research* 26, 1025-1058.
- Villamena, F.A., De La Cruz, A.A., 2001. Caffeine selectivity of divinylbenzene crosslinked polymers in aqueous media. *Journal of Applied Polymer Science* 82, 195-205.
- Vollath, D., Szabo, D.V., Fuchs, J., 1999. Synthesis and properties of ceramic - Polymer composites. *Nanostructured Materials* 12, 433-438.

- Vorderbruggen, M.A., Crivello, J., Wu, K., Breneman, C.M., 1999. Use of cationic aerosol photopolymerization to form silicone microbeads in the presence of molecular templates (vol 8, pg 1106, 1996). *Chemistry of Materials* 11, 1398-1398.
- Whitby, K.T., 1961. GENERATOR FOR PRODUCING HIGH CONCENTRATIONS OF SMALL IONS. *Review of Scientific Instruments* 32, 1351-&.
- Widmann, J.F., Aardahl, C.L., Johnson, T.J., Davis, E.J., 1998. Encapsulation of levitated microparticles. *Journal of Colloid and Interface Science* 199, 197-205.
- Wu, D., Xu, F., Sun, B., Fu, R., He, H., Matyjaszewski, K., 2012. Design and Preparation of Porous Polymers. *Chemical Reviews* 112, 3959-4015.
- Wulkow, M., 2008. Computer Aided Modeling of Polymer Reaction Engineering-The status of Predici, 1-Simulation. *Macromolecular Reaction Engineering* 2, 461-494.
- Xiong, M.N., Gu, G.X., You, B., Wu, L.M., 2003. Preparation and characterization of poly(styrene butylacrylate) latex/nano-ZnO nanocomposites. *Journal of Applied Polymer Science* 90, 1923-1931.
- Yang, Z.Q., Huck, W.T.S., Clarke, S.M., Tajbakhsh, A.R., Terentjev, E.M., 2005. Shape-memory nanoparticles from inherently non-spherical polymer colloids. *Nature Materials* 4, 486-490.
- Ye, Q., He, W.D., Ge, X.W., Jia, H.T., Liu, H.R., Zhang, Z.C., 2002. Formation of monodisperse polyacrylamide particles by radiation-induced dispersion polymerization. I. Synthesis and polymerization kinetics. *Journal of Applied Polymer Science* 86, 2567-2573.
- Ye, S., Cramer, N.B., Bowman, C.N., 2011. Relationship between Glass Transition Temperature and Polymerization Temperature for Cross-Linked Photopolymers. *Macromolecules* 44, 490-494.
- Yoshida, M., Roh, K.-H., Lahann, J., 2007. Short-term biocompatibility of biphasic nanocolloids with potential use as anisotropic imaging probes. *Biomaterials* 28, 2446-2456.
- Yuwono, A.H., Liu, B.H., Xue, J.M., Wang, J., Elim, H.I., Ji, W., Li, Y., White, T.J., 2004. Controlling the crystallinity and nonlinear optical properties of transparent TiO<sub>2</sub>-PMMA nanohybrids. *Journal of Materials Chemistry* 14, 2978-2987.
- Zaikov, G., Rakovsky, S., Anachkov, M., 2012. Ozone and its reactions with diene rubbers. *Chemistry and Chemical Technology* 6, 307-319.
- Zebel, G., 1958. Zur Theorie des Verhaltens elektrisch geladener Aerosole. *Kolloid-Zeitschrift* 157, 35-50.
- Zeng, H., Sun, S., 2008. Syntheses, properties and potential applications of multicomponent magnetic nanoparticles. *Advanced Functional Materials* 18, 391-400.

Zhang, B., Liao, Y.-C., Girshick, S.L., Roberts, J.T., 2008. Growth of coatings on nanoparticles by photoinduced chemical vapor deposition. *Journal of Nanoparticle Research* 10, 173-178.

Zhang, L., Ranade, M.B., Gentry, J.W., 2004. Formation of organic coating on ultrafine silver particles using a gas-phase process. *Journal of Aerosol Science* 35, 457-471.

Zhu, S., Tian, Y., Hamielec, A.E., Eaton, D.R., 1990. Radical trapping and termination in free-radical polymerization of MMA. *Macromolecules* 23, 1144-1150.

# Ertan Akgün

---

Place and Date of Birth:  
Walenstadt, Switzerland  
20.08.1984



*Remaining private information is hidden.*

## EDUCATION

- 02/2010 – 06/2014      PhD in Chemical Engineering  
                                 Karlsruhe Institute of Technology
- 10/2007 – 08/2009      Diploma in Chemical Engineering  
                                 Karlsruhe Institute of Technology  
                                 Grade: 1.6 / 1.0
- 09/2002 – 09/2007      B.Sc. in Chemical Engineering  
                                 Ege University  
                                 Grade: 90.41 / 100 (with distinction)

## SCIENTIFIC PUBLICATIONS

- Patents
  - Ertan Akgün, Wolfgang Gerlinger, Michael Wörner  
Aerosol Photopolymerization, US 20130079482 A1
  - Ertan Akgün, Stephanie Sigmund, Wolfgang Gerlinger, Bernd Sachweh,  
Gerhard Kasper, Michael Wörner  
Finely Divided Particles of Core-Shell Structure, US 20140061026 A1

- Peer Reviewed Journal Articles
  - Ertan Akgün, Jürgen Hubbuch, Michael Wörner  
Perspectives of Aerosol-Photopolymerization: Nanoscale Polymer Particles  
Chemical Engineering Science 101, 248-252, 2013
  - Ertan Akgün, Jürgen Hubbuch, Michael Wörner  
Perspectives of Aerosol-Photopolymerization: Organic-Inorganic Hybrid  
Nanoparticles  
Colloid and Polymer Science, 292, 1241-1247, 2014
  - Ertan Akgün, Jürgen Hubbuch, Michael Wörner  
Perspectives of Aerosol-Photopolymerization: Nanostructured Polymeric  
Materials  
Macromolecular Materials and Engineering, DOI: 101002/mame.201400032,  
2014
  - Ertan Akgün, Stephanie Sigmund, Jörg Meyer, Jürgen Hubbuch, Michael Wörner,  
Gerhard Kasper  
Defined Polymer Shells on Nanoparticles via a Continuous Aerosol-Based Process  
Nanoparticle Research, 16, 2533, 2014
  - Ertan Akgün, Alex Muntean, Jürgen Hubbuch, Marco Sangermano, Michael Wörner  
Cationic Aerosol-Photopolymerization  
Macromolecular Materials and Engineering, DOI: 10.1002/mame.201400211
  
- Conference Talks
  - Ertan Akgün, Wolfgang Gerlinger, Michael Wörner, Bernd Sachweh, Jürgen  
Hubbuch  
Organic-inorganic hybrid nanoparticles via aerosol-photopolymerization  
6<sup>th</sup> International Conference on Surfaces, Coatings and Nano-Structured  
Materials, October 17-20, 2011, Krakow, Poland
  - Ertan Akgün, Wolfgang Gerlinger, Michael Wörner, Bernd Sachweh, Jürgen  
Hubbuch  
Production of nanocaps by aerosol-photopolymerization  
World Polymer Congress, June 24-29, 2012, Blacksburg, USA
  - Ertan Akgün, Wolfgang Gerlinger, Michael Wörner, Bernd Sachweh, Jürgen  
Hubbuch  
Different hybrid and single-phase nanoparticles by aerosol-  
photopolymerization  
European Aerosol Conference, September 2-7, 2013, Granada, Spain

- Stephanie Sigmund, Ertan Akgün, Jörg Meyer, Michael Wörner, Wolfgang Gerlinger, Gerhard Kasper  
Continuous, electrostatic controlled synthesis of organic-inorganic composite particles  
European Aerosol Conference, September 2-7, 2013, Granada, Spain
- Ertan Akgün, Wolfgang Gerlinger, Michael Wörner, Bernd Sachweh, Jürgen Hubbuch,  
Nanoskalige Hybridpartikel und nicht-kugelförmige Partikel mittels Aerosol-Photopolymerisation  
ProcessNet-Jahrestagung, September 10-13, 2012, Karlsruhe, Germany
- Ertan Akgün, Wolfgang Gerlinger, Bernd Sachweh, Jürgen Hubbuch, Michael Wörner  
Aerosol-photopolymerization for hybrid nanoparticles with different structures  
3<sup>rd</sup> International Conference on Multifunctional, Hybrid and Nanomaterials, March 3-7, 2013, Sorrento, Italy
- Ertan Akgün, Marcel Vranceanu, Bernd Sachweh, Jürgen Hubbuch, Michael Wörner  
Perspectives of aerosol-photopolymerization  
European Polymer Congress, June 16-21, 2013, Pisa, Italy
- Ertan Akgün, Marcel Vranceanu, Bernd Sachweh, Jürgen Hubbuch, Michael Wörner  
Substance release kinetics of nanoparticles generated by aerosol-photopolymerization  
European Aerosol Conference, September 1-6, 2013, Prague, Czech Republic
  
- Conference Posters
  - Ertan Akgün, Wolfgang Gerlinger, Michael Wörner, Bernd Sachweh, Jürgen Hubbuch  
Aerosol-photopolymerization for the production of nanoscale acrylic polymer particles  
8<sup>th</sup> European Congress of Chemical Engineering, September 25-29, 2011, Berlin, Germany
  - Ertan Akgün, Jürgen Hubbuch, Michael Wörner  
Hybrid nanostructures via aerosol-photopolymerization  
Nano-structure in disperse systems: production, characterization and functionality, November 12-13, 2012, Karlsruhe, Germany

- Stephanie Sigmund, Ertan Akgün, Jörg Meyer, Michael Wörner, Wolfgang Gerlinger, Gerhard Kasper  
Continuous generation of organic-inorganic hybrid nanoparticles via charge controlled coagulation  
Nano-structure in disperse systems: production, characterization and functionality, November 12-13, 2012, Karlsruhe, Germany
- Ertan Akgün, Stephanie Sigmund, Wolfgang Gerlinger, Bernd Sachweh, Jürgen Hubbuch, Gerhard Kasper, Michael Wörner  
An integrated gas-phase process to generate core-shell nanoparticles via bipolar coagulation with subsequent photopolymerization  
3<sup>rd</sup> International Conference on Multifunctional, Hybrid and Nanomaterials, March 3-7, 2013, Sorrento, Italy
- Stephanie Sigmund, Ertan Akgün, Jörg Meyer, Michael Wörner, Gerhard Kasper  
Synthesis of tailored organic-inorganic nanostructures by charge controlled coagulation  
European Aerosol Conference, September 1-6, 2013, Prague, Czech Republic

## SCIENTIFIC KNOWLEDGE

- Generation and characterization of nano - and microscale particles
- Stabilization and separation of nanoparticle dispersions
- Polymer and - hybrid particle technology
- Generation of nanostructured materials
- Modeling and simulation in polymer reaction engineering
- Applied photochemistry and spectroscopy

## SOFT SKILLS

- Teaching  
Exercises of the lecture “Measurement Technology and Instrumental Analysis”
- Mentoring  
Mentoring of diploma and bachelor students, summer internship students, and scientific assistant students
- Workshops  
Attended the workshops “Team Management“ and “Intercultural Communication with Focus on Africa”

## LANGUAGE SKILLS

- German: business fluent
- English: business fluent
- Turkish: native speaker